Doctoral Thesis

Touching Autism Spectrum Disorder: Somatosensory Abnormalities in Shank3b and Cntnap2 Mouse Models

Ph.D. Candidate:
Luigi Balasco

Supervisor:
Prof. Yuri Bozzi

Doctoral Programme in Cognitive and Brain Sciences
Center for Mind/Brain Sciences - CIMeC
University of Trento

XXXIV Cycle

Acknowledgments

Questi anni di dottorato sono stati i più belli e faticosi della mia vita. Mi sento così cambiato che se guardo indietro mi riconosco appena. Sarà che ho perso gran parte dei capelli, ma per quelli mi piace incolpare mia moglie. In questi anni ho imparato tanto dal punto di vista personale e professionale e molto lo devo alle persone che ho incrociato. Ho sempre cercato di prendere il meglio dalle persone che hanno fatto parte di questo viaggio, che abbiano percorso un tratto di strada insieme a me o semplicemente incrociato lungo la strada.

Ho un debito enorme nei confronti di Yuri, in questi anni sei stato più di un supervisor. Hai saputo credere in me e mi hai dato le responsabilità che cercavo ma soprattutto mi hai concesso mille e più occasioni. Occasioni di provare senza la paura di sbagliare, occasioni di conoscere senza pregiudizio, occasioni di mettersi in gioco senza giudizio. I tuoi consigli e la tua guida sono stati preziosi e sono convinto che non si fermeranno qui. Per me sei un punto di riferimento e d'ispirazione.

Un ringraziamento speciale va a tutti i ragazzi che hanno lavorato duramente con me durante questi anni. Lorenzo, Francesca, Romina Evgenia, Alessandra, Enrica. Mi sento di dire che non solo abbiamo fatto squadra, ma ci siamo soprattutto divertiti e non sbaglio a chiamarvi amici.

Un sentito grazie ad Andrea Grigoli, mi hai accolto come uno di famiglia in lab e sei stato un amico più che collega durante i tempi passati insieme al CIBIO. Ho imparato più io da te che viceversa. Tu, insieme con Maria Elena, Simona, Anja, Gabriele, Ivan e Antonio siete le persone che più mi mancheranno del CIBIO.

Voglio esprimere la mia gratitudine ad Alessandro Gozzi i cui preziosi commenti durante i nostri incontri annuali sono stati d'ispirazione. Ancora, voglio ringraziare Giovanni Provenzano. I tuoi consigli ed il tuo punto di vista sulle cose della vita e del lavoro sono stati preziosi. Non dimenticherò facilmente il tuo "Don Luì, sveeeglia" a Sorrento.

Un ringraziamento va alla mia seconda famiglia del CIMEC: Michela, Erika, Veronika, Tommaso, Grazia. Le chiacchiere e le risate insieme sono state il collante di questo lavoro.

Voglio ringraziare anche i miei amici sparsi per il mondo: Marco P., Paolo, Emanuele, Nicolò, F. Pintozzi, Caterina e Marco S. Nonostante la lontananza ci siete sempre. Vi auguro un futuro radioso.

Ancora, i miei amici di sempre Pierpaolo, Francesco, Marino, Daniela e Simona per esserci sempre e per ricordarmi da dove provengo. Siete la famiglia che ho scelto. So di poter contare sempre su di voi.

Se da ragazzino mi aveste chiesto “cosa vuoi fare da grande?” beh, io avrei risposto “lo scienziato pazzo!” tra le risate dei miei genitori. Se è vero che la pazzia è dietro l’angolo devo profondamente ringraziare la mia famiglia per aver supportato il mio sogno di bambino.

Questa tesi è dedicata a mia moglie, Anna, che mi ha dato una spintarella fuori la porta (Gandalf, sei tu?). Sono sempre più convinto che questo traguardo è anche il tuo traguardo. La tua forza d’animo e la tua caparbietà sono d’ispirazione per me, il tuo amore un pilastro.

Content disclaimer

The content of the thesis presented here belongs to the following publications:

- Balasco Luigi, Provenzano Giovanni and Bozzi Yuri (2020) Sensory Abnormalities in Autism Spectrum Disorders: A Focus on the Tactile Domain, From Genetic Mouse Models to the Clinic. Frontiers in Psychiatry 10:1016. doi: 10.3389/fpsyt.2019.01016

- Balasco Luigi, Pagani Marco, Pangrazzi Luca, Chelini Gabriele, Ciancone Chama Alessandra Georgette, Shlosman Evgenia, Mattioni Lorenzo, Galbusera Alberto, Iurilli Giuliano, Provenzano Giovanni, Gozzi Alessandro, Bozzi Yuri (2022) Abnormal whisker-dependent behaviors and altered cortico-hippocampal connectivity in Shank3b$^{-/-}$ mice, Cerebral Cortex, https://doi.org/10.1093/cercor/bhab399

- Balasco Luigi, Pagani Marco, Pangrazzi Luca, Chelini Gabriele, Viscido Francesca, Ciancone Chama Alessandra Georgette, Galbusera Alberto, Provenzano Giovanni, Gozzi Alessandro, Bozzi Yuri (2022) Somatosensory cortex hyperconnectivity and impaired whisker-dependent responses in Cntnap2$^{-/-}$ mice, Neurobiology of Disease, https://doi.org/10.1016/j.nbd.2022.105742.

- Ciancone Chama Alessandra Georgette, Bozzi Yuri, Balasco Luigi (2022) Gene expression profiling in trigeminal ganglia from Cntnap2$^{-/-}$ and Shank3b$^{-/-}$ mouse models of autism spectrum disorder, bioRxiv 2022.10.23.513403; doi: https://doi.org/10.1101/2022.10.23.513403

These manuscripts here reported are a result of a collaborative effort. Specifically, the resting state functional magnetic resonance imaging (rs-fMRI) results presented here have been performed by Dr. Marco Pagani[12] and Dr. Alessandro Gozzi[1] to whom goes my acknowledgments and gratitude. Moreover, the automated whisker stimulation apparatus used with Shank3b head fixed mice was developed by Dr. Giuliano Iurilli[3], who also has my deepest appreciation. We refer to the Author Contribution Section of the papers for full details. For completeness and cohesion in reading, the results are included in this thesis.

[1]Functional Neuroimaging Laboratory, Center for Neuroscience and Cognitive Systems, Istituto Italiano di Tecnologia, 38068 Rovereto, TN, Italy

[2] Autism Center, Child Mind Institute, New York, NY, USA

[3]Systems Neurobiology Laboratory, Center for Neuroscience and Cognitive Systems, Istituto Italiano di Tecnologia, 38068 Rovereto, TN, Italy

Abstract

Autism spectrum disorders (ASDs) represent a heterogeneous group of neurodevelopmental disorders characterised by deficits in social interaction and communication, and by restricted and stereotyped behaviour. The diagnosis of autism is based on behavioural observation of the subject as research has not yet identified specific markers. Today, several studies show that disturbances in sensory processing are a crucial feature of autism. Indeed, around 90% of individuals diagnosed with autism show atypical responses to various sensory stimuli. These sensory abnormalities (described as hyper- or hypo-reactivity to sensory stimulation) are currently recognised as diagnostic criteria for autism. Among the sensory defects, tactile abnormalities represent a very common finding impacting the life of autistic individuals. It has been shown how abnormal responses to tactile stimuli not only correlate with the diagnosis of autism but also predict its severity. Indeed hypo-responsiveness to tactile stimuli is associated with greater severity of the main symptoms of autism. To date, the neural substrates of these behaviours are still poorly understood.

Over the years, the use of genetically modified animal models has enabled a major step forward in the study of the aetiology of autism spectrum disorders. Interestingly, several animal models that carry autism-related mutations also show deficits of a sensory nature. This is the case with the Shank3b$^{-/-}$ and Cntnap2$^{-/-}$ mouse models, strains in which the expression of the gene in question is suppressed. The SHANK3 gene encodes for a crucial protein in the structure of the postsynaptic density of glutamatergic synapses. In humans, haploinsufficiency of SHANK3 causes the Phelan-McDermid syndrome, a neurodevelopmental disorder characterised by ASD-like behaviour, developmental delay, intellectual disability and absent or severely delayed speech. Individuals with Phelan-McDermid syndrome often

show dysfunctions in somatosensory processing, including disturbances in tactile sensitivity. CNTNAP2 codes for CASPR2, a transmembrane protein of the neurexin superfamily involved in neuron-glia interactions and clustering of potassium channels in myelinated axons. Missense mutation in CNTNAP2 is causative of cortical dysplasia-focal epilepsy syndrome (CDFE), a rare disorder characterized by epileptic seizures, language regression, intellectual disability, and autism. Following these findings, mice lacking the Shank3b isoform (Shank3b$^{-/-}$) and Cntnap2 gene (Cntnap2$^{-/-}$) show autistic-like behaviours.

In this study, we used an interdisciplinary approach (behavioural, molecular, and imaging techniques) to study the neuronal substrates of whisker-mediated behaviours in genetic mouse models of ASD. We performed two behavioural tests, namely the textured novel object recognition test (tNORT) and the whisker nuisance test (WN) to have in-depth insight in whisker dependent behaviours. Following behavioural assessment, through a molecular approach, we investigated the neural underpinnings of this aberrant behaviour. We evaluated neuronal activation in key brain areas involved in the processing of sensory stimuli via c-*fos* mRNA in situ hybridization. Finally, using a seed-based approach in resting-state functional magnetic resonance imaging (rsfMRI) we probed the functional connectivity phenotype of these mutant mice. The contribution of the peripheral nervous system to sensory processing was also assessed via RT-qPCR at the level of the trigeminal ganglion.

Sensory abnormalities that characterize ASDs represent a symptom of primary relevance in the life of autistic individuals. Scientific research has only recently addressed this important aspect and animal models represent a useful preclinical tool to investigate the causal role of genetic mutations in the aetiology of ASDs. In such context, the complementary

approach used in this work represents a crucial step to the understanding of sensory-related deficits which characterize ASD.

Table of contents

Introduction

Autism Spectrum Disorders (ASDs) in the scope of sensory abnormalities.

Autism spectrum disorders (ASDs) and autism are general terms for a heterogeneous group of neurodevelopmental conditions characterized by challenges in social skills such as interactions and communication deficits, accompanied by restricted and stereotyped behaviours (DSM-V: American Psychiatric Association 2013). Being autism a spectrum of conditions, both strengths and unique abilities are associated with the disorder as well as severe challenges. For this reason, autism is defined in terms of deficits and symptoms following the definition of the American Psychiatric Association's Diagnostic and Statistical Manual of Mental Disorders (DSM). Several studies also indicate that abnormal sensory processing represents a crucial feature of ASD. About 90% of autistic individuals show atypical responses to different types of sensory stimuli (Robertson and Baron-Cohen 2017), and sensory abnormalities (described as both hyper- and hypo-reactivity to sensory input) are currently recognized as diagnostic criteria of ASD (DSM-V: American Psychiatric Association 2013) demonstrating its primary importance in the description of autism. Abnormal sensory reactivity represents a crucial issue in autism research since it likely contributes to other ASD symptoms such as anxiety, stereotyped behaviours, as well as cognitive and social dysfunctions (Ben-Sasson et al., 2007; Sinclair et al., 2017).

The correlation among autism and sensory deficits is not a novelty. Formerly, Dr. Kanner one of the first to describe autism, included different atypical sensory behaviours in his analysis (including heightened sensitivity to noise and touch, attraction to visual patterns and spinning objects, finger-stimming in front of the eyes) although considering them as secondary phenomenon (Kanner 1943). The

researchers Bergman and Escalona were the first instead to describe a group of children who were particularly reactive to "unusual sensitivities" in several sensory modalities (Bergman and Escalona 1947) hypothesizing that an early developmental onset of sensitivity to sensory stimuli would cause social withdrawal in childhood. Dr. Eveloff later described different behavioural difficulties faced by autistic children (Eveloff 1960). He proposed that altered sensory processing in autism might represent the effect of the lack of early experiences of environmental stimuli, therefore, interfering with the development of self-representations. Dr. Wing noted the "detail-oriented" behaviour of autistic children, showing that they have significantly more sensory processing abnormalities than typically developing (TD) children (Wing 1969). She was the first to suggest including abnormal sensory perceptual features as a proper diagnostic tool into 'basic impairments in autism'. However, this was not included in the first diagnostic criteria for autism by DSM in 1980 (DSM-3: American Psychiatric Association 1980). Another line of research came in parallel in the same years from the field of occupational therapy (OT). Drs. Ayres and Robbins formulated the theory of sensory integration (SI) dysfunction to describe several neurological disorders including autism (Ayres and Robbins 1979). This theory tried to relate sensory processing deficits with behavioural abnormalities and had the merit to define SI in terms of behavioural responses identifying for example tactile defensiveness and fight-or-flight reactions. However, sensory processing disorder was not still considered a disorder per se. With Dr. Rutter, the theory of "social-perception" took hold in 1983 (Rutter 1983). He concluded the sensory symptoms found in the autistic population were the result of deficits in social cognition. It is not the processing of a sensory stimulus per se that creates difficulties in the autistic subject, but rather the processing of stimuli of emotional nature (i.e., those that possess a social content). Finally, only in 2013 sensory processing deficits were included for the

first time among the international diagnostic criteria of autism in the revision of the Diagnostic and Statistical Manual of Mental Disorders (DSM-V).

From a clinical point of view, sensory deficits are documented already in the 6th month of life of infants later diagnosed with autism (Baranek et al., 2013; Esters et al., 2015). This gives us dual information, firstly that sensory symptoms anticipate social and communication deficits (Estes et al., 2015), and secondly that abnormal sensory traits could be predictive of the autistic condition (Turner-Brown et al., 2013). This appears strikingly evident when considering that not only the vast majority of individuals diagnosed with autism experience atypical reactivity to sensory stimuli (Marco et al., 2011; Robertson and Baron-Choen 2017), but also that this affects every sensory modality: smell (Galle et al., 2013; Rozenkrantz et al., 2015), taste (Tavassoli et al., 2012), audition (Bonnel et al., 2003), vision (Simmons et al., 2009), and touch (Marco et al., 2012; Puts et al., 2014). It seems clear that understanding the neurobiological bases underlying these sensory processing deficits represents a new challenge for ASD research, specifically aiming to identify early biomarkers and novel possible therapeutic strategies for these disorders.

Tactile Sensitivity in ASD.

The typical description of sensory processing abnormalities in autistic individuals falls in the terminology of "over-responsiveness", "under-responsiveness", and "failure to habituate". Over-responsiveness, also called hyper-sensitivity, refers to children being more "reactive" to sensory stimulation compared to controls (Grandin 1992, Baranek et al., 1994), often associated with negative emotion or active avoidance of stimulation. However, the terminology used in clinical reports and questionnaires often fails in separating "over-responsiveness" from "impaired habituation". Moreover, it is unclear whether this refers to

the hyper-excitability of the sensory cortex or the expression of negative emotions to tactile stimulation. Conversely, under-responsiveness, also described as hypo-sensitivity, is characterized by reduced reactivity to sensory stimulation and sensory seeking (Baranek et al., 1997). Both over- and under-responsiveness then fall under the general term of tactile defensiveness (Baranek et al., 1994), which describes both abnormal emotional responses to tactile stimulation as well as withdrawal/avoidance of a stimulation.

The majority of studies investigating tactile dysfunction in ASD have traditionally focused on parent and teacher reports and questionnaires. Several studies described tactile abnormalities using sensory profiles (SP; Mikkelsen et al., 2018; Rogers et al., 2003b; Ben-Sasson et al., 2007; Foss-Feig et al., 2012; Cascio et al., 2016). Other tests including the Infant/Toddler Sensory Profile (ITSP), Infant-Toddler Social and Emotional Assessment (ITSEA), Autism Diagnostic Interview-Revised (ADI-R), and Autism Diagnostic Observation Schedule-Generic (ADOS-G), revealed that toddlers with ASD show higher under responsiveness and stimulus avoidance as well as low frequency of seeking behaviours compared to TD controls (Ben-Sasson et al., 2007). Foss-Feig and colleagues investigated both under- and over-responsiveness to tactile stimuli in children with ASD through three measures of sensory processing: Tactile Defensiveness and Discrimination Test-Revised (TDDT-R), the Sensory Experiences Questionnaire (SEQ), and the Sensory Profile (SP). They reported that heightened levels of tactile seeking behaviour were associated with more severe levels of social and repetitive behaviours. Additionally, heightened levels of hypo-responsiveness to tactile stimuli were associated with more severe levels of social and non-verbal communication impairments as well as increased repetitive behaviours. Conversely, over-responsiveness was not correlated with any of the core symptoms of ASD (Foss-Feig et al.,

2012). Most studies on tactile processing so far have focused on children, however, there are also studies (Crane et al., 2009; Tavassoli et al., 2014) showing that abnormal sensory processing is also present in adults.

These studies, although informative indicators of tactile abnormalities in ASD, they lack objectivity in the strict sense since they are based on subjective assessments of both behavioural and emotional responses to touch (Mikkelsen et al., 2018). Moreover, they appear to be inconsistent concerning the pattern of response, correlation among measures, and diagnostic terms. In addition, different types of reports were used in different studies. All such aspects render these studies difficult to be compared; moreover, they do not always correlate to clinical observation, nor do they provide indicators of possible neuronal dysfunctions.

More recently, researchers have preferred a psychophysics approach to study tactile functionality in ASD in a more objective modality. Some of these studies have shown how the detection of tactile stimuli is impaired in both adults and children with ASD (Blakemore et al., 2006), despite conflicting evidence (O'Riordan et al., 2006; Guclu et al., 2007, Cascio et al., 2008). It is possible to speculate that these differences result from the different types of stimulation used (i.e., flutter, vibration, sinusoidal, or constant) as well as its location. Although these works have the merit of bringing greater objectivity to the study of tactile abnormalities in ASD, it remains unclear whether underlying sensory mechanisms are altered, or it is the emotional response to sensory input that leads to issues in the filtering of the signal resulting in hyper/hypo-responsiveness.

Imaging studies have also tried to investigate the underlying neural mechanism of abnormal tactile sensitivity in ASD. Since tactile stimuli are part of the somatosensory world and as such rely on subcortical and cortical brain regions, researchers focused on possible differences in

these brain areas between ASD and TD control subjects. Neuroimaging research provides evidence that the neural underpinnings of the behavioural signs of ASD involve both dysfunctional integration of information across brain networks and basic dysfunction in primary cortices (Lainhart 2015). Children with ASD who show negative responses to sensory stimuli also display increased functional activation in sensory processing areas (such as sensory cortices) and brain areas involved in emotional processing (including the amygdala and the prefrontal cortex) (Green et al., 2013). Although these studies provide us with useful indications of cortical function in autism, discrepancies exist across studies. Moreover, the variability in neural responses appears to be higher in ASD (Dinstein et al., 2012; Haigh et al., 2016). A possible explanation could be sought in the type of stimulation involved (i.e., passive vs. active) as well as in the high heterogeneity of ASD (Marco et al., 2011). In addition, a limit of these studies lies in the complexity to compare findings in children with those obtained in adolescents and adults.

Several studies suggest that ASD pathogenesis might involve an imbalance between excitation and inhibition (E/I imbalance). This hypothesis is supported by several lines of evidence showing that the γ-aminobutyric acid (GABA) system is altered in ASD, and that may relate to alterations in sensation and symptoms in both animal models and humans. A pivotal role of GABAergic dysfunction in ASD was first hypothesized in the early 2000s by Hussman (Hussman 2001) and Rubenstein and Merzenich (Rubenstein and Merzenich 2003), even if the key role of GABA in shaping the neural response to tactile stimulation (Dykes et al., 1984; Juliano et al., 1989), as well as in brain development and cortical plasticity (Mccormick 1989; Markram et al., 2001), was known from many years. Several genetic, neuropathological, and neuroimaging studies showed that GABAergic dysfunctions occur in ASD

(Bozzi et al., 2018), and defective GABAergic neurotransmission has been suggested as a potential candidate in sensory deficits in ASD (Leblanc and Fagiolini 2011). In the tactile domain, a study investigating tactile detection thresholds in TD children was the first to report that tactile sensitivity was associated with GABRB3 genetic variation in typically developing children (Tavassoli et al., 2012), confirming findings from animal model studies. The GABRB3 gene, coding for the β3 subunit of the GABA receptor channel, is one of the many candidate genes to be associated with autism (Delorey 2005; Abrahams and Geschwind 2008). Moreover, GABA levels were shown to be reduced in the sensorimotor cortex and positively correlated with worsened detection thresholds in children with ASD; in addition, GABA levels were not correlated with adaptation or frequency discrimination as for TD children (Puts et al., 2017). Taken together, these results suggest that altered inhibition could explain some of the behavioural features of tactile abnormalities in ASD.

Somatosensory functioning and social behaviour.

It is clear from these studies that altered sensory processing has revealed to be an important feature in the clinical description of ASD. It has been proposed that sensory stimuli and social behaviours may have a reciprocal influence on each other throughout development (Gliga et al., 2014). This idea is reinforced form findings of early abnormal sensory sensitivity to stimuli predicting later joint attention and language development (Baranek et al., 2013) and higher levels of social impairment in adults with ASD (Hilton et al., 2010). Touch is considered one of the most basic ways to sense the external world (Barnett 1972) and has been reported to have a significant role in role in several social aspects such as communication (Hertenstein et al., 2006b), developing social bonds (Dunbar 2010), and overall physical development and connectivity of brain areas (Bjornsdotter et al., 2014; Brauer et al., 2016). For this reason, the skin has been proposed by some authors as a "social

organ" (Morrison et al., 2007). It has been suggested that irregularities in touch and tactile perception may be associated with broad levels of social dysfunction in ASD. Furthermore, a lack of social touch can lead to higher levels of anxiety, stress, and depression (Hertenstein 2002), aspects which are commonly seen in the ASD population (Ghaziuddin et al., 2002; Kerns et al., 2012).

When discussing dysfunctions of the somatosensory system, it is important to consider the sensory processing cascade in its entirety. Starting from the periphery (i.e., the skin, where the mechanical stimuli are transduced in electrical signals), moving to the intermediate stations (i.e., spinal cord and/or brainstem, where the electrical signals are delivered through neuronal ascending pathways), reaching subcortical and cortical brain areas (i.e., primary somatosensory cortex and other higher function somatosensory processing areas, where integration/codification of the information occurs), sensory information can undergo more or less severe modifications. Indeed, abnormal development or interaction in any of these steps could ideally lead to abnormal sensory processing. Moreover, since proper tactile perception is of importance in early development as well as in forming social and physical relationships (Hertenstein et al., 2006a), a possible relation between tactile abnormalities and social behaviours could be a matter of fact. For this reason, when assessing the behavioural outcomes of relevant social/sensory tasks performed by mouse models of ASD, it is at least necessary, when possible, to correlate the behavioural response to a potential neurobiological defect. Indeed, even though humans and animals have evolved under different evolutionary pressures making social behaviours much harder to compare, molecular and cellular functions are strongly conserved and so appear to be mostly comparable. However, what must be kept in mind is that social behaviours are not unitary behaviour with a unique neurobiological basis, but rather

different aspects of social behaviour show different neural substrates. Moreover, the modulation of environmental cues, the type of sensory stimulation, and the role of conspecific actions in shaping the social response adds complexity to our understanding of social behaviour in animals (including humans) (Chen et al., 2018).

Studying autism spectrum disorders in mice.

It has long been known that ASD has a high degree of heritability: studies on monozygotic twins revealed a peak of concordance of 90% compared to 10% of dizygotic twins and siblings (Bailey et al., 1995; Le Couteur et al., 1996). However, only recent efforts and technological advancements in genetics made it possible to identify a plethora of gene variants associated with ASD. These variants have been found in several hundreds of different genes and cover the entire spectrum of mutations, from single-nucleotide variants (SNVs) to copy number variants (CNVs), including inherited as well as de novo mutations (Huguet et al., 2013; De La Torre-Ubieta get al., 2016). Several genetic mutations in ASD have been associated with genes coding for proteins involved in synaptic functions, such as SHANK (Durand et al., 2007), CNTNAP (Alarcon et al., 2008, Arking et al., 2008), NLGN (Jamain et al., 2003; Lawson-Yuen et al., 2008), and NRXN (Kim et al., 2008). Some examples of CNVs associated with ASD include chromosomal loci 15q11-q13 (Christian et al., 2008), 16p11.2 (Fernandez et al., 2010), and the UBE3A (Glessner et al., 2009), NRXN1 (Kim et al., 2008), and CNTN4 (Fernandez et al., 2004) genes. In adding complexity to the understanding of ASD pathophysiology, a subset of single gene mutations associated with ASD is also responsible for other neurodevelopmental disorders, including FMR1 in fragile X syndrome, TSC1 in tuberous sclerosis, and MECP2 in Rett syndrome. The tremendous progress made in identifying all these genes associated with ASD has subsequently resulted in the generation of several ASD mouse models, through which it is possible to infer the

effect of single mutations, thus advancing our understanding of the biological bases underpinning this complex syndrome. A multitude of mouse models has been generated by knock-out and knock-in mutations in ASD candidate genes. In developing new mouse models, it is important to consider different aspects such as face validity (i.e., resemblance to human symptoms), construct validity (i.e., similarity to the causes of the disease), and predictive validity (i.e., expected responses to treatments that are effective in the human disease), with the best animal model keeping together the three validity criteria (Crawley 2004). This is a fundamental aspect of autism, especially if we consider that autism is a typical human condition. Given the complex phenotypic and genetic heterogeneity of ASD, developing a mouse model keeping together all these aspects represents a challenge for every researcher. Since the diagnosis of ASD is mainly given by the analysis of behavioural aspects rather than physiological criteria, and being mice, like humans, a social species displaying an extensive variety of social behaviours, neuroscientists tried to develop and refine behavioural paradigms that could be relevant to the human condition. The symptoms however may be uniquely human and are often highly variable among individuals, so it appears clear that designing mouse behavioural assays relevant to autistic symptoms represents a unique challenge. However, different behavioural paradigms have been developed considering the two core symptoms of the human disorder (social/communication defects and repetitive behaviours) and revealed to be qualitatively efficient and reproducible (Silverman et al., 2010).

Shank3b and Cntnap2 mouse models of ASD.

In this work, we used Shank3b and Cntnap2 mutant mice as models for the Phelan McDermid (PMS) and cortical dysplasia-focal epilepsy (CDFE) respectively, two syndromic forms of autism. PMS is caused by mutations in the SHANK3 gene which codes for the SH3 and multiple

ankyrin repeat domain protein 3 (Monteiro & Feng, 2017). This protein belongs to the family of Shank proteins and therefore acts as a major scaffolding protein within the postsynaptic density of excitatory neurons (Jiang & Ehlers, 2013). As a syndrome, PMS is described by intellectual disability, speech and developmental delay, and importantly ASD-related behaviours such as problems in communication and social interaction (Phelan & McDermid, 2010), as well as sensory hypo reactivity to tactile stimulation (Tavassoli et al., 2021).

CDFE is caused by a recessive nonsense mutation in the CNTNAP2 gene which codes for CASPR2. CASPR2 (Cntnap2) is part of the neurexin family of transmembrane proteins and is involved in neuron-glia interactions, potassium channel clustering on myelinated axons, dendritic arborization, and spine development (Poliak et al., 1999; Poliak et al., 2003; Anderson et al., 2012). CDFE syndrome is a rare disorder characterized by intellectual disability, ASD-like behaviours, language regression, and focal epileptic seizures from childhood.

Mice lacking Shank3 and Cntnap2 genes display autistic-like characteristics such as repetitive grooming and impaired social interaction among others thus widely considered reliable models to study ASD-like symptoms relevant to these syndromes (Peça et al., 2011; Peñagarikano et al., 2011; Vogt et al., 2018). Interestingly, Shank3b-/- mutant mice display aberrant whisker-independent texture discrimination and over-reactivity to tactile stimuli applied to hairy skin (Orefice et al. 2016). More recent findings showed that developmental loss of Shank3 in peripheral somatosensory neurons (that causes over-reactivity to tactile stimuli) also results in ASD-like behaviours in adulthood (Orefice et al. 2019). Instead, Cntnap2 is expressed in primary sensory organs and in brain regions involved in sensory processing (Gordon et al., 2016), suggesting a role for the Cntnap2 gene in sensory neurotransmission. In keeping with the Cntnap2 expression pattern,

studies indicate that a lack of Cntnap2 results in sensory dysfunction. Cntnap2-/- mice display enhanced hypersensitivity to noxious and thermal stimuli applied to hindpaws, which has been related to enhanced excitability of dorsal root ganglion neurons (Dawes et al., 2018). Moreover, despite reports of intact firing rate and amplitude in cortical neurons of Cntnap2-/- mice (Peñagarikano et al., 2011), lack of Cntnap2 has been shown to impair synaptic transmission in cortical neurons in vitro (Anderson et al., 2012) and layer 2/3 pyramidal neurons of the somatosensory cortex following whisker stimulation (Antoine et al., 2019). Circuit connectivity is also impaired in sensory cortical areas of Cntnap2 mutant mice (Choe et al., 2021), suggesting a broad neuronal network remodelling in these mutants.

While core deficits of ASD have been extensively covered, the neural substrates of whisker-dependent behaviours have been poorly investigated in these models.

Somatosensory system organisation in mice and humans.

The somatosensory system in mammals conveys sensory information from receptors located in the skin, muscles, and joints to the brain. In mice, the somatosensory system is dominated by the input coming from the facial vibrissae: the neuronal representation of whiskers in the primary somatosensory cortex (the barrel field) occupies more than two-thirds of its total area (Paxinos 2013). The anatomical and functional organization of the somatosensory system is highly conserved and is based on two major ascending components: the dorsal column system and the trigeminal system. The first-order sensory neurons are the dorsal root ganglion cells and the trigeminal ganglion cells that collect information from the receptors located in the body and the face, respectively. While the dorsal root ganglion (DRG) neurons send their central processes to make a synapse in the spinal cord, the trigeminal ganglion cells make a synapse in the hindbrain. The main

hindbrain nucleus receiving afferents from the whisker system is the spinal trigeminal nucleus (Sp). The whisker macro representation starts to be appreciable at the level of the hindbrain in concrete structures called "barrelettes" (Ma 1991). The spinal cord and hindbrain nuclei in turn project to specialized somatosensory nuclei of the thalamus: the ventral posterior group (VP). The initial anatomical separation of the two systems is interrupted at the level of the thalamus, which represents a relay station for all sensory stimuli. The VP region of the thalamus is subdivided into a large medial portion (VPM), which receives afferents from the trigeminal system, and a smaller lateral portion (VPL) which instead receives afferents from the limbs and the trunk. The size of each subdivision of VP is proportional to the number of afferents, so the VPM appears to be larger than the VPL. Moreover, even from the VPM it is possible to appreciate a representation of individual facial whiskers, the so-called "barreloids" (Van Der Loos 1976). Somatosensory processes also terminate in clusters of heterogeneous thalamic nuclei (the posterior group, Po) lying medial, dorsal, and caudal to VPM. The largest component of the Po forms the medial subdivision (PoM), which also receives inputs from the whisker pad providing a parallel source of information to the primary somatosensory (S1) cortex (Diamond et al., 1992). In rodents, two further clusters of nuclei have been identified in this region of the thalamus: the reticular nucleus of the thalamus (Rt) and the zona incerta (ZI). These two clusters do not receive somatosensory input from the brainstem or spinal cord but being packed with GABAergic neurons and strongly projecting to the VP, they are thought to play an important role in modulating the output of VP (Lavallee and Deschenes 2004). All somatosensory stimuli converge onto the primary (S1) and secondary (S2) somatosensory cortices. S1 is dorsolateral in the rostral part of the neocortex, whereas S2 is located laterally to S1. The primary somatosensory cortex in mice is dominated by the barrel field (S1BF), containing the representation of single facial

whiskers. In 1970, Woolsey and Van Der Loos were the first to report these distinct anatomical structures named “barrels” (Woolsey and Van Der Loos 1970). Further divisions of the S1 are the forelimb area (S1FL), the trunk area (S1Tr), and the hindlimb area (S1HL), with each of these areas characterized by a thick condensed layer IV. Figure 1 schematically reports the organization of the somatosensory pathways in mice.

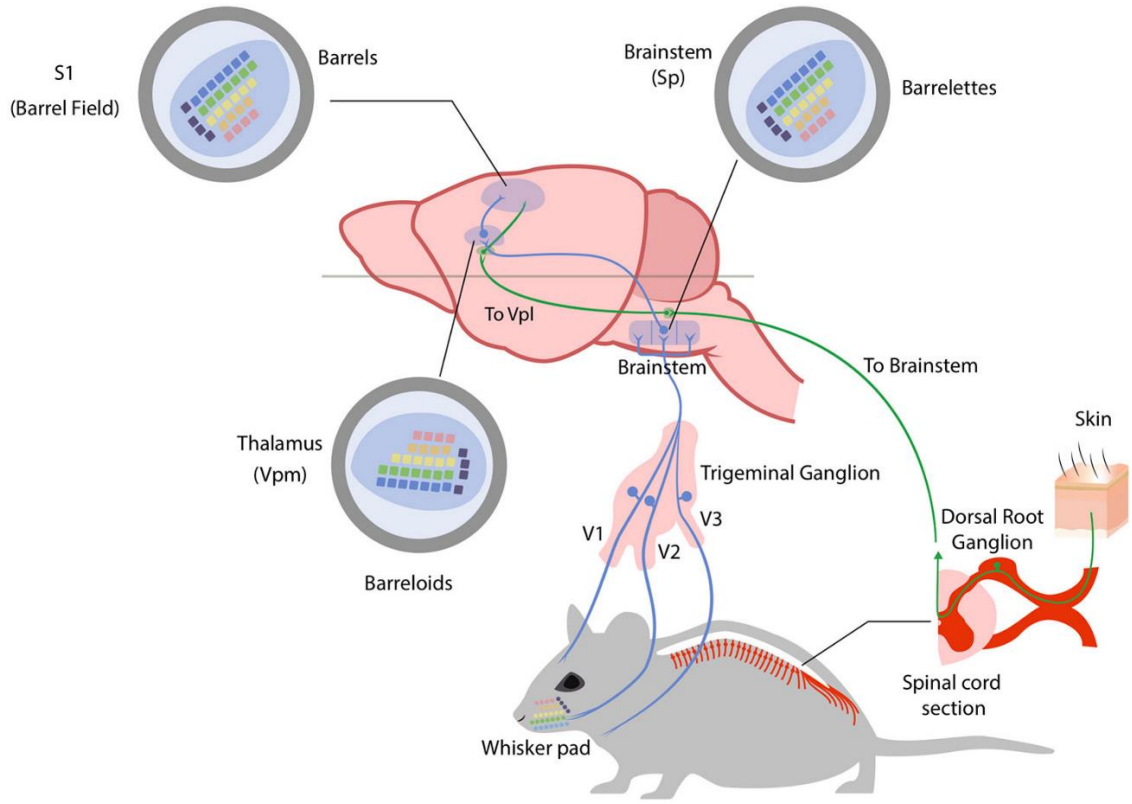

Fig. 1. The mouse somatosensory system. Somatosensory stimuli coming from the head region of the mouse are conveyed to the brain through trigeminal ganglion neurons. Neuronal fibers are depicted in blue (for the trigeminal ganglion pathway) and green (for anterior and lateral spinothalamic pathways). The ophthalmic (V1), maxillary (V2) and mandibular (V3) branches of trigeminal ganglion process region-specialized somatosensory information with the maxillary branch (V2) innervating the whiskers. Here whiskers are indicated and colour-coded to best follow their brain representations (whisker pad). Trigeminal ganglion neurons project to brainstem nuclei (spinal trigeminal nuclei – Sp) where they form an inverted neuronal representation of single whiskers (barrelettes). Trigeminothalamic fibers in turn project to the ventral posteromedial nucleus in the thalamus (Vpm) where again single whiskers are represented and shifted in orientation (barreloids). Finally, thalamocortical axons from the Vpm reach the primary somatosensory cortex (S1) in the barrel field, forming the final neuronal representation of single whiskers (barrels). Somatosensory stimuli coming from the body of the mouse are instead conveyed to the brainstem through dorsal root ganglia (DRG) neurons. The main difference in this system is the fact that somatosensory stimuli are conveyed to the ventral posterolateral nucleus of the thalamus (Vpl) before reaching the sensory cortex. See text for references.

As compared to the mouse, the human somatosensory system presents important similarities and differences. Somatosensory receptors located in the skin are essentially the same, and the anatomy of the ascending pathway organization is maintained in both species. The organization of the somatosensory cortex found in mice is comparable to that found in mammals with relatively little expansion of the neocortex (Hill and Walsh 2005). Much of the somatosensory cortex in these mammals is represented by two distinct systematic representations of the contralateral body surface, named the first (primary) representation, or S-I, and the second representation, or S-II. The larger S-I represents the body from tail to mouth in a mediolateral cortical sequence, while the smaller S-II has a head-to-tail mediolateral (or dorsoventral) cortical sequence (Kaas 2004). Instead, the somatosensory cortex in higher primates (including humans) contains more subdivisions than the somatosensory cortex in non-primates. Experiments on the organization of the anterior parietal cortex in macaque monkeys defined S-I as a broad region including cytoarchitectonic areas 3 (3a and 3b), 1, and 2 of Brodmann, though Kaas argues that only area 3b should be considered primary somatosensory cortex (Kaas 2004; Nelson et al., 1980). Area 3b, indeed, forms a complete representation of the body surface. In mice, two whiskers that are adjacent to each other on the animal's face are represented in adjacent cortical barrels, and the barrel field constitutes a topographic map. Similarly, a topographical organization of the somatosensory cortex (the so-called homunculus) is present in humans (Penfield and Boldrey 1937). As for the cortical representation of the whiskers in mice and rats, the homunculus is a topographic map because neighbouring sites on the skin are represented at neighbouring sites in the cortex. The whiskers are the critical touch organ in rats and mice, whereas in humans and other primates, the fingertips are their equivalent. Each fingertip is innervated by axons

from 250–300 sensory neurons (a comparable number as the whisker) and because individual axons terminate in multiple receptor structures, the density of mechanoreceptors is remarkably high (over 1,000 per cm2). One important way in which fingerprint touch differs from whisker touch is that primates manipulate objects with their hands whereas rodents do not manipulate objects with their whiskers. This difference is evident when comparing the mechanism for sensing texture. For mice and rodents in general, the firing rate of neurons in the barrel cortex differs from rough to smooth surface (Lottem and Azouz 2009). In primates, the perception of coarse textures is based on the difference in firing rate between adjacent slowly adapting neurons (Connor and Johnson 1992); the perception of fine surfaces is based on vibrations in the skin, transduced by rapidly adapting Pacinian receptors (Hollins and Bensmaia 2007). Finally, important differences have been found in the structure of supragranular layers 2 and 3 of the mouse and human somatosensory cortex (Jabaudon 2017). Figure 2 schematically reports the somatotopic representation of the mouse and human primary somatosensory cortex.

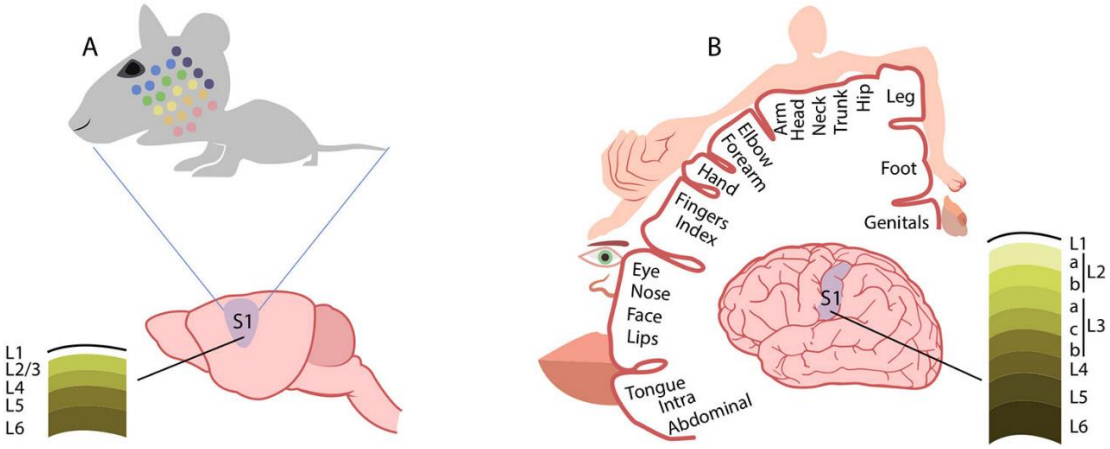

Fig. 2. Comparison of cortical somatosensory representation in mice and humans. Distorted representation of body areas in the mouse (A) and human (B) primary somatosensory cortex (S1). In both species, S1 somatosensory maps reflect the extent of cortical areas devoted to the processing of sensory information from different parts of the body. In mice, the altered proportions of the head and whisker pad with respect to other body regions mirror the extent of innervation from these areas. Similarly, in humans, the cortical somatosensory representation is enlarged for those regions, such as the hands and the lips, that are densely innervated by sensory fibers. Conversely, the structure of supragranular layers 2 and 3 markedly differ between the mouse (A) and human (B) somatosensory cortex.

Thus, in this work, we used the primary somatosensory cortex of the mouse as a proxy to investigate sensory processing in human ASD.

Material and Methods

Animals.

All experimental procedures were performed following Italian and European directives (DL 26/2014, EU 63/2010) and were reviewed and approved by the University of Trento animal care committee and the Italian Ministry of Health. Animals were housed in a 12 h light/dark cycle with food and water available ad libitum. Surgical procedures when needed were performed under anaesthesia and all efforts were made to minimize suffering. The mating strategy included heterozygous mice (Shank3b$^{+/-}$ x Shank3b$^{+/-}$ and Cntnap2$^{+/-}$ x Cntnap2$^{+/-}$) to generate the wild-type (WT) and knockout (KO) homozygous littermates used in this study. Genotyping was performed by standard PCR according to the protocol available on The Jackson Laboratory website (https://www.jax.org/strain/017688 for Shank3b and https://www.jax.org/strain/017482 for Cntnap2). For Shank3b: twenty-one mice (11 Shank3b$^{+/+}$ and 10 Shank3b$^{-/-}$) were used for fMRI experiments and sixty-seven mice (36 Shank3b$^{+/+}$ and 31 Shank3b$^{-/-}$) were used for behavioural testing. A subset of sixteen animals subjected to the WN test (9 Shank3b$^{+/+}$ and 7 Shank3b$^{-/-}$) was used for c-*fos* mRNA in situ hybridization. An additional group of eleven mice (6 Shank3b$^{+/+}$ and 5 Shank3b$^{-/-}$) received only sham stimulation and were used as controls for in situ hybridization experiments (no difference in WN scores was detected between genotypes in this additional group of animals). Seven mice (three stimulated and four controls) per genotype were used for the c-*fos* mRNA study following whisker stimulation under anaesthesia. Finally, twenty adult (6 months old - 10 Shank3b$^{+/+}$ and 10 Shank3b$^{-/-}$) and six juvenile (P30 - 3 Shank3b$^{+/+}$ and 3 Shank3b$^{-/-}$) sex-matched mice were used for RT-qPCR in the trigeminal ganglia. For Cntnap2: Twenty-six mice (13 Cntnap2$^{+/+}$ and 13 Cntnap2$^{-/-}$) were used for fMRI experiments. Fifty-three mice (26 Cntnap2$^{+/+}$ and 27 Cntnap2$^{-/-}$

) were used for the open field test. A subset of thirty animals (15 Cntnap2$^{+/+}$ and 15 Cntnap2$^{-/-}$) also performed the textured novel object recognition test (tNORT). Twelve mice were used for c-*fos* mRNA in situ hybridization (6 Cntnap2$^{+/+}$ and 6 Cntnap2$^{-/-}$) following either anaesthesia or whisker stimulation. Ten adult animals (5 Cntnap2$^{+/+}$ and 5 Cntnap2$^{-/-}$) were used in the RT-qPCR study in the cerebral cortex. Finally, twenty adult (6 months old - 10 Cntnap2$^{+/+}$ and 10 Cntnap2$^{-/-}$) and ten juvenile (P30 - 5 Cntnap2$^{+/+}$ and 5 Cntnap2$^{-/-}$) sex-matched mice were used for RT-qPCR in the trigeminal ganglia. The stage of the oestrous cycle was not monitored for female animals used in this study. Previous studies showed that similar group sizes are sufficient to obtain statistically significant results in fMRI (Pagani et al. 2019), behavioural, and in situ hybridization studies (Tripathi et al., 2009; Provenzano et al., 2014; Chelini et al., 2019) as well as RT-qPCR studies (Sgadò et al., 2013b). All experiments were performed blind to genotype. Animals were assigned a numerical code by an operator who did not take part in the experiments and codes were associated with genotypes only for data analysis.

Open field test (OF).

Mice were habituated to the testing arena before texture discrimination assessment, for two consecutive days (Fig. 3). During these two sessions, each animal was placed in an empty arena (40 cm × 40 cm × 40 cm) and allowed to freely explore. The walls of the arena were smooth and grey-coloured. Sessions were recorded and mice were automatically tracked using EthoVisionXT (Noldus) to evaluate their locomotor behaviour. Distance travelled and time spent in the centre/borders were analysed.

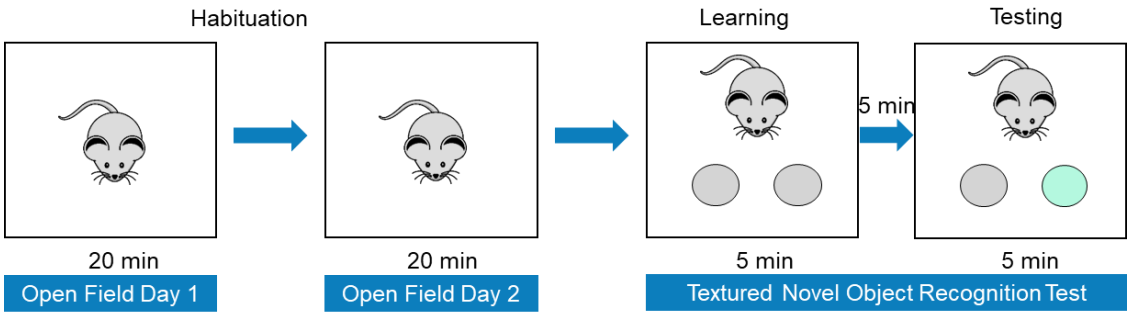

Fig. 3. Open field (OF) and textured novel object recognition test (tNORT) experimental design. Animals are habituated for two days in an open-field arena for 20 minutes before the tNORT. The tNORT consist of two phases: in the learning phase a mouse is presented with two identically textured objects (grey circles); in the testing phase the same mouse is presented with an already encountered textured object (grey circle) and a novel textured object (water green circle). For specifics about the objects see text. Both learning and testing phase as well as the retention phase last 5 minutes.

Textured novel object recognition test (tNORT).

Whisker-mediated texture discrimination was assessed as described in previously published protocols (Wu et al. 2013), with minor adjustments (Fig. 3). Textured novel object recognition (tNORT) was performed in the same arena used for open field testing. On the third day, mice were presented with custom-made cylinder objects (1.5 cm radius base × 12 cm height) covered in garnet sandpaper (Fig. 4). The grit (G) of the objects (i.e., the coarseness of the sandpaper) was chosen according to previously published protocols (Wu et al. 2013; Domínguez-Iturza et al. 2019), to favour whisker interaction. A 120 G sandpaper (very fine) was used as the familiar textured object, whereas a 40 G sandpaper (very coarse) was used for the novel textured object. Many identical objects were created for each grit of sandpaper used in this study to avoid repetitive use of the same object across the testing period. This reduced the likelihood that mice would identify a particular object based solely on odour cues. Additionally, the test was conducted in the penumbra (4 lux) to prevent any potential visual confounders caused by sandpaper grit. Adult mice lack the visual acuity necessary to distinguish between the grit of the two items at this level of light (Schmucker et al. 2005). During the first session of the test (learning phase), mice were placed in the arena with two identically textured objects (object A and object B; 120 G) and they were free to investigate the objects with their whiskers for 5 min. Mice were then removed and held in a separate transport cage for 5 min. This brief period was chosen to minimize hippocampal-mediated learning (Wu et al. 2013). In the second session of the test (testing phase), the two objects were replaced with a third, identically textured object (familiar, 120 G) and a new object with a different texture (novel, 40 G). Mice were then returned to the arena and allowed to explore with whiskers for 5 min. The short time of interaction (5 min) was selected to encourage the investigation through whiskers but not of paws/body. The

textured objects were placed in the centre of the arena, equidistant to each other and the walls and mice were placed in the arena facing away from the two objects. The position of the novel versus the familiar object was counterbalanced and pseudorandomized between subjects. Since mice have an innate preference for novel stimuli, an animal that can discriminate between the textures of the objects spends more time investigating the novel textured object, whereas an animal that cannot discriminate between the textures is expected to investigate the objects equally. The testing arena was cleaned with 70% ethanol between sessions and between animals to disguise olfactory cues. The amount of time mice spent actively investigating each of the objects was assessed during both the learning and testing phases. Investigation through whiskers was defined as directing the nose towards the object with less than 2 cm from the nose to the object or touching the nose to the object. Resting, grooming, and digging next to, or sitting on, the object was not considered an investigation. Mice that had a total investigation time of less than 2 s during either learning and testing phases were excluded from the analysis due to poor exploratory activity (Wu et al., 2013). The activity of the mice during the learning and testing phase was recorded with a video camera centred above the arena and automatically tracked using EthoVisionXT (Noldus). The performance of the mice in the tNORT was expressed by the preference index. The preference index is the ratio of the amount of time spent exploring any one of the two objects in the learning phase or the novel one in the testing phase over the total time spent exploring both objects, expressed as a percentage [i.e., A/(B + A) × 100 in the learning session and novel/(familiar + novel) × 100 in the testing session].

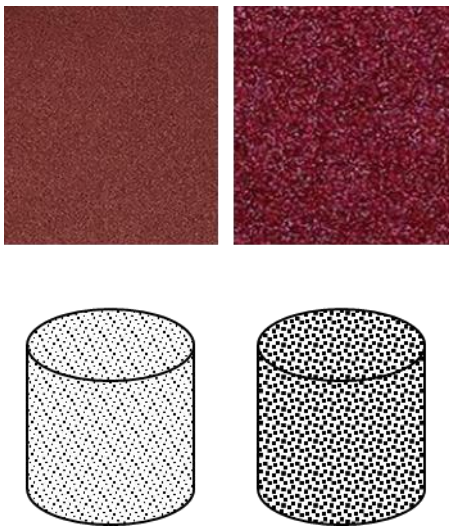

Fig. 4. Textured custom-made objects. The textured objects employed in the tNORT consisted of cylinders wrapped with sandpaper of different grit (G). The grit of the sandpaper used was 120G (very fine texture - top left) and 60G (very coarse texture - top right). The resulting objects presented many small intersperse particles (bottom left – for fine texture) or large intersperse particles (bottom right – for coarse texture). The difference in the appearance of the garnet sandpaper was minimized by the reduced light conditions in which the test was performed (4lux). In such conditions, the low visual acuity of the mouse prevents the discrimination of the objects based on visual experiences.

Whisker nuisance test (WN).

The whisker nuisance (WN) test was used to assess the behavioural reactions to direct whisker stimulation in freely moving mice (Fig. 5; Balasco et al., 2019, Chelini et al., 2019, Pizzo et al., 2020). For 2 days before the test, animals were allowed to habituate for 30 min to a novel empty cage (experimental cage). To facilitate the habituation to the novel environment, home-cage bedding was placed overnight in the experimental cage and removed right before the introduction of the mouse. On test day, mice were acclimated to the experimental environment for 30 min, before the beginning of the testing phase. The testing phase included four recorded sessions that lasted five minutes each. In the first (sham) session, a wooden stick was introduced in the experimental cage, avoiding direct contact with the animal. The behaviours assessed in this session served as a baseline for the subsequent part of the test. The following three sessions consisted of a bilateral whisker stimulation by continuously deflecting vibrissae using the wooden stick. To dissect the behavioural responses to mechanical whisker stimulation, multiple behavioural categories were defined and separately quantified while being blind to the genotype and experimental settings. The identified categories included freezing, guarded behaviour, evasion, and response to stick. Freezing was scored when the animal was immobile in a defensive posture (i.e., with curved back, protracted neck and stretched limbs, or fully hunched posture). Guarded behaviour corresponded to a defensive posture when the animal was not immobile. Evasion was defined as the active avoidance of the stick by either running in the opposite direction or walking backwards while keeping eye contact with the stick. Finally, the response to stick was split in two sub-categories: climbing and startle. Climbing was counted each time the animal attempted active exploration of the stick by rearing on the hindlimbs. Startle was evaluated as a sudden and

uncoordinated avoidance movement. While freezing, guarded behaviour, and evasion were quantified as the time spent in each behaviour, both climbing and startle were quantified as the number of events detected over the total time of observation.

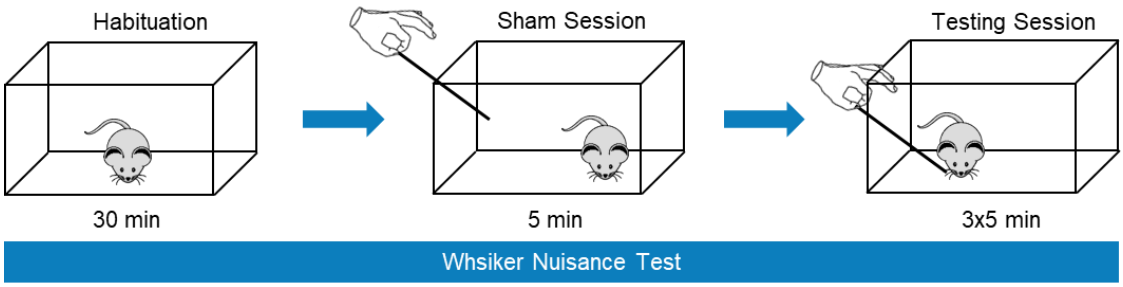

Fig. 5. Whisker nuisance (WN) test experimental design. Mice are habituated in an experimental cage for 30 minutes for 2 days before the start of the test. On testing day mice are placed in the very same experimental cage for 30 minutes. This is followed by the sham session, lasting 5 minutes, in which the animal is presented with a wooden stick without any physical contact with the whiskers. Following the sham session, the proper testing session start. The animal is then stimulated with a wooden stick on its whiskers in three trials of 5 minutes each with one minute of inter trial interval. Both sham and testing sessions are recorded for successive behavioural phenotyping.

Behavioural analysis.

Statistical analyses of behavioural data were performed with GraphPad Prism 8.0 software, with the level of significance set at $p < 0.05$. Statistical analysis was performed by Mann-Whitney test or two/three-way ANOVA followed by Tukey's or Bonferroni's post-hoc multiple comparisons, as appropriate.

Whisker stimulation in head-fixed awake mice.

All surgeries used standard aseptic procedures as previously described (Iurilli and Datta, 2017). Briefly, mice were deeply anaesthetized with 5% isoflurane (by volume in O2) and mounted in a stereotaxic head holder/gas mask apparatus. Isoflurane was then lowered until mice reached a stable anaesthetic state (typically 1,5–2%). Mice were injected with 0.1 mg/kg buprenorphine for pain management. Mice's heads were shaved, and the eyes were covered with a thin layer of petroleum jelly. Following a local injection of bupivacaine (1-5 µl, 0.2-1.0 mg/kg) as a local anaesthetic, the surgical area was cleaned with an antiseptic solution (70% isopropanol followed by 10% iodine solution) and the scalp removed with a scalpel and fine scissors. The periosteum was removed with a scalpel and the skull was cleaned and dried with sterile cotton swabs. The exposed skull was covered with a thin layer of cyanoacrylate glue. A head plate was fixed to the exposed skull with dental cement that was used to cover any exposed part of the skull. Mice were allowed to recover from the surgery for one day before starting a three-day habituation to the behavioural apparatus. During the habituation and the following whisker stimulation protocol, mice sit in a custom-made 3D-printed plastic tube (5 cm diameter) with their head anchored to a custom-made head holder through the head plate. The whisker stimulator consisted of a 2.5 cm2 square of sandpaper held by a rod attached to a servomotor. The servomotor was powered and controlled by an Arduino Uno microcontroller. The whisker stimulator

was positioned ≈0.8 cm away from the mouse's right face and moved in the anterior-posterior direction with a 10deg angle and a frequency of 6 strokes/second for three sessions of five minutes each, with a minute of inter-trial interval. Only during the habituation phase, the whisker stimulator was operated on the animal without touching the whiskers to habituate the mouse to the noise of the servomotor.

Whisker stimulation under anaesthesia (WS).

Mice were anaesthetized with an intraperitoneal injection of urethane (20% solution in sterile double-distilled water, 1.6 g/kg body weight) and head-fixed on a stereotaxic apparatus. Urethane anaesthesia was chosen as it preserves whisker-dependent activity in the somatosensory cortex (Unichenko et al. 2018). WS protocol consisted of three consecutive sessions (5 min each, with 1 min intervals) of continuous touch of the whiskers with a stick (bilateral stimulation), thus reproducing the stimulation protocol used in the WN test.

c-*fos* mRNA in situ hybridisation.

For in situ hybridization experiments, mice were sacrificed 20 min after the end of either sham, WN, anaesthesia or WS. Brains were rapidly removed, rinsed in ice-cold PBS (phosphate buffered saline), placed in OCT Tissue Tek embedding medium (Sakura, CA, USA) and frozen on dry ice. Frozen brains in OCT blocks were stored at −80 °C until cryostat sectioning. Coronal cryostat sections (20µm thick) were mounted on SuperFrost™ slides (Thermo-Scientific), air-dried, and stored at -80°C. In situ hybridization experiments were performed using a digoxigenin-labelled riboprobe. The signal was detected by an alkaline phosphatase-conjugated anti-digoxigenin antibody followed by alkaline phosphatase staining. The experimental protocol is described as follows. Frozen sections were air-dried and fixated in 4% paraformaldehyde. Sections were washed in PBS and acetylated in 0.0265 M acetic anhydride/0.1 M

triethanolamine. Sections were then hybridized for 12-16h at 65°C with digoxigenin-labelled c-*fos* riboprobe in hybridization buffer (50% formamide, 0.3 M NaCl, 10 mM Tris-HCl pH 8.0, 2 mM EDTA, 10% dextran sulphate, 10 mM phosphate buffer pH 8.0, 1x Denhardt's solution, 0.5 mg/mL yeast RNA). Slides were washed twice in 50% formamide/1x standard saline citrate (SSC) for 1h at 55°C and then rinsed with maleic acid buffer (100 mM maleic acid, 150 mM NaCl, Tween 20 0,1%, pH 7.5) at 20°C. Sections were incubated for 2h at 20°C with blocking solution (2x Blocking reagent Roche in MABT, 10% normal goat serum). Following the blocking phase, sections were incubated with alkaline phosphatase anti-digoxigenin antibody (1:2000 in blocking solution) for 12h at +4°C. Slides were then washed three times with MABT and then incubated for 10 minutes with alkaline phosphatase buffer (AP, NaCl 100mM, MgCl2 50mM, Tris pH9,5 100mM, Tween 20 0,1% e Levamisole 5 mM). Following AP buffer incubation, sections were exposed to alkaline phosphatase chromogenic substrates (NBT/BCIP Roche, 20 µl/ml) for 24-36h to produce a visible coloured product. Brain slices from different experimental paradigms were processed together to exclude possible batch effects. Sense riboprobes, used as a negative control, revealed no detectable signal (data not shown). Digital images from four to eight sections per animal were acquired at the level of the S1/dorsal hippocampus using a Zeiss AxioImager II microscope at 10× primary magnification. Since we could not exclude that in freely moving mice subjected to WN c-*fos* mRNA induction occurred in S1 subfields different from the whisker-specific one, the signal was quantified in the whole S1 and not only in the barrel cortex. For consistency, the same quantification was performed in other experimental conditions. Brain areas were identified according to the Allen Mouse Brain Atlas (https://mouse.brain-map.org).

In situ hybridization data analysis.

Utilizing the ImageJ program (https://imagej.net/Downloads), captured images were converted to 8-bit (grey-scale), inverted, and processed to determine the intensity of the c-*fos* mRNA signal (Fig. 6). Mean signal intensity was measured in different counting areas drawn to identify S1 cortical layers, hippocampal subfields, and other regions of interest. Mean signal intensity was then divided by the background calculated in the acellular layer 1. Statistical analysis was performed by unpaired t-test or one-way ANOVA followed by Tukey's for post hoc multiple comparisons as appropriate.

Fig. 6. **In situ hybridization data analysis pipeline.** Following c-*fos* ish, images are acquired as a mosaic image of an entire coronal section (left). Images are converted in an 8-bit greyscale (centre) and inverted resulting in white dots showing c-*fos* mRNA expressing neurons (right). mRNA expression is calculated as mean signal intensity in the area of interest. Mean signal intensity values are divided by signal intensity calculated in layer 1 to normalize for background noise.

Quantitative reverse transcription – polymerase chain reaction (RT-qPCR).

Total RNAs were extracted from the cerebral cortex of Cntnap2 mutant mice and controls as well as from trigeminal ganglia of adult and young mutant (Shank3b$^{-/-}$ and Cntnap2$^{-/-}$) and control mice (Shank3b$^{+/+}$ and Cntnap2$^{+/+}$) with RNeasy Mini Kit (QUIAGEN). Retro-transcription reactions to cDNA were performed with a SuperScript™ VILO™ cDNA Synthesis Kit (Invitrogen) according to the manufacturer's protocol. RT-qPCR was performed in a CFX96TM Real-Time System (Bio-Rad, USA), using SYBR Green master mix (Bio-Rad). Primers (Sigma) were designed on different exons to avoid the amplification of genomic DNA (Table 1). The CFX3 Manager 3.0 (Bio-Rad) software was used to perform expression analyses (Sgadò et al., 2013). Mean cycle threshold (Ct) values from replicate experiments were calculated for each marker and β-actin (used as a standard for quantification), and then corrected for PCR efficiency and inter-run calibration. The expression level of each mRNA of interest was then normalized to that of β-actin for both genotypes.

Primers.

Five genes were selected for testing via RT-qPCR on adult cerebral cortex tissue from Cntnap2 mutant and control mice. The selected genes reflect the main markers of excitatory (vGlut1 and vGlut2) and inhibitory (Gad1, Gad2 and Pvalb) neurotransmission. Forty-eight genes were selected for testing via RT-qPCR on adult TG tissue, whereas a subset of genes was selected for testing in juvenile TG tissue. Genes were selected to identify specific markers of sensory, inhibitory, and excitatory neurons, as well as neuroinflammation and neuroprotection. Primer specificity was verified using the In-Silico PCR (UCSC Genome Browser) and Primer Blast (NCBI) resources. Primer sequences are listed in Table 1.

Gene expression analysis.

For RT-qPCR experiments performed in the cerebral cortex of Cntnap2 mutant and control mice, the relative expression levels of each marker (normalized to that of β-actin) were compared from at least triplicate experiments. Raw Ct values resulting from qRT-PCR experiments performed on trigeminal ganglia were normalised and calculated into fold change values via the Livak method. Fold change (FC) represents the expression ratio of KO groups ($Shank3b^{-/-}$ or $Cntnap2^{-/-}$) relative to their respective WT controls ($Shank3b^{+/+}$ or $Cntnap2^{+/+}$). Therefore, fold changes lower than 1 represent a downregulation in the expression of a target gene while those greater than 1 report an upregulation of the target gene relative to the control sample. Statistical analysis was performed by unpaired t-test using the GraphPad Prism 8 software with a significance level set at $p<0.05$.

Resting state-functional magnetic resonance imaging (rs-fMRI).

Resting state functional MRI connectivity is a technique to map spatiotemporal synchronization of spontaneous BOLD fluctuations across brain regions in human clinical (Di Martino et al., 2014) and rodent studies (Pagani et al., 2021; Zerbi et al., 2021) to describe alterations of brain networks in autism and other neuropsychiatric disorders. Functional connectivity analyses reported here were carried out on the rs-fMRI scans acquired for previous studies (Liska et al., 2018 for Ctnap2; Pagani et al., 2019 for Shank3b). A total of twenty-one adult Shank3b (n=11 WT and n=10 KO) and twenty-six Cntnap2 (n=13 WT and n=13 KO). The protocol for animal preparation employed is described as follows. Animals were anaesthetized with isoflurane (5% induction), intubated and artificially ventilated (2% maintenance). After surgery, isoflurane was discontinued and replaced with halothane (0.7%). Recordings started 45 min after isoflurane cessation. Functional scans were acquired with a 7 T MRI scanner (Bruker Biospin, Milan, Italy)

using a 72-mm birdcage transmit coil and a 4-channel solenoid coil for signal reception. For each animal, in vivo anatomical images were acquired with a fast spin echo sequence (repetition time [TR] = 5500 ms, echo time [TE] = 60 ms, matrix 192 × 192, field of view 2 × 2 cm, 24 coronal slices, slice thickness 500 µm). Cocenterd single-shot BOLD rs-fMRI time series were acquired using an echo planar imaging (EPI) sequence with the following parameters: TR/TE 1200/15 ms, flip angle 30°, matrix 100 × 100, field of view 2 × 2 cm, 24 coronal slices, slice thickness 500 µm for 500 volumes.

Functional connectivity analysis.

Raw time-series were pre-processed and denoised as previously reported prior to mapping rs-fMRI connectivity (Liska et al., 2018; Coletta et al., 2020). To account for the impacts of T1 equilibration, the first 50 volumes were eliminated. After that, time series were despiked, motion-corrected, and registered to a standard group-averaged BOLD reference template (Pagani et al., 2016). Motion traces of head realignment parameters and mean ventricular signal were then used as nuisance covariates and regressed out from each time course. All time-series received band-pass filtering (0.01-0.1 Hz) and spatial smoothing (FWHM = 0.6 mm) prior to functional connectivity mapping. Functional connectivity of brain regions associated with whisker-mediated behaviours was mapped using seed-based correlation analysis in both mutant mouse lines. Specifically, in Shank3b mice, bilateral seeds of 3 × 3 × 1 voxels were placed in the dorsal hippocampus, S1, and ventral posteromedial nucleus of the thalamus (VPM) to probe impaired functional connectivity between these regions and the rest of the brain. Figures 24 and 25 show where the bilateral seeds used for mapping were located. Whereas, for Cntnap2 mice, bilateral seeds were placed in the primary somatosensory (S1) cortex and ventral postero-medial nucleus (VPM) of the thalamus. The location of the bilateral seeds employed for

mapping is indicated in Fig. 26. Functional connectivity was measured with Pearson's correlation and r-scores were transformed to z-scores using Fisher's r-to-z transform before group-level statistics. Voxel-wise intergroup differences for seed-based mapping were assessed using a 2-tailed Student's t-test ($t > 2$, $p < 0.05$) and family-wise error (FWER) cluster-corrected using a cluster threshold of $p = 0.01$. To quantify rs-fMRI alterations we also carried out functional connectivity measures in cubic regions of interest ($3 \times 3 \times 1$ voxels). A 2-tailed Student's t-test was used to determine the statistical significance of these region-by-region intergroup effects ($t > 2$, p 0.05).

Shank3b$^{-/-}$ mice show hypo-locomotor behaviour in the open field arena.

We initially evaluated Shank3b$^{-/-}$ and control mice in an open field arena, taking advantage of the extended tNORT habituation, to test for general locomotor activity and generalized anxiety. In both testing days, Shank3b$^{-/-}$ mice were significantly less mobile than control littermates in terms of distance travelled (Fig. 7A; two-way ANOVA, Shank3b$^{+/+}$ vs. Shank3b$^{-/-}$; main effect of genotype $F(1, 56) = 86.93$; $P < 0{,}0001$; main effect of testing days $F(1, 56) = 52.05$, $P < 0{,}0001$; post hoc Tukey's test, Shank3b$^{+/+}$ vs. Shank3b$^{-/-}$ within day 1 and 2, $P < 0.0001$), average speed (Fig. 7B; two-way ANOVA Shank3b$^{+/+}$ vs. Shank3b$^{-/-}$; main effect of genotype $F(1, 56) = 90.56$; $P < 0{,}0001$; main effect of testing days $F(1, 56) = 58.65$, $P < 0{,}0001$; post hoc Tukey's test, Shank3b$^{+/+}$ vs. Shank3b$^{-/-}$ within day 1 and 2, $P < 0.0001$), and time spent moving (Fig. 7C; two-way ANOVA Shank3b$^{+/+}$ vs. Shank3b$^{-/-}$; main effect of genotype $F(1, 56) = 100.1$; $P < 0{,}0001$; main effect of testing days $F(1, 56) = 78.83$, $P < 0{,}0001$; post hoc Tukey's test, Shank3b$^{+/+}$ vs. Shank3b$^{-/-}$ within day 1 and 2, $P < 0.0001$) compared to control littermates. Between testing days, the same metrics were significantly reduced in both genotypes (Fig. 7A, B and C; Tukey's post hoc following two-way ANOVA, Shank3b$^{+/+}$ day 1 vs. Shank3b$^{+/+}$ day 2 and Shank3b$^{-/-}$ day 1 vs. Shank3b$^{-/-}$ day 2; $P < 0.0001$), indicating habituation to the novel environment. Over the course of the two habituation days, both genotypes also spent comparable amounts of time in the centre and the borders of the open field arena (Fig. 7D three-way ANOVA, Shank3b$^{+/+}$ vs. Shank3b$^{-/-}$; main effect of genotype $F(1, 112) = 0.03368$, $P = 0.8547$; main effect of days $F(1, 112) = 0.4418$, $P = 0.5076$; main effect of arena regions $F(1, 112) = 4081$, $P < 0{,}0001$). Finally, throughout both testing days, Shank3b$^{-/-}$ and control mice both preferred the arena's borders (Fig. 7D; Tukey's post hoc following three-

way ANOVA, centre vs. borders within Shank3b$^{+/+}$ and centre vs. borders within Shank3b$^{-/-}$; $P < 0.0001$), indicating a shared anxious behaviour. No sex differences were found in the behaviour analysed (two-way ANOVA, Shank3b$^{+/+}$ vs Shank3b$^{-/-}$, main effect of sex $p > 0.05$ for distance travelled, average speed, and time spent moving or in centre/borders; data not shown).

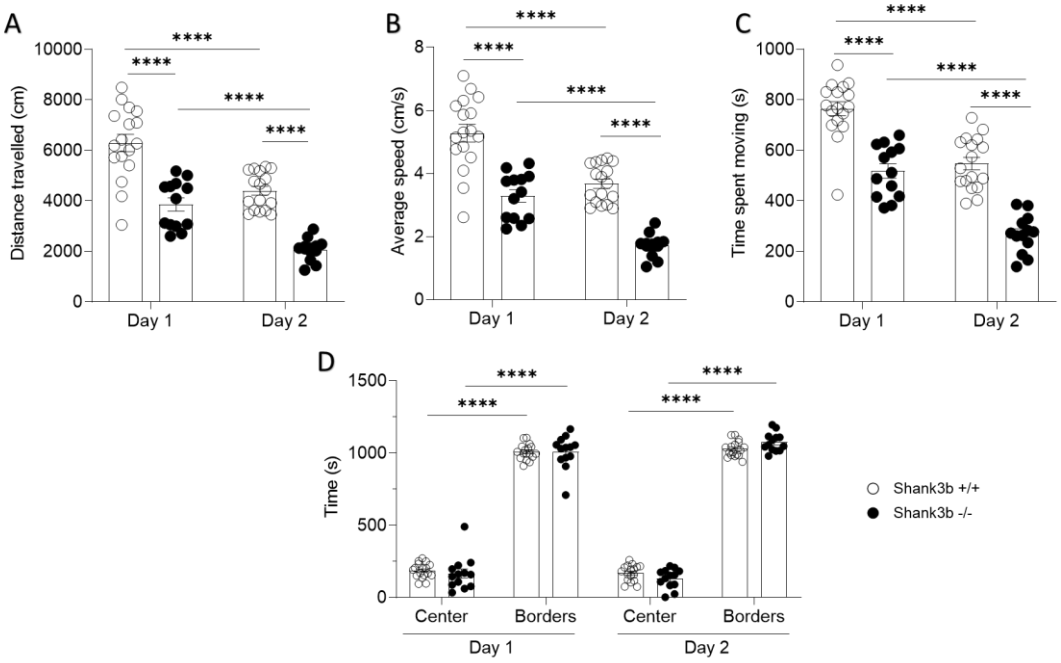

Fig 7. Shank3b$^{-/-}$ mice exhibit hypo-locomotion. (A, B and C) Quantification of open field performance by Shank3b$^{+/+}$ and Shank3b$^{-/-}$ mice revealed that Shank3b$^{-/-}$ mice travel less (A), with a reduced speed (B) and spend less time moving (C) over the two days of the test, as compared to controls (****$P < 0.0001$, Tukey's test following two-way ANOVA). Both Shank3b$^{+/+}$ and Shank3b$^{-/-}$ mice spent significantly more time in borders as compared to the centre of the arena (D, ****$P < 0.0001$, Tukey's test following three-way ANOVA), but the total time spent in centre and borders did not significantly differ between genotypes (D, $P > 0.05$, Tukey's test following three-way ANOVA). All plots report the mean values ± SEM; each dot represents one animal. Genotypes are as indicated (n = 17 Shank3b$^{+/+}$ and n = 13 Shak3b$^{-/-}$).

Cntnap2$^{-/-}$ mice show hyper-locomotor behaviour in the open field arena.

We also assessed Cntnap2$^{-/-}$ and control mice in the open field arena. Previous studies demonstrated that Cntnap2$^{-/-}$ mice and rats have greater locomotor activity in the open field arena (Penagarikano et al., 2011; Scott et al., 2018). We replicated these findings in our settings by showing that Cntnap2$^{-/-}$ mice display a significantly increased distance travelled and average speed (Fig. 8A and B; Mann-Whitney test, Cntnap2$^{-/-}$ vs Cntnap2$^{+/+}$; $p = 0.0093$) as compared to wild-type littermates. Additionally, both genotypes spent a comparable amount of time in the centre and borders of the open field arena (Fig. 8C; Tukey's post hoc following two-way ANOVA, Cntnap2$^{+/+}$ vs Cntnap2$^{-/-}$ within the centre; $p = 0.5150$; Cntnap2$^{+/+}$ vs Cntnap2$^{-/-}$ within borders; $p = 0.5132$) despite having a preference for border regions (Fig. 8C; Tukey's post hoc following two-way ANOVA, centre vs borders within Cntnap2$^{+/+}$ and centre vs borders within Cntnap2$^{-/-}$; $p < 0.0001$), indicating a similar level of anxiety. No sex differences were found in the behaviour analysed (two-way ANOVA, Cntnap2$^{+/+}$ vs Cntnap2$^{-/-}$, main effect of sex $p > 0.05$ for distance travelled, average speed, and time spent in centre/borders; data not shown).

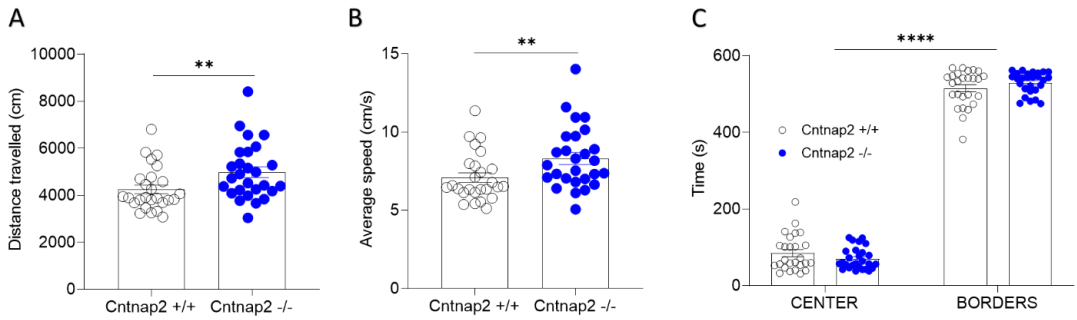

Fig 8. Shank3b$^{-/-}$ mice exhibit hyper-locomotion. (A, B and C) Quantification of open field performance by Cntnap2$^{+/+}$ and Cntnap2$^{-/-}$ mice revealed that Cntnap2$^{-/-}$ mice travel less (A) and with a reduced speed (B), as compared to controls (**P < 0.01, Mann-Whitney test). Both Cntnap2$^{+/+}$ and Cntnap2$^{-/-}$ mice spent significantly more time in borders as compared to the centre of the arena (C, ****P < 0.0001, Tukey's test following two-way ANOVA), but the total time spent in the centre and borders did not significantly differ between genotypes (C, P > 0.05, Tukey's test following two-way ANOVA). All plots report the mean values ± SEM; each dot represents one animal. Genotypes are as indicated (n = 26 Cntnap2$^{+/+}$ and 27 Cntnap2$^{-/-}$)

Shank3b$^{-/-}$ and Cntnap2$^{-/-}$ mice display impairments in texture discrimination through whiskers.

According to human studies, autism is associated with abnormal sensory responses. To test the presence of a similar dysfunction in Shank3 and Cntnap2 mutant mice, we assessed both mutant mouse lines and controls in a whisker-dependent version of tNORT (Wu et al., 2013) using custom-made objects that differ only by texture (Fig. 3 and 4, see Materials and Methods for specifics). Both Shank3b$^{-/-}$ and Cntnap2$^{-/-}$ spent a comparable total amount of time exploring the object with whiskers in both the learning and testing phase compared to their wild-type littermates (Fig. 9A and B for Shank3b mice and Fig. 9C and D for Cntnap2 mice; unpaired t-test, Shank3b$^{+/+}$ vs. Shank3b$^{-/-}$ and Cntnap2$^{+/+}$ vs Cntnap2$^{-/-}$; $P > 0.05$), indicating that mutant mice have preserved exploration through whiskers and did not exhibit an aversion to the objects.

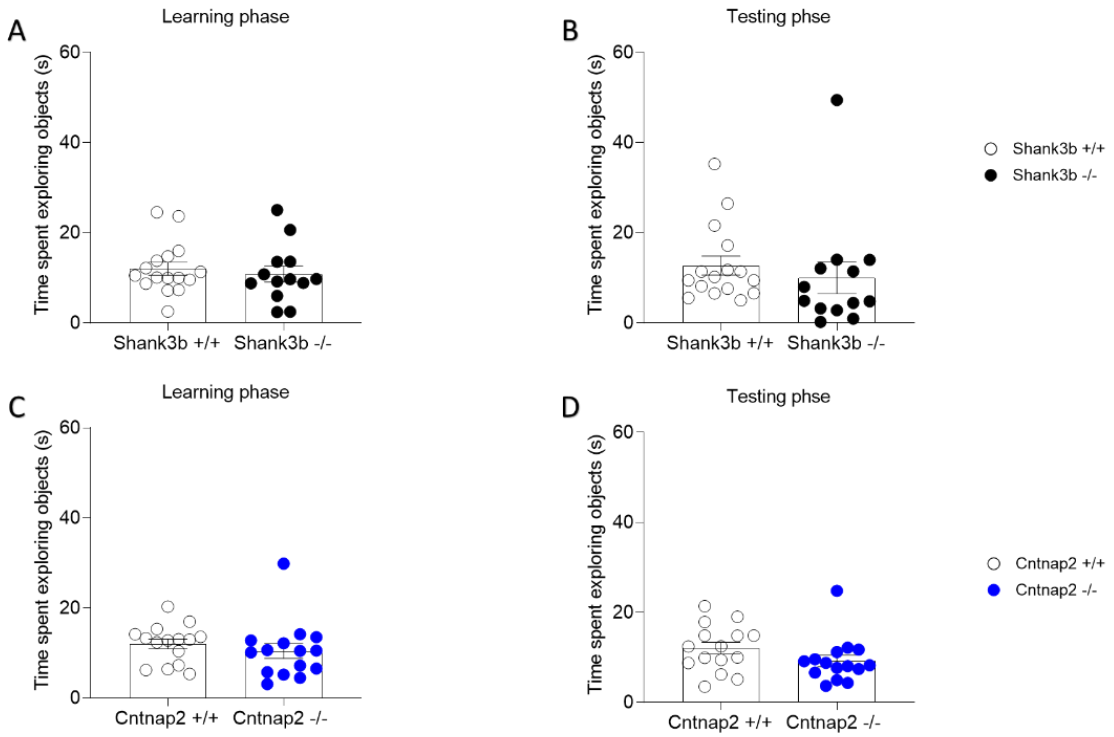

Fig 9. The amount of time spent whisking the objects in learning and testing phase do not differ between genotypes. A and B show the total time spent whisking the objects by Shank3b$^{+/+}$ and Shank3b$^{-/-}$ in both the learning and testing phase of tNORT (P>0.05, unpaired t-test Shank3b$^{+/+}$ vs Shnk3b$^{-/-}$). C and D show the total time spent whisking the objects by Cntna2$^{+/+}$ and Cntnap2$^{-/-}$ in both the learning and testing phase of tNORT (P>0.05, unpaired t-test Cntnap2$^{+/+}$ vs Cntnap2$^{-/-}$). All plots report the mean values ± SEM; each dot represents one animal. Genotypes are as indicated (n = 16 Shank3b$^{+/+}$ and n = 13 Shak3b$^{-/-}$; n = 15 Cntnap2$^{+/+}$ and 15 Cntnap2$^{-/-}$).

In the learning phase of tNORT Shank3b$^{-/-}$ and control mice did not show a preference for one of the equally textured objects (Fig. 10A, two-way ANOVA, main effect of objects $F(1, 54) = 3.637$, $p = 0.0618$). The same was also found when testing for Cntnap2$^{-/-}$ and control mice (Fig. 10C, two-way ANOVA, main effect of objects $F(1, 56) = 0{,}2320$, $p = 0.6319$). During the testing phase, we showed that only one genotype of both mouse lines showed a preference for the novel textured object (Fig. XB and C; two-way ANOVA, interaction between genotype and objects $F(1, 54) = 28.29$, $P<0{,}0001$ in Shank3b and $F (1, 56) = 9{,}368$, $P=0{,}0034$ in Cntnap2). Specifically, Shank3b$^{+/+}$ and Cntnap2 $^{+/+}$ mice spent a significantly larger amount of time exploring the novel object (Fig. 10B and D), testifying a preference for the novel texture exploration through whiskers. Conversely, Shank3b $^{-/-}$ mice preferred the familiar texture objects (Fig. XB; Tukey's post hoc following two-way ANOVA, familiar object vs novel object within Shank3b$^{+/+}$, $p = 0.003$ and Shank3b$^{-/-}$, $p = 0.0134$), while Cntnap2$^{-/-}$ mice spent comparable time exploring the novel and the familiar object, (Fig. 10D; Tukey's post hoc following two-way ANOVA, familiar object vs novel object within Cntnap2$^{+/+}$, $p < 0.0001$ and Cntnap2$^{-/-}$, $p = 0.2033$). No sex differences were found in both mouse lines in the preference index during both learning and testing phases (three-way ANOVA, Shank3b$^{+/+}$ vs Shank3b$^{-/-}$, and Cntnap2$^{+/+}$ vs Cntnap2$^{-/-}$ main effect of sex $p > 0.05$ in learning and testing phases). These results suggest that Shank3b and Cntnap2$^{-/-}$ mice display impaired whisker-mediated texture discrimination.

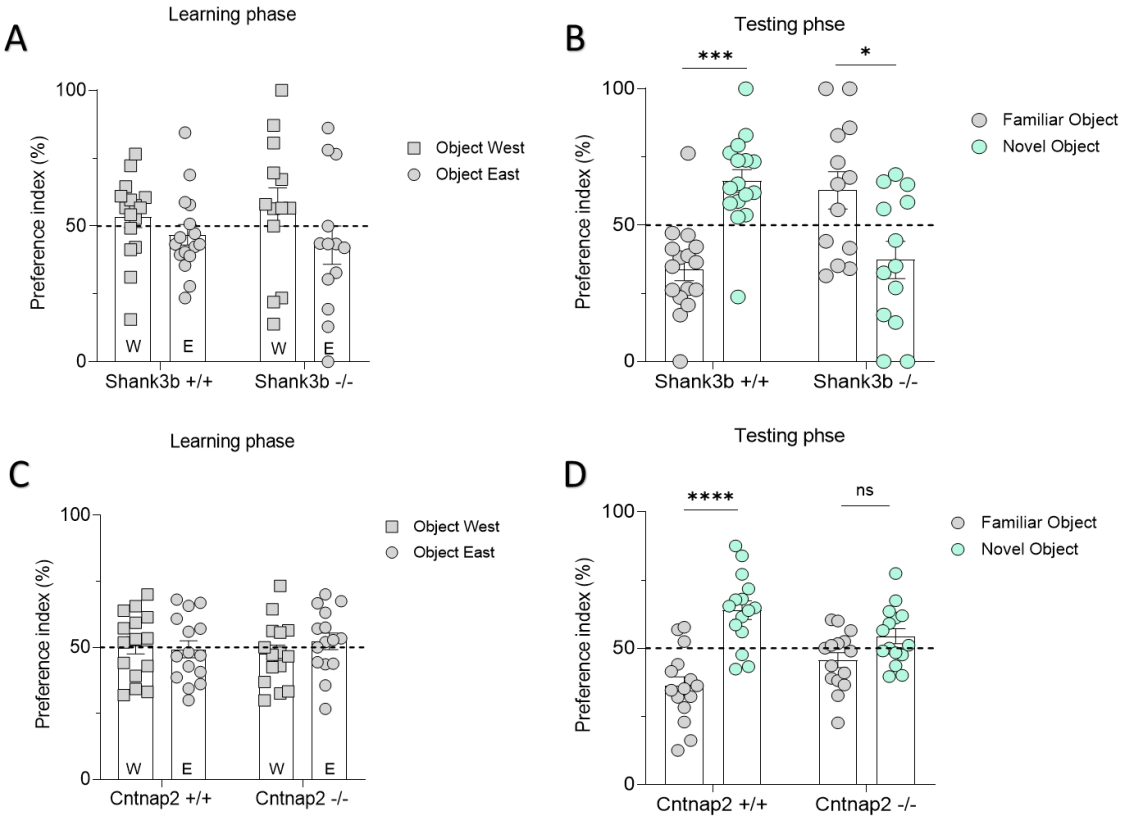

Fig. 10. Shank3b$^{-/-}$ and Cntnap2$^{-/-}$ mice exhibit abnormal whisker dependent texture discrimination. (A-D) Quantification of tNORT performances by Shank3b and Cntnap2 mutant mice and relative controls. Preference index (%) for familiar objects did not differ between Shank3b$^{+/+}$ and Shank3b$^{-/-}$ (A) as well as between Cntnap2$^{+/+}$ and Cntnap2$^{-/-}$ mice (C) in the learning phase ($p > 0.05$, Tukey's test following two-way ANOVA). In the testing phase, Shank3b$^{-/-}$ did not show a preference for the novel textured object but for the familiar one as compared with Shank3b$^{+/+}$ mice (B, ***$p < 0.001$ for Shank3b$^{+/+}$ and $p<0.05$ for Shank3b$^{-/-}$, Tukey's test following two-way ANOVA). Cntnap2$^{-/-}$ mice did not show a preference for the novel textured object, as compared to Cntnap2$^{+/+}$ mice (D, ****$p < 0.0001$ for Cntnap2$^{+/+}$ and $p>0.05$ for Cntnap2$^{-/-}$, Tukey's test following two-way ANOVA. All plots report the mean values ± SEM; each dot represents one animal. Genotypes are as indicated (n = 16 Shank3b$^{+/+}$ and n = 13 Shak3b$^{-/-}$; n = 15 Cntnap2$^{+/+}$ and 15 Cntnap2$^{-/-}$).

Shank3b$^{-/-}$ mice are hyporeactive to repetitive whisker stimulation.

We then evaluated the behavioural responses of Shank3b$^{-/-}$ and control mice to repetitive whisker stimulation via the whisker nuisance test (WN; Balasco et al., 2019, Chelini et al., 2019). Following a sham session that allowed to set the baseline of behavioural responses, Shank3b$^{-/-}$ and control mice were repeatedly stimulated with a wooden stick during three consecutive sessions of 5 min each (Fig. 5). Different behavioural responses (freezing, guarded behaviour, evasion, climb and startle) were quantified (Fig. 5; see Materials and Methods). Overall, there were no behavioural differences between Shank3b$^{+/+}$ and Shank3b$^{-/-}$ mice during the pre-stimulation (sham) session with both genotypes showing comparable guarded behaviour and evasiveness (Fig. 11B and C; Kolmogorov–Smirnov test; Shank3b$^{+/+}$ vs. Shank3b$^{-/-}$, $P > 0.05$). Both genotypes did not climb or were startled by the stick presentation during the sham session (Fig. 11D and E; Kolmogorov–Smirnov test; Shank3b$^{+/+}$ vs. Shank3b$^{-/-}$, $P > 0.05$). However, Shank3b$^{-/-}$ displayed a significant increase in the time spent freezing during sham session compared with controls (Fig. 11A; Kolmogorov–Smirnov test, Shank3b$^{+/+}$ vs. Shank3b$^{-/-}$; $P = 0.006$). A significant effect of genotype was found for evading, climbing, and startle behaviours (Fig. 11C, D and E; two-way ANOVA, main effect of genotype $F(1, 140) = 8,33$ for evading; $F(1, 140) = 9,49$ for climbing; $F(1, 140) = 6,98$ for startle; $P < 0.01$) with Shank3b$^{-/-}$ mice being hyporeactive to whisker stimulation. No differences between genotypes were found for freezing and guarded behaviours (Fig. 11A and B; two-way ANOVA, main effect of genotype $F (1, 140) = 0,4420$ for freezing and $F (1, 140) = 1,499$ for guarded; $P > 0.05$). A marked effect of trials was found for all behaviour analysed (Fig. 11A-E; two-way ANOVA, main effect of trial $F(3, 140) = 14,83$ for freezing; $F(3, 140) = 14,12$ for guarded; $F(3, 140) = 22,06$ for evading; $F(3, 140) = 46,09$ for climbing; $F(3, 140) = 12,60$ for startle; $P < 0.0001$) indicating habituation to repetitive whisker

stimulation. In the first trial, both genotypes exhibited a similar fearful response testified by higher scores in freezing, guarded, and evading behaviours compared to the sham session (Fig. 11A, B and C; Bonferroni's test following two-way ANOVA; trial 1 vs. sham within Shank3b$^{+/+}$ and Shank3b$^{-/-}$, $P < 0.05$). However, Shank3b$^{-/-}$ mice spent significantly less time evading compared to controls (Fig. 11C), while no difference was observed in freezing and guarded behaviours during trial 1 (Fig. 11A and B; Kolmogorov–Smirnov test; Shank3b$^{+/+}$ vs. Shank3b$^{-/-}$ within trial 1, $P < 0.05$ for evading, $P > 0.05$ for freezing and guarded). Additionally, Shank3b$^{-/-}$ mice had significantly less curiosity toward the stimulus, as seen by the fact that they engaged in significantly fewer climbing behaviours during trial 3 compared to controls (Fig. 11D; Kolmogorov–Smirnov test; Shank3b$^{+/+}$ vs. Shank3b$^{-/-}$ within trial 3, $P = 0.004$). Finally, no major differences in behavioural scores were observed between the sexes within the two genotypes (data not shown).

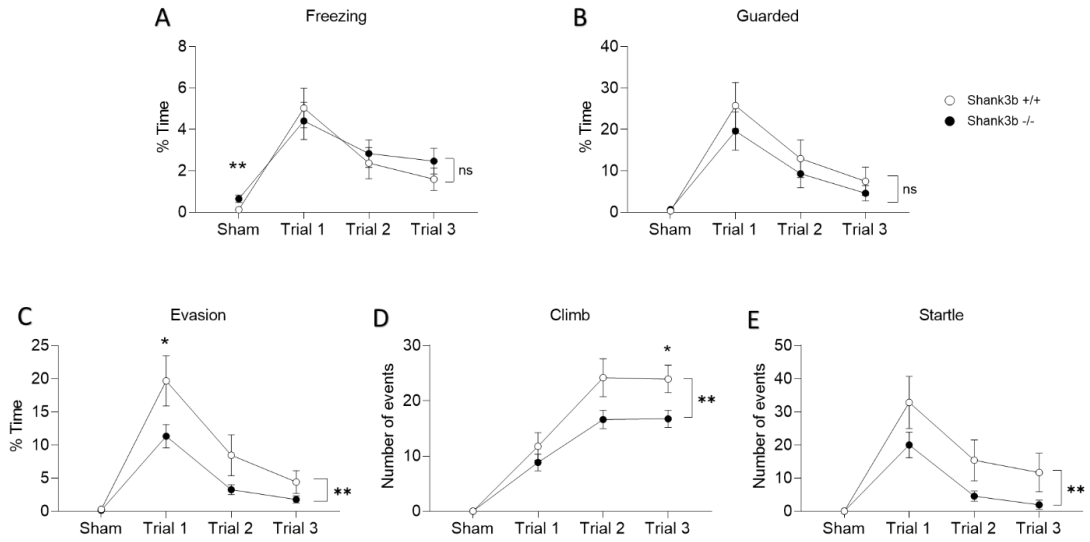

Fig. 11. Shank3b$^{-/-}$ mice are hyporeactive to whisker stimulation showing reduced evading and exploratory behaviours but intact fearful behaviours in WN. Time spent in freezing (A), guarded behaviour (B), and evading (C) are expressed as % over the total time of observation in each session. The number of climbing events (D) and startle events (E) in response to the stick presentation are expressed as the total number of events. All plots report mean values ± SEM. *P < 0.05, **P < 0.01, Kolmogorov–Smirnov test and two-way ANOVA. Genotypes are as indicated (n = 19 Shank3b$^{+/+}$ and 18 Shank3b$^{-/-}$)

These findings suggest that Shank3b$^{-/-}$ mice are less likely to take proactive actions in response to intrusive whisker stimulation compared to control mice. The animal's ability to experience fear is not affected by Shank3b deficiency, but its ability to react to novel and intrusive stimuli is severely disrupted.

Cntnap2$^{-/-}$ mice are not affected by whisker stimulation.

We also quantified the behavioural responses to repetitive whisker stimulation via the WN in Cntnap2$^{-/-}$ and control mice and found that mutant mice behave similarly to their wild-type littermates in each behaviour analysed (Fig. 12A-E; two-way ANOVA main effect of genotype, Cntnap2$^{+/+}$ vs Cntnap2$^{-/-}$ in each behaviour $P > 0.05$). As seen for Shank3b mice, also Cntnap2$^{+/+}$ and Cntnap2 mice showed comparable levels of freezing, guarded behaviour, and evasiveness during the sham session (Fig. 12A, B and C; Kolmogorov–Smirnov test; Cntnap2$^{+/+}$ vs. Cntnap2$^{-/-}$, $P > 0.05$). Both genotypes did not show climbs or startle following stick presentation during the sham session (Fig. 12D and E; Kolmogorov–Smirnov test; Cntnap2$^{+/+}$ vs. Cntnap2$^{-/-}$, $P > 0.05$). Cntnap2$^{+/+}$ and Cntnap2$^{-/-}$ showed habituation to repetitive whisker stimulation across trials (Fig. 12A-E; two-way ANOVA, main effect of trial $F(3, 108) = 9{,}897$ for freezing, $F(3, 108) = 9{,}348$ for guarded behaviour, $F(3, 108) = 18{,}84$ for evasion, $F(3, 108) = 39{,}97$ for climbs and $F(3, 108) = 22{,}36$ for startle; $P<0{,}0001$) but no differences were found between genotypes in each trial analysed (Kolmogorov–Smirnov test; Cntnap2$^{+/+}$ vs. Cntnap2$^{-/-}$ in trial 1, trial 2 and trial 3, $P > 0.05$) indicating a preserved behavioural response following direct whisker simulation.

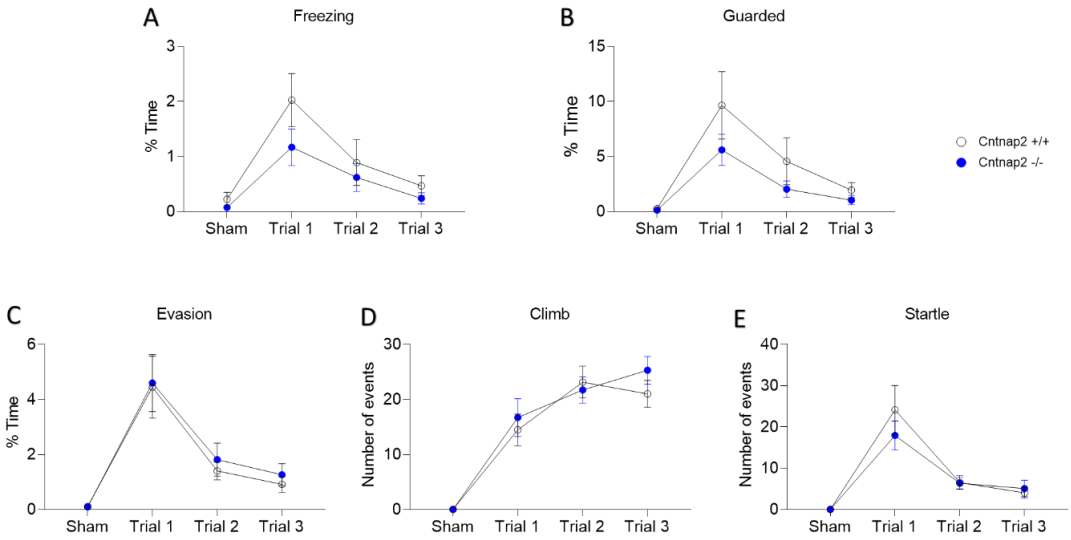

Fig. 12. Cntnap2$^{-/-}$ and Cntnap2$^{+/+}$ mice show comparable behaviours following repetitive whisker stimulation in WN. Time spent in freezing (A), guarded behaviour (B), and evading (C) are expressed as % over the total time of observation in each session. The number of climbing events (D) and startle events (E) in response to the stick presentation are expressed as the total number of events. All plots report mean values ± SEM. P > 0.05 Kolmogorov-Smirnov test and two-way ANOVA. Genotypes are as indicated (n = 15 Cntnap2$^{+/+}$ and 14 Cntnap2$^{-/-}$)

Shank3b$^{-/-}$ mice lack c-*fos* induction in S1 and Hp following whisker stimulation.

Aberrant texture discrimination through whiskers and sensory hypo-responsiveness to whisker stimulation in Shank3b$^{-/-}$ mice led us to investigate the neuronal underpinnings of these whisker-dependent behaviours. We looked for c-*fos* mRNA expression as a proxy to infer neuronal activity in response to sensory stimulation (Filipkowski et al., 2000, Chelini et al., 2019) and quantified in-situ hybridization (ISH) signals in key brain regions involved in the processing of tactile sensory information. Firstly, c-*fos* mRNA induction was quantified in the primary somatosensory cortex (S1) of Shank3b$^{+/+}$ and Shank3b$^{-/-}$ mice following either a sham or WN session (Fig. 13A and B).

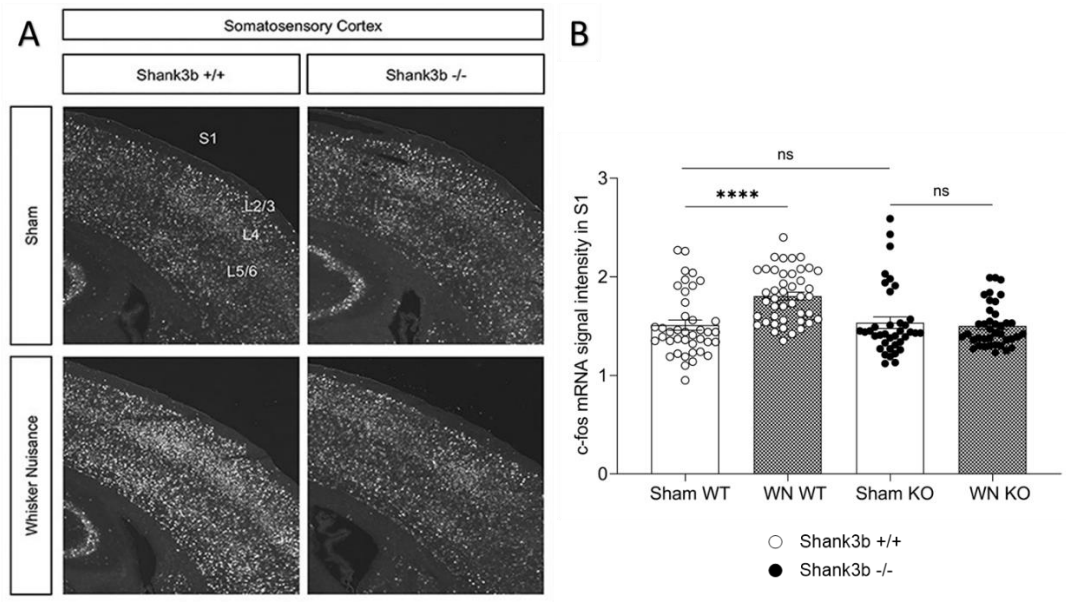

Fig. 13. Shank3b$^{-/-}$ mice lack c-*fos* mRNA induction in S1 and following WN. (A). Schematic of Sham (top) and WN test (bottom). (B) Representative images of c-*fos* mRNA in situ hybridization in S1 of Shank3b$^{+/+}$ and Shank3b$^{-/-}$ mice, 20 min following sham or WN. Scale bars, 500 µM. (C) Quantification of c-*fos* mRNA signal intensity in S1 following Sham and WN. Values are expressed as mean signal intensities ±SEM (see Materials and Methods). ****$P < 0.0001$, Tukey post hoc test following one-way-ANOVA ($n = 44$ sections from nine Shank3b$^{+/+}$ mice and 40 sections from seven Shank3b$^{-/-}$ mice following WN and $n = 43$ sections from six Shank3b$^{+/+}$ mice and 37 sections from five Shank3b$^{-/-}$ mice following sham). Genotypes and treatments are as indicated. Abbreviations: L2–6, S1 cortical layers; S1, primary somatosensory cortex.

Following the sham session, both genotypes showed comparable levels of c-*fos* mRNA expression (Fig. 13A and B; Tukey post-hoc following one-way ANOVA, $P > 0.05$). While whisker stimulation induced an increase in c-*fos* mRNA expression in the S1 of Shank3b$^{+/+}$ mice (Fig. 13A and B; Tukey post-hoc following one-way ANOVA, Sham vs WN in Shank3b$^{+/+}$, $P < 0.0001$), no differences were found between Sham and WN in Shank3b$^{-/-}$ mice (Fig. 13A and B; Tukey post-hoc following one-way ANOVA, Sham vs WN in Shank3b$^{+/+}$, $P > 0.05$). c-*fos* mRNA expression was also upregulated in S1 layers of Shank3b$^{+/+}$ mice but not in Shank3b$^{-/-}$ mice following WN, as compared to sham control (Fig. 14A, B and C; Tukey post-hoc following one-way ANOVA, Sham vs WN in Shank3b$^{+/+}$, $P < 0.0001$).

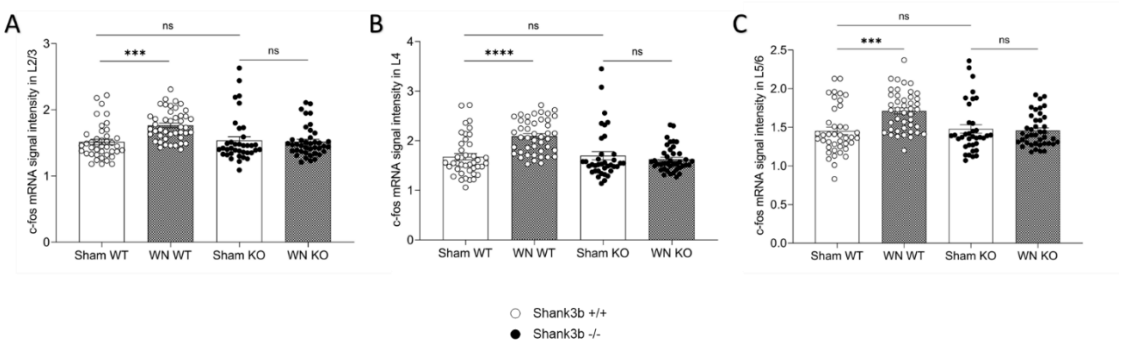

Fig.14. c-*fos* mRNA expression is upregulated in S1 layers of Shank3b$^{+/+}$ mice but not Shank3b$^{-/-}$ mice following WN, as compared to sham. (A-C) Quantification of c-*fos* mRNA signal intensity in S1 layers following sham and WN. Values are expressed as mean signal intensities ±SEM. ***p<0.001, ****p<0.0001, Tukey post-hoc test following one-way ANOVA (n=44 sections from 9 Shank3b$^{+/+}$ mice and 40 sections from 7 Shank3b$^{-/-}$ mice following WN and n=43 sections from 6 Shank3b$^{+/+}$ mice and 37 sections from 5 Shank3b$^{-/-}$ mice following sham). Genotypes, treatments, and S1 cortical layers (L2-6) are as indicated.

We also analysed the hippocampus (Hp) of Shank3b$^{+/+}$ and Shank3b$^{-/-}$ mice following either Sham or WN. The hippocampus receives afferents from the S1 and is affected by the sensory stimulation of the whiskers (Lavenex and Amaral., 2000; Bellistri et al., 2013; Gener et al., 2013). In our settings, c-*fos* mRNA levels in the hippocampus did not differ between Sham and WN animals in both genotypes (Fig. 15A and B; $P > 0.05$, one-way ANOVA).

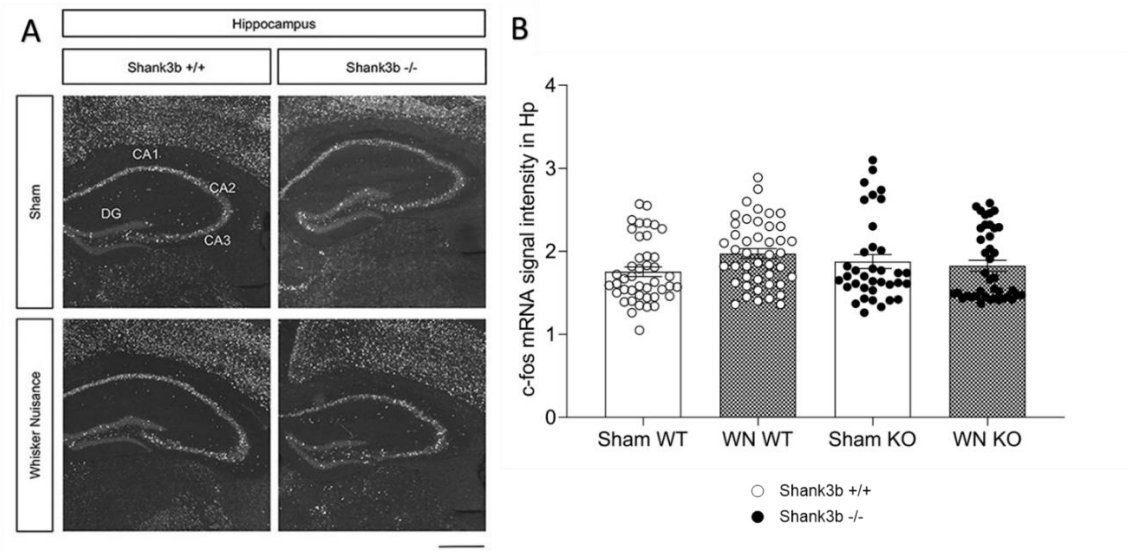

Fig. 15. No differences c-*fos* mRNA induction in Hp and following WN in Shank3b$^{-/-}$ mice. (A). Representative images of c-*fos* mRNA in situ hybridization in Hp of Shank3b$^{+/+}$ and Shank3b$^{-/-}$ mice, 20 min following sham or WN. Scale bars, 500 µM. (B) Quantification of c-*fos* mRNA signal intensity in the Hp following sham and WN. Values are expressed as mean signal intensities ±SEM (see Materials and Methods). $P > 0.05$, one-way-ANOVA ($n = 44$ sections from nine Shank3b$^{+/+}$ mice and 40 sections from seven Shank3b$^{-/-}$ mice following WN and $n = 43$ sections from six Shank3b$^{+/+}$ mice and 36 sections from five Shank3b$^{-/-}$ mice following sham). Genotypes and treatments are as indicated. Abbreviations: CA1/2/3, hippocampal pyramidal cell layers; DG, dentate gyrus; Hp, hippocampus.

To exclude the possibility that lack of c-*fos* induction found in S1 was a general endophenotype of Shank3b$^{-/-}$ mice we also analysed other brain regions such as the motor cortex (M Ctx), the medial thalamic nuclei (Mtn), the ventral postero-medial nucleus of the thalamus (Vpn) and the amygdala (Amy). No differences were found in c-*fos* mRNA expression between the two genotypes in these brain regions analysed (Fig. 16A-D; one-way ANOVA, Sham vs WN in Shank3b$^{+/+}$ and Shank3b$^{-/-}$, $P > 0.05$).

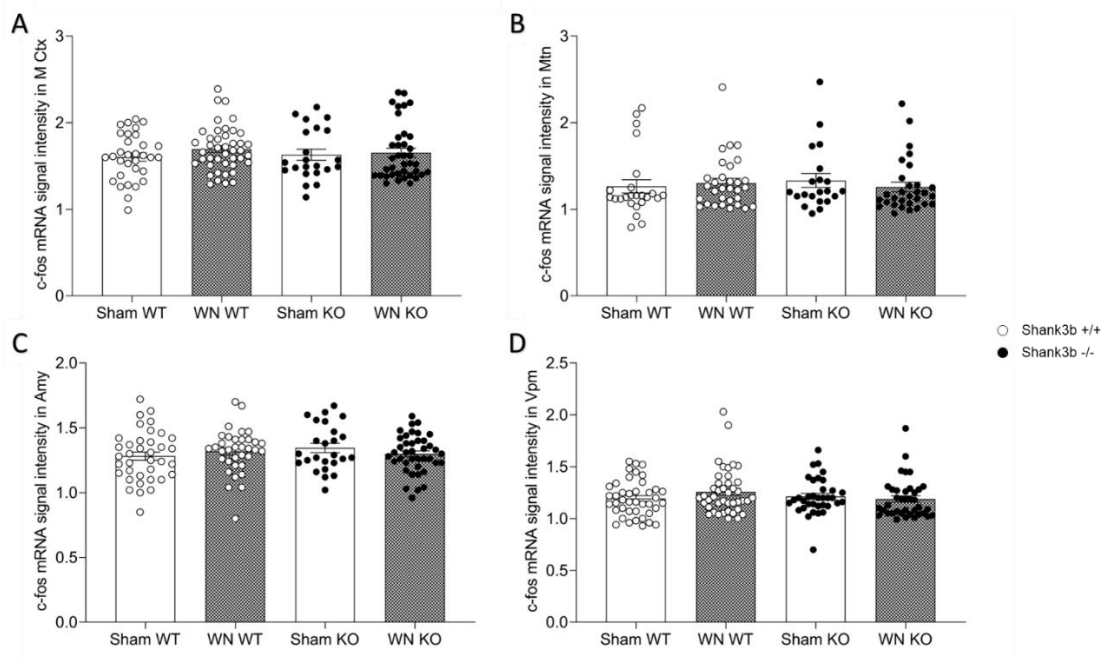

Fig. 16. Shank3b$^{+/+}$ and Shank3b$^{-/-}$ mice did not show any difference in c-*fos* mRNA signal intensity following WN test in other brain regions analysed. Values are expressed as mean signal intensities ±SEM. One-way-ANOVA, p>0.05 (n=44 sections from 9 Shank3b$^{+/+}$ mice and 40 sections from 7 Shank3b$^{-/-}$ mice following WN and n=43 sections from 6 Shank3b$^{+/+}$ mice and 37 sections from 5 Shank3b$^{-/-}$ mice following sham). Genotypes are as indicated. Abbreviations: M Ctx, motor cortex; Mtn, medial thalamic nuclei; Vpm, ventral postero-medial nucleus of thalamus; Amy, amygdala.

To further study the whisker-dependent responses of S1 and Hp, we then carried out a procedure of automated unilateral whisker stimulation in head-fixed awake animals. A significant upregulation of c-*fos* mRNA expression was found in the stimulated S1 (i.e., contralateral to whisker stimulation) for both genotypes (Fig. 17A and B; Tukey's post hoc following one-way ANOVA, Stim vs. No Stim $P < 0.0001$ in Shank3b$^{+/+}$ and $P = 0.0008$ in Shank3b$^{-/-}$). However, Shank3b$^{-/-}$ mice had lower levels of c-*fos* mRNA expression in the stimulated S1 than Shank3b$^{+/+}$ control mice (Fig. XB; Tukey's post hoc following one-way ANOVA, Shank3b$^{+/+}$ Stim vs. Shank3b$^{-/-}$ Stim, $P = 0.0128$). Both genotypes did not show differences in c-*fos* mRNA expression in the unstimulated S1 (located ipsilateral to the stimulation) (Fig. 17A and B; Tukey's post hoc following one-way ANOVA, Shank3b$^{+/+}$ No Stim vs. Shank3b$^{-/-}$ No Stim, $P = 0.0906$). Additionally, measurement of the c-*fos* mRNA in the hippocampus showed that, when compared to stimulated Shank3b$^{+/+}$ controls, the activation of c-*fos* was considerably lower in Shank3b$^{-/-}$ mice (Fig. 17C and D; unpaired t-test $P = 0.0001$). In the other brain regions examined, there was no variation in c-*fos* expression between the two genotypes. The other region analysed showed no modulation of c-*fos* mRNA expression between the two genotypes (Fig. 17E-H; unpaired t-test and one way-ANOVA, $P > 0.05$).

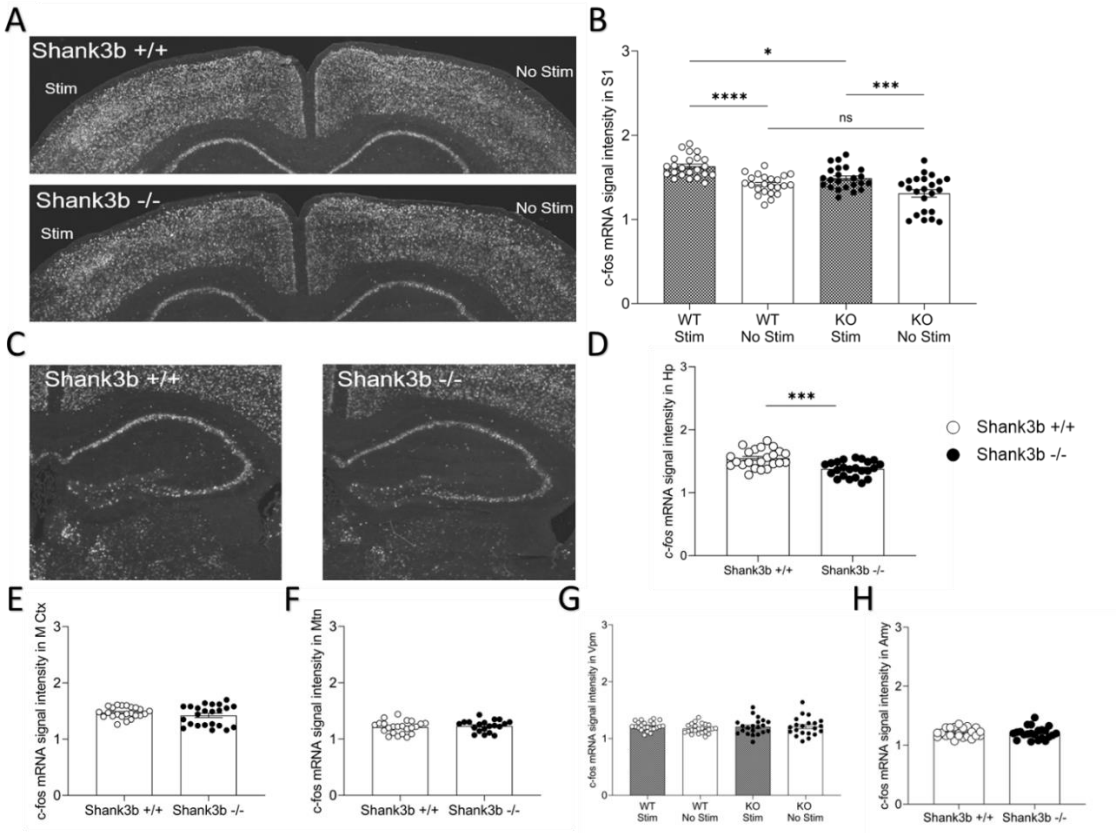

Figure 17. Shank3b$^{-/-}$ mice show reduced c-*fos* mRNA expression in S1 and hippocampus following automated whisker stimulation in head-fixed awake animals. (A, C) Representative images of c-*fos* mRNA in situ hybridization in S1 (A) and hippocampus (C) of Shank3b$^{+/+}$ and Shank3b$^{-/-}$ mice, 20 min following whisker stimulation in head-fixed awake animals. (B, D) Quantification of c-*fos* mRNA signal intensity in S1 (C) and hippocampus (D) of Shank3b$^{+/+}$ and Shank3b$^{-/-}$ mice. Quantification of c-*fos* mRNA signal intensity in other brain regions did not show differential modulation of c-*fos* expression (E-H). Values are expressed as mean signal intensities ±SEM. *p<0.05 ***p<0.001 ****p<0.0001, Tukey post-hoc test following one-way ANOVA (B, G) and unpaired t-test (D, E, F, and H). n=23 sections from 3 Shank3b$^{+/+}$ mice and 23 sections from 3 Shank3b$^{-/-}$. Genotypes and treatments are as indicated. Abbreviations: Stim, contralateral to stimulation; No Stim, ipsilateral to stimulation; S1, primary somatosensory cortex; Hp, hippocampus; M Ctx, motor cortex; Mtn, medial thalamic nuclei; Vpm, ventral postero-medial nucleus of thalamus; Amy, amygdala.

Finally, we examined c-*fos* mRNA induction following a protocol of whiskers stimulation (intended to mimic the stimulation of WN) in anaesthetised Shank3b$^{+/+}$ and Shank3b$^{-/-}$ mice (WS, Fig. 18A and B). We decided to perform c-*fos* ish in anaesthetised animals as this condition allows us to better dissect the neuronal responses without possible confounds given by basal neuronal activation in awake mice. Following anaesthesia only, in situ hybridization experiments revealed equivalent expression of c-*fos* mRNA in S1 and the hippocampus of both genotypes (Fig. 18C and D; Tukey post-hoc test following one-way ANOVA, $P > 0.05$ in S1 and Hp). Conversely, WS induced a significant upregulation of c-*fos* mRNA in both S1 (Fig. 18A) and Hp (Fig. 18B) of Shank3b$^{+/+}$ but not Shank3b$^{-/-}$ mice compared to unstimulated controls (Fig. 18C and D; Tukey post-hoc test following one-way ANOVA anaesthesia vs. WS $P < 0.0001$ in Shank3b$^{+/+}$ S1 and HP).

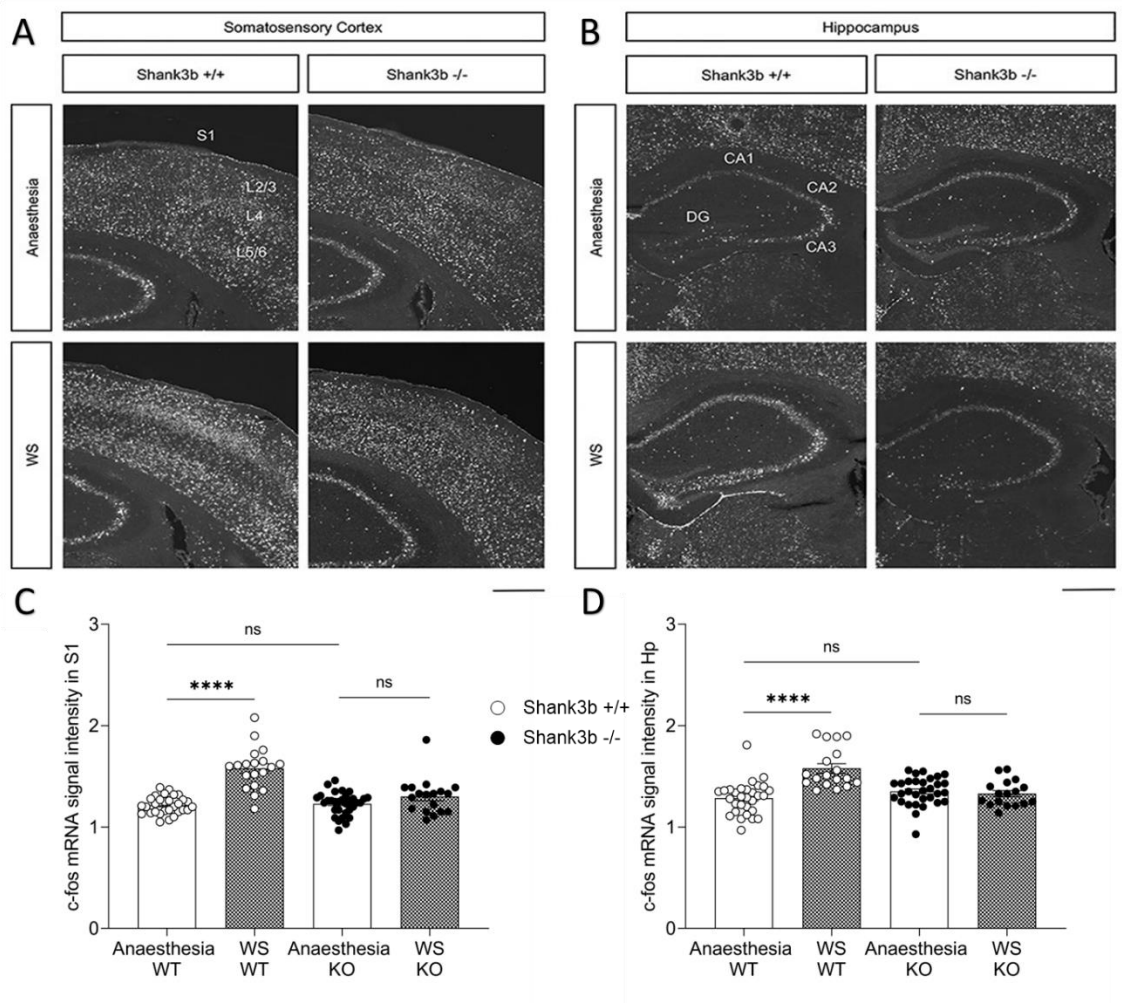

Fig. 18. Shank3b$^{-/-}$ mice lack c-*fos* mRNA induction in S1 and following whisker stimulation under anaesthesia. (A, B) Representative images of c-*fos* mRNA in situ hybridization in S1 (A) and Hp (B) of Shank3b$^{+/+}$ and Shank3b$^{-/-}$ mice, 20 min following anaesthesia or whisker stimulation under anaesthesia. Scale bars, 500 µm. (C, D) Quantification of c-*fos* mRNA signal intensity in S1 (C) and hippocampus (D) of Shank3b$^{+/+}$ and Shank3b$^{-/-}$ mice. Values are expressed as mean normalized signal intensities ±SEM. ****P < 0.0001 Tukey post hoc test following one-way-ANOVA (n = 19 sections from three Shank3b$^{+/+}$ mice and 18 sections from three Shank3b$^{-/-}$ mice following WS and n = 30 sections from four Shank3b$^{+/+}$ mice and 32 sections from four Shank3b$^{-/-}$ mice following anesthesia). Genotypes and treatments are as indicated. Abbreviations: CA1/2/3, hippocampal pyramidal cell layers; DG, dentate gyrus; Hp, hippocampus; L2–6, S1 cortical layers; S1, primary somatosensory cortex.

In addition to the activation of the S1, whisker stimulation under anaesthesia also induced an over-expression of c-*fos* mRNA in the cortical layers of Shank3b$^{+/+}$ mice but not in Shank3b$^{-/-}$ mice compared to anaesthetised unstimulated controls (Fig. 19A-C; Tukey post-hoc test following one-way ANOVA, anaesthesia WT vs WS WT vs. WS $P < 0.0001$; anaesthesia KO vs WS KO $P > 0.05$).

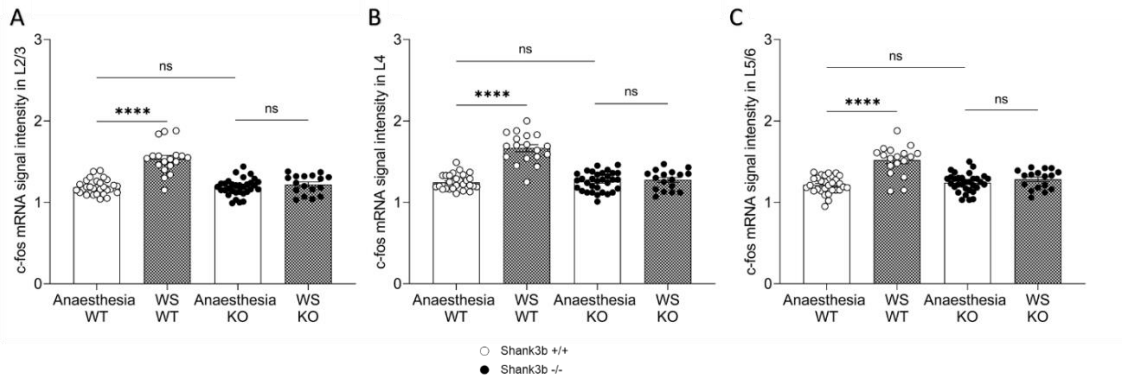

Fig. 19. c-*fos* mRNA expression is upregulated in S1 layers of Shank3b$^{+/+}$ but not Shank3b$^{-/-}$ mice following whisker stimulation under anaesthesia (WS) compared to anaesthesia only controls. (A-C) Quantification of c-*fos* mRNA signal intensity in S1 layers following WS and anaesthesia only. Values are expressed as mean signal intensities ±SEM. ****p<0.0001, Tukey post-hoc test following one-way ANOVA (n=19 sections from 3 Shank3b$^{+/+}$ mice and 18 sections from 3 Shank3b$^{-/-}$ mice following WS and n=30 sections from 4 Shank3b$^{+/+}$ mice and 32 sections from 4 Shank3b$^{-/-}$ mice following anaesthesia). Genotypes, treatments, and S1 cortical layers (L2-6) are as indicated.

Moreover, WS induced a significant c-*fos* mRNA upregulation in the ventral postero-medial nucleus of the thalamus (VPM, somatosensory thalamus, which receives afferents from whiskers via brainstem nuclei and projects to S1 layer 4; Petersen 2007; Diamond et al., 2008) and amygdala of Shank3b$^{+/+}$ but not Shank3b$^{-/-}$ mice, as compared to controls (Fig. 20C and D; Tukey post-hoc test following one-way ANOVA, anaesthesia WT vs WS WT vs. WS $P < 0.001$ for Vpm and $P < 0.0001$ for Amy; anaesthesia KO vs WS KO $P > 0.05$). No difference in c-*fos* mRNA expression was detected between the two genotypes in other brain regions analysed (Fig. 20A and B; one-way ANOVA, Sham vs WN in Shank3b$^{+/+}$ and Shank3b$^{-/-}$, $P > 0.05$).

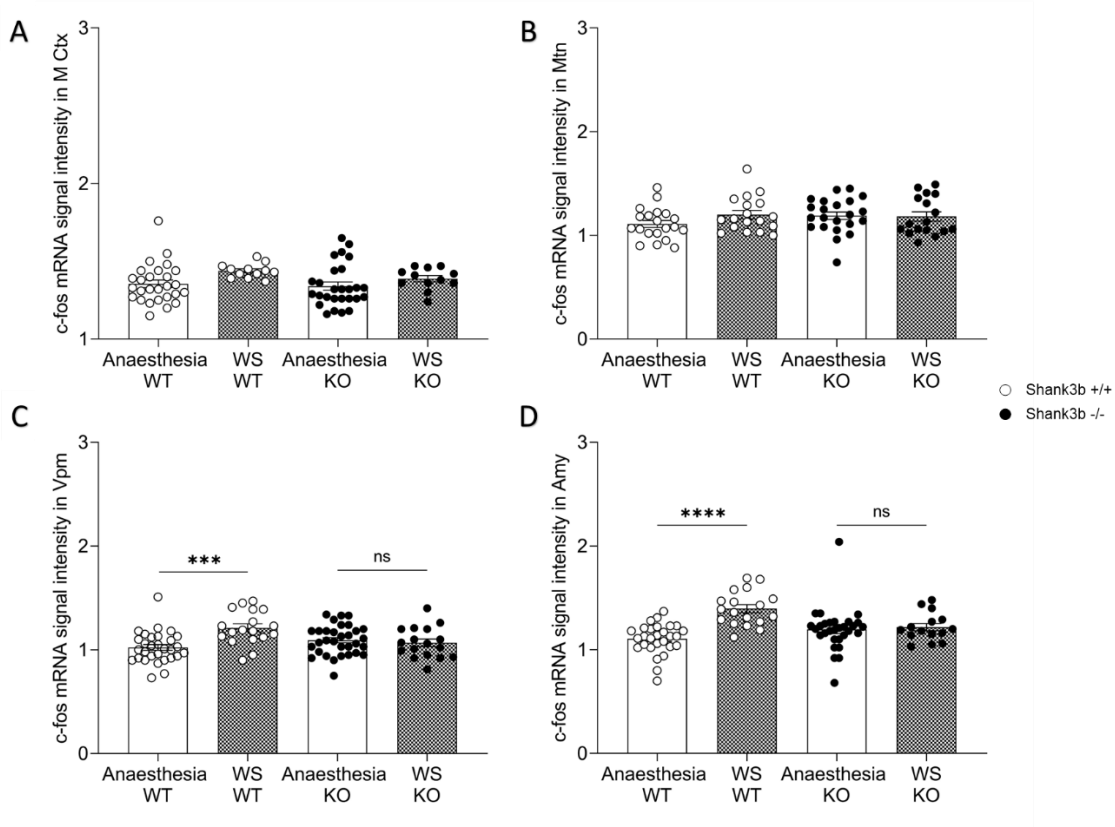

Fig.20. c-*fos* mRNA expression in other brain regions from Shank3b$^{+/+}$ and Shank3b$^{-/-}$ mice following whisker stimulation under anesthesia (WS) or anaesthesia only. (A, B) Shank3b$^{+/+}$ and Shank3b$^{-/-}$ mice did not show any difference in c-*fos* mRNA in the motor cortex (M Ctx, A) and medial thalamic nuclei (Mtn, B) in the two experimental conditions. (C, D) c-*fos* mRNA upregulation was detected only in the ventral postero-medial nucleus of the thalamus (Vpm, C) and amygdala (Amy, D) of Shank3b$^{+/+}$ mice. Values are expressed as mean signal intensities ±SEM. ***p<0.001 in Vpm, ****p<0.0001 in Amy and p>0.05 for all other brain areas, Tukey post-hoc test following one-way-ANOVA (n=19 sections from 3 Shank3b$^{+/+}$ mice and 18 sections from 3 Shank3b$^{-/-}$ mice following WS and n=30 sections from 4 Shank3b$^{+/+}$ mice and 32 sections from 4 Shank3b$^{-/-}$ mice following anaesthesia). Genotypes and treatments are as indicated.

Altogether these findings indicate that in Shank3b$^{-/-}$ mice, whisker stimulation does not result in c-*fos* mRNA induction in both S1 and hippocampus as for Shank3b$^{+/+}$ mice, suggesting impaired crosstalk between these two areas in Shank3b mutants.

Cntnap2$^{-/-}$ mice show increased c-*fos* expression in S1 following WS.

Despite being unaffected in the WN test (Fig. 12), Cntnap2$^{-/-}$ show a marked impairment in whisker-mediated texture discrimination (Fig. 10) compared to wild-type littermates. Therefore, we decided to investigate also in this mouse model the pattern of c-*fos* mRNA expression following WS (Fig. 21). WS induced c-*fos* mRNA expression in S1 of both genotypes, as compared to anaesthetized unstimulated animals; however, whisker-stimulated Cntnap2$^{-/-}$ mice showed a more pronounced c-*fos* induction in S1 (Fig. 21A). Quantification of c-*fos* mRNA mean signal intensity confirmed these observations (Fig. 21B; Tukey's post hoc following one-way ANOVA, anaesthesia Cntnap2$^{+/+}$ vs anaesthesia Cntnap2$^{-/-}$ $p > 0.05$; anaesthesia vs. WS $p = 0{,}0001$ in Cntnap2$^{+/+}$ and $p < 0{,}0001$ in Cntnap2$^{-/-}$; WS Cntnap2$^{+/+}$ vs WS Cntnap2$^{-/-}$, $p = 0{,}0062$).

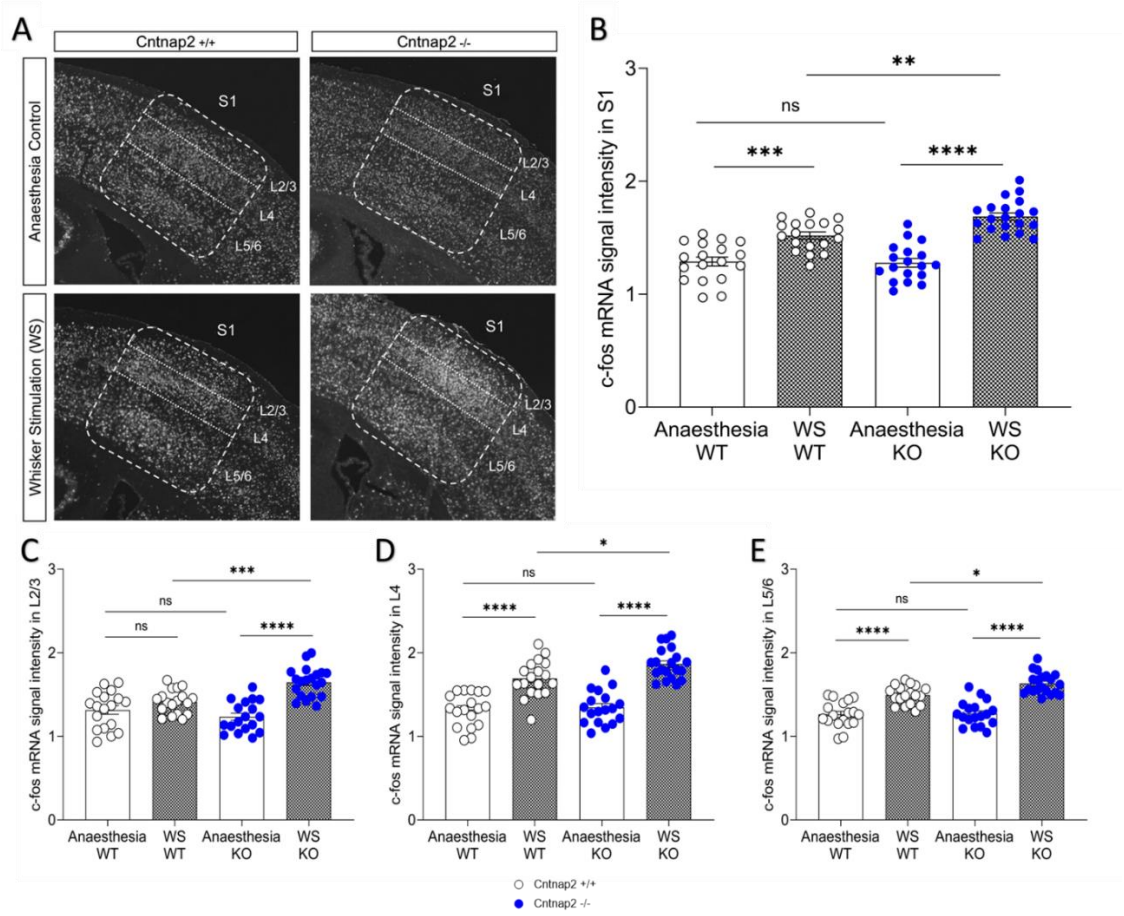

Fig.21. Increased neuronal activation in S1 of Cntnap2$^{-/-}$ mice following whisker stimulation under anaesthesia. (A). Representative images of c-*fos* mRNA in situ hybridization in S1 (white staining) of Cntnap2$^{+/+}$ and Cntnap2$^{-/-}$ mice, 20 min following anaesthesia only or whisker stimulation under anaesthesia (WS). Scale bar: 500 µm. (B) Quantification of c-*fos* mRNA signal intensity in S1. (C-E) Quantification of c-*fos* mRNA signal intensity in S1 layers 2/3 (C), 4 (D), and 5/6 (E). Values are expressed as mean normalized signal intensities ± SEM (n = 4–8 sections from 3 animals per genotype). **p < 0.01, ***p < 0.001, ****p < 0.0001. Genotypes and treatments are as indicated. Abbreviations: S1, primary somatosensory cortex; L2–6, S1 cortical layers.

Analysis of c-*fos* mRNA expression in cortical layers of S1 also revealed a similar pattern in L2/3, L4 and L5/6 (Fig. 21C-E; Tukey's post hoc following one-way ANOVA, anaesthesia vs WS $p < 0{,}0001$ in L2/3, L4, and L5/6). WS instead induced a similar c-*fos* mRNA upregulation in the somatosensory thalamus (VPM; Fig. 22A) and hippocampus (Fig. 22B) of both Cntnap2$^{+/+}$ and Cntnap2$^{-/-}$ mice, compared to anaesthetized unstimulated animals. No difference in c-*fos* mRNA signal intensity was detected between the two genotypes in other brain regions analysed, such as the motor cortex (Fig. 22C), medial thalamic nuclei (Fig. 22D) and amygdala (Fig. 22E).

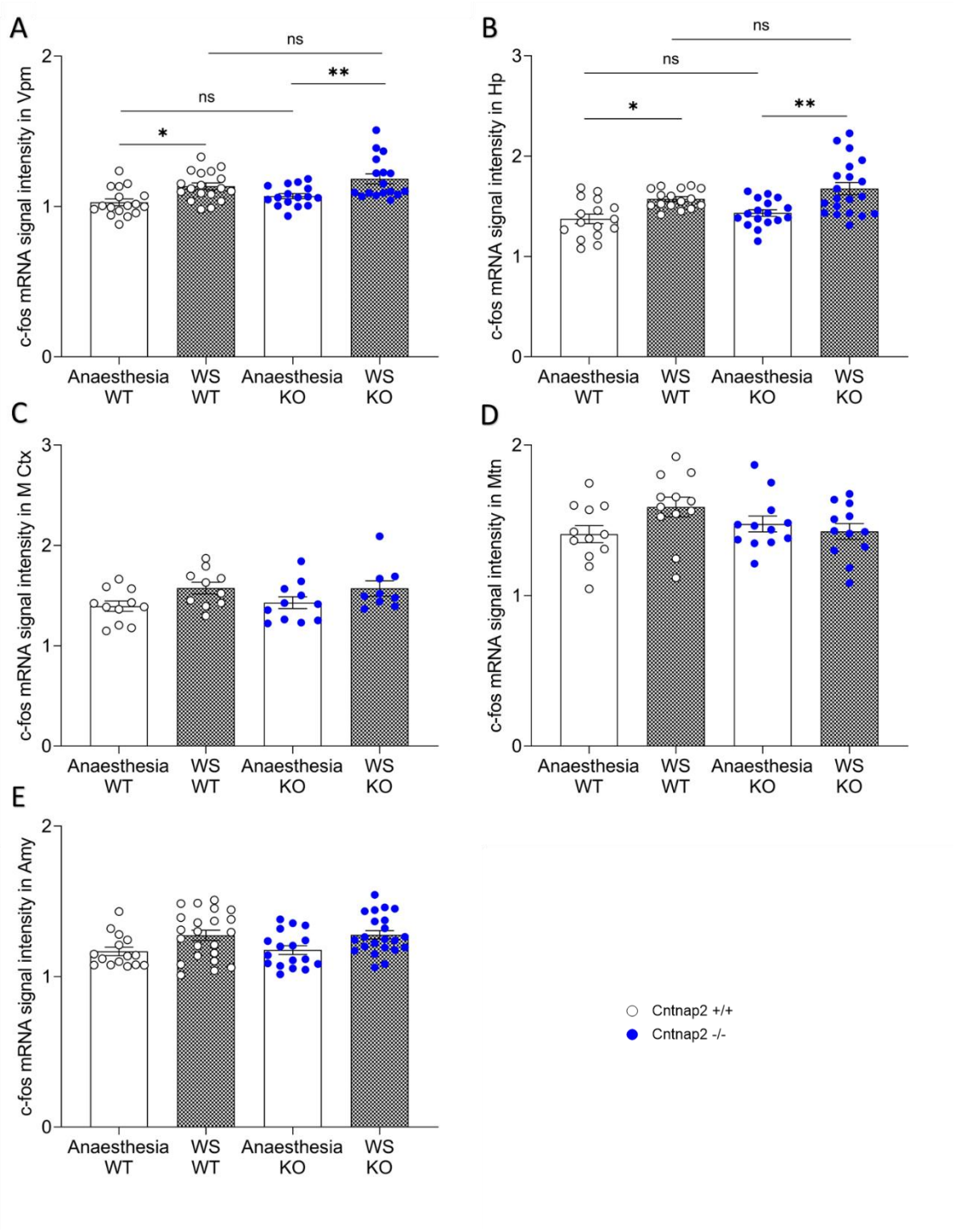

Fig. 22. c-*fos* mRNA expression in other brain regions from Cntnap2$^{+/+}$ and Cntnap2$^{-/-}$ mice following whisker stimulation under anesthesia (WS) or anesthesia only. (A, B) c-*fos* mRNA upregulation was detected in the ventral postero-medial nucleus of the thalamus (Vpm, A) and hippocampus (Hp, B) of Cntnap2$^{-/-}$ and control mice following WS. (C-E) Cntnap2$^{+/+}$ and Cntnap2$^{-/-}$ mice did not show any difference in c-*fos* mRNA in the motor cortex (M Ctx, C), medial thalamic nuclei (Mtn, D) and amygdala (Amy, E) in the two experimental conditions. Values are expressed as mean signal intensities ±SEM. *$p < 0.05$ **$p < 0.01$, Tukey post-hoc test following one-way-ANOVA (n = 2–8 sections from 3 animals per genotype). Genotypes and treatments are as indicated.

These results suggest that despite showing comparable behavioural responses following the WN test, Cntnap2$^{-/-}$ mice display an increased c-*fos* expression in the S1 following stimulation of the whisker under anaesthesia.

Excitatory neurotransmission markers are over-expressed in the cortex of Cntnap2$^{-/-}$ mice.

We next used RT-qPCR to assess the expression of excitatory (vesicular glutamate transporters vGLUT1 and 2) and inhibitory (glutamic acid decarboxylase GAD1 and 2, parvalbumin Pvalb) markers in the neocortex of adult Cntnap2$^{+/+}$ and Cntnap2$^{-/-}$ mice. c-*fos* is a general marker of neuronal activation. Therefore, we used RT-qPCR to infer a putative involvement of excitatory vs inhibitory circuit in Cntnap2$^{-/-}$ mice evaluating the expression of the main markers of excitatory/inhibitory neurotransmission. vGLUT1 and 2 mRNAs were overexpressed in Cntnap2$^{-/-}$ mice compared to controls (*$p < 0.05$ unpaired t-test), while mRNA levels of inhibitory markers did not differ between the two genotypes (Fig. 23).

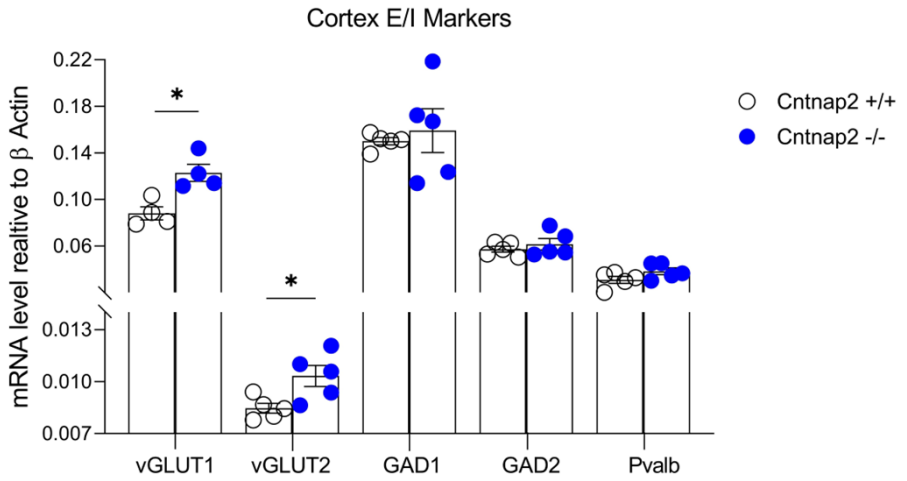

Fig. 23. Expression of excitatory and inhibitory neuron markers in the neocortex of Cntnap2$^{-/-}$ mice. Quantification of vGLUT1, vGLUT2, GAD1, GAD2, and Pvalb mRNA expression (RT-qPCR) in the neocortex of adult Cntnap2$^{+/+}$ and Cntnap2$^{-/-}$mice. For both genotypes, the expression level of each mRNA of interest was normalized on the expression of the β-actin reference gene, and the relative expression of each target was calculated (mean ± SEM of at least 4 replicates from pools of 5 animals per genotype; each dot represents a technical replicate; *$p < 0.05$ unpaired t-test.

These results suggest that an increased excitation/inhibition (E/I) ratio might underlie S1 overactivation and somatosensory discrimination deficits of Cntnap2$^{-/-}$ mice.

rs-fMRI connectivity mapping of Shank3b$^{-/-}$ showed hypoconnectivity between Hp and S1.

Previous research has demonstrated that Shank3b deletion results in significantly altered cortico-cortical functional connectivity (Pagani et al. 2019). Here we examined the rs-fMRI connectivity of the dorsal hippocampus, a part of the brain characterized by a reduced c-*fos* signal in Shank3b mutants, to see whether the regional deficits seen upon repetitive whisker stimulation could be connected to similarly impaired hippocampus-S1 functional synchronization (Fig. 24 and 25). Interestingly, reduced functional connectivity between the dorsal hippocampus and S1 was reported by rs-fMRI mapping ($|t| > 2$, P 0.05, and FWER cluster-corrected using a cluster threshold of P = 0.01, Fig. 24A). Quantification of rs-fMRI signal in regions of interest confirmed impaired functional connectivity between hippocampus and S1 ($t = 3.57$, $P = 0.002$, Fig. 5B), which, like the hippocampus, we found lacking activation by sensory stimuli in Shank3b$^{-/-}$ mice (Fig. 13, 15, 17 and 18).

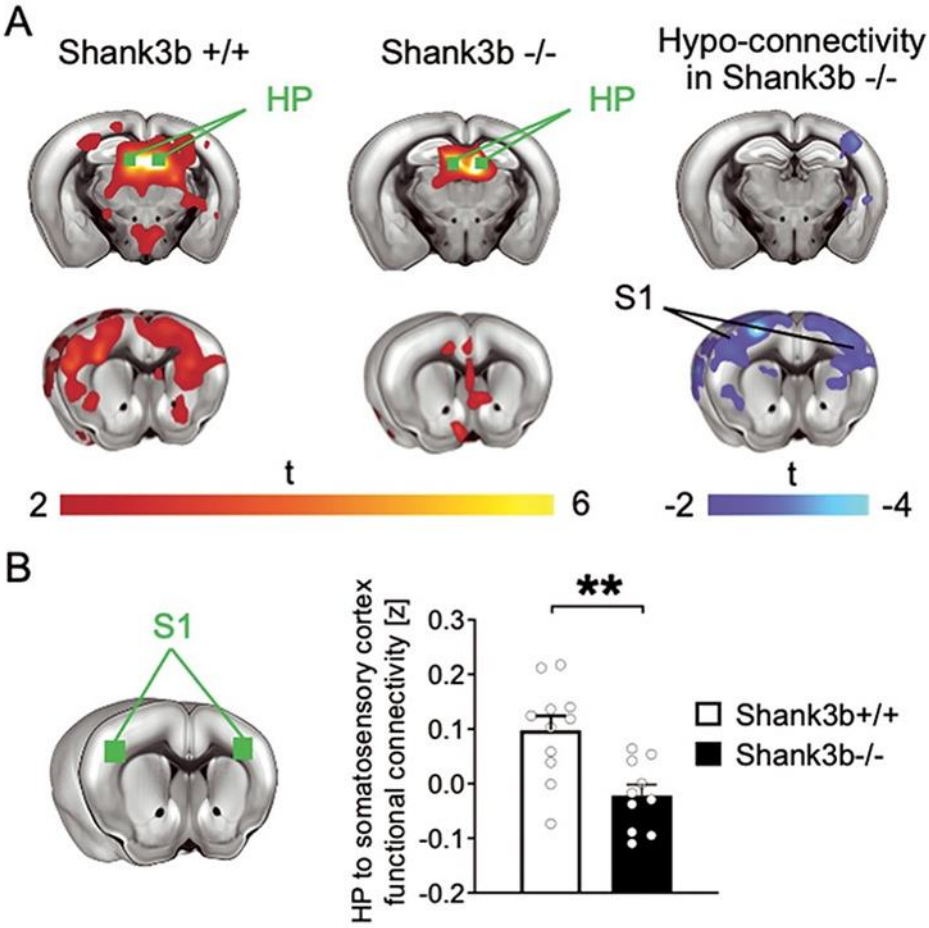

Fig. 24. Impaired functional connectivity between hippocampus and primary somatosensory cortex (S1) in Shank3b$^{-/-}$ mice. (A) Seed-based connectivity maps of the dorsal hippocampus in Shank3b$^{+/+}$ and Shank3b$^{-/-}$ mice. Red-yellow represents brain regions showing significant rs-fMRI functional connectivity with the dorsal hippocampus (HP) in Shank3b$^{+/+}$ (left) and Shank3b$^{-/-}$ mice (middle). The seed region is depicted in green. Brain regions showing significantly reduced rs-fMRI connectivity in Shank3b$^{-/-}$ mutants with respect to Shank3b$^{+/+}$ control littermates are depicted in blue/light blue (right). (B) Functional connectivity was also quantified in reference volumes of interest (green) placed in S1. Error bars represent SEM. **P < 0.01 (unpaired t-test, n = 11 Shank3b$^{+/+}$ and 10 Shank3b$^{-/-}$; each dot represents one animal). Genotypes are as indicated.

To rule out the existence of connectivity alterations between VPM and S1, and between these two regions and the brainstem trigeminal nucleus (TN), we then performed a seed-based connectivity analysis of the VPM and S1. Shank3b$^{-/-}$ animals had intact rs-fMRI connectivity between the trigeminal nucleus and S1 following seed-based mapping of the VPM ($|t| > 2$, $P < 0.05$ and FWER cluster-corrected using a cluster threshold of $P = 0.01$, Fig. 25A). Similarly, Shank3b$^{-/-}$ mice had preserved connectivity between the VPM and TN when the seed was placed in the S1 ($|t| > 2$, $P < 0.05$ and FWER cluster-corrected using a cluster threshold of $P = 0.01$, Fig. 25B). The presence of unaltered rs-fMRI connectivity between the VPM and S1 was confirmed by quantifications in regions of interest ($t = 0.68$, $P = 0.50$, Fig. 25C).

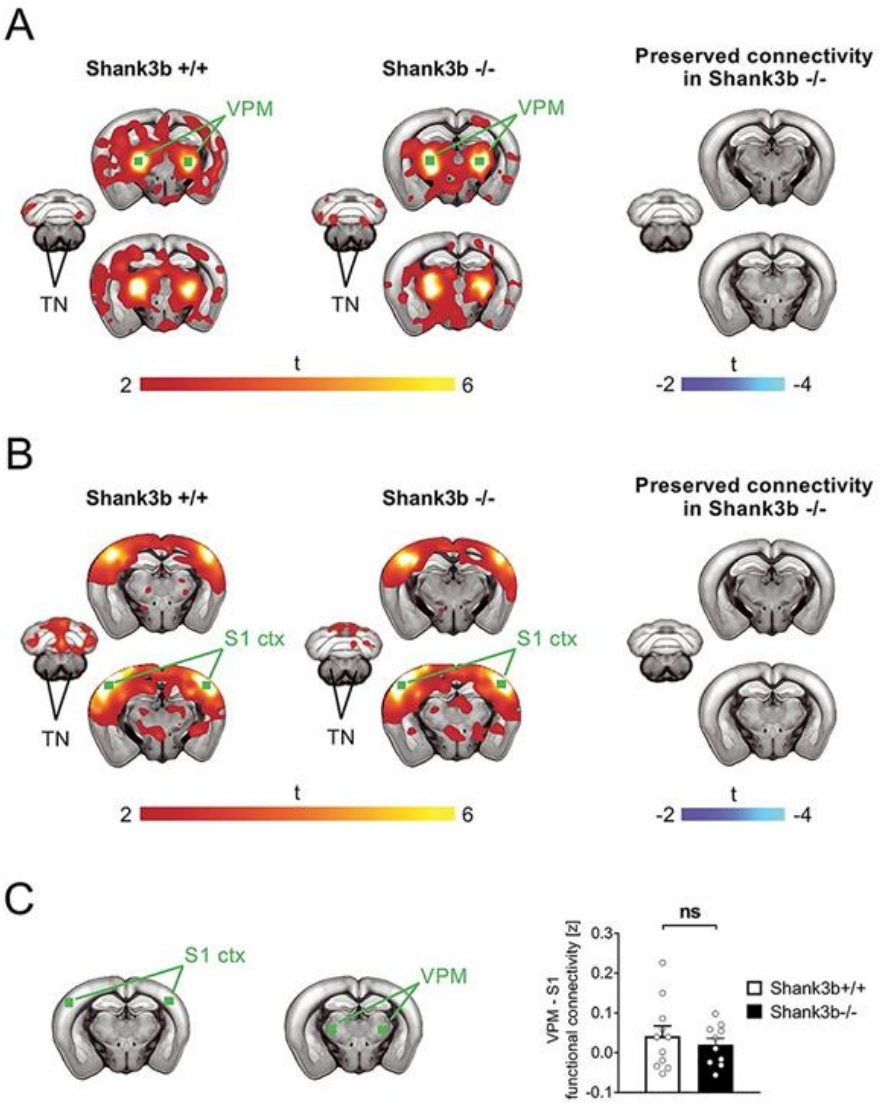

Fig. 25. Preserved functional connectivity between VPM, S1 and TN in Shank3b$^{-/-}$ mice. (A) Seed-based connectivity maps of the VPM in Shank3b$^{+/+}$ and Shank3b$^{-/-}$ mice. Red-yellow represents brain regions showing significant rs-fMRI functional connectivity with the VPM in Shank3b$^{+/+}$ (left) and Shank3b$^{-/-}$ mice (middle). Seed region is depicted in green. Intergroup genotype-dependent comparisons show unimpaired connectivity of the VPM in Shank3b$^{-/-}$ mice (right). (B) Seed-based connectivity maps of S1 in Shank3b$^{+/+}$ and Shank3b$^{-/-}$ mice. Red-yellow represents brain regions showing significant rs-fMRI functional connectivity S1 in Shank3b$^{+/+}$ (left) and Shank3b$^{-/-}$ mice (middle). Seed region is depicted in green. Intergroup genotype-dependent comparisons show preserved functional connectivity of S1 in Shank3b$^{-/-}$ mice (right). (C) Region-based quantifications confirmed that functional connectivity between VPM and S1 was unimpaired in Shank3b$^{-/-}$ mice, as quantified in reference volumes of interest (green) (unpaired t-test, t = 0.68, P = 0.50, n = 11 Shank3b$^{+/+}$ and n = 10 Shank3b$^{-/-}$ mice; each dot represents one animal). Error bars represent SEM.

These results suggest that a compromised functional coupling between the hippocampal and somatosensory areas may be the origin of the reduced cortical-hippocampal response shown in Shank3b mutants.

rs-fMRI connectivity mapping of Cntnap2$^{-/-}$ mice showed hyperconnectivity within S1s.

Previous studies reported that homozygous loss of Cntnap2 leads to profoundly altered prefronto-cortical functional coupling (Liska et al., 2018). Here we probed the rs-fMRI connectivity of S1 in Cntnap2 to investigate functional synchronization in somatosensory areas (Fig. 26A). Notably, voxelwise rs-fMRI connectivity mapping of S1 revealed increased functional connectivity within S1 ($t > 2$, $p < 0.05$ and FWER cluster-corrected using a cluster threshold of $p = 0.01$, Fig. 2A). Unilateral quantifications of rs-fMRI signal in regions of interest confirmed functional over-connectivity within the right ($t = 3.11$, $p = 0.005$, Fig. 26B, top panel) and left S1 ($t = 3.41$, $p = 0.002$, Fig. 26B, bottom panel). To rule out the presence of thalamo-cortical functional connectivity alterations in Cntnap2 mutants, we carried out voxelwise rs-fMRI connectivity mapping of the ventral posterior medial thalamic nucleus (VPM), which receives afferents from whiskers via brainstem nuclei and projects to S1 layer 4 (Petersen, 2007). Our analysis revealed unimpaired rs-fMRI of the VPM in Cntnap2 mutants as compared to wild-type littermates ($t > 2$, $p < 0.05$ and FWER cluster-corrected using a cluster threshold of $p = 0.01$, Fig. 26C). Preserved rs-fMRI connectivity of the VPM was confirmed by region-wise unilateral quantifications between right S1 and VPM ($t = 0.53$, $p = 0.063$, Fig. 26D, top panel) and between left S1 and VPM ($t = 0.51$, $p = 0.067$, Fig. 26D, bottom panel). Our set of functional connectivity analyses also revealed unimpaired rs-fMRI connectivity between S1 and VPM, and TN. These findings indicate an aberrant over-synchronization within somatosensory areas in Cntnap2 mutants.

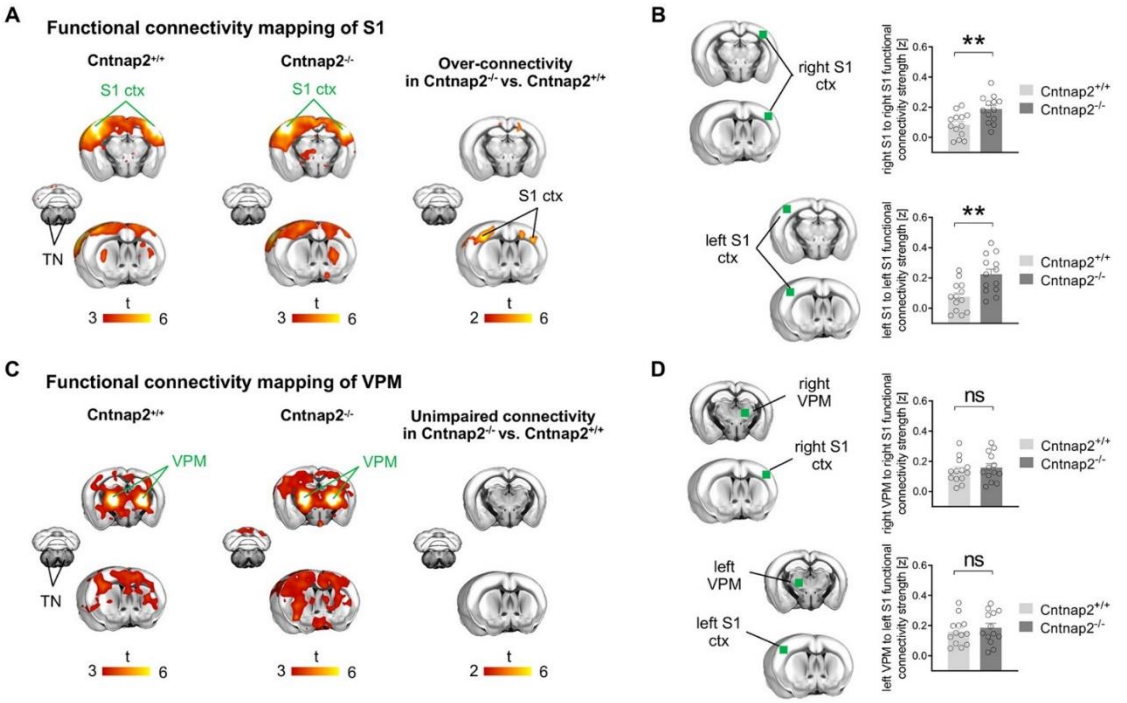

Fig. 26. Increased functional connectivity within the somatosensory cortex of Cntnap2$^{-/-}$ mice. (A) Seed-based connectivity maps of S1 cortex in Cntnap2$^{+/+}$ and Cntnap2$^{-/-}$ mice. Red-yellow represents brain regions showing significant rs-fMRI functional connectivity with the S1 in Cntnap2$^{+/+}$ (left) and Cntnap2$^{-/-}$ mice (middle). The seed region is depicted in green lettering. Brain regions showing rs-fMRI over-connectivity in Cntnap2$^{-/-}$ mice with respect to Cntnap2$^{+/+}$ control littermates are depicted in red-yellow (right). (B) Functional connectivity within the S1 was also quantified in unilateral reference volumes of interest (green). (C) Seed-based connectivity maps of the VPM. Red-yellow represents brain regions showing significant rs-fMRI functional connectivity with the VPM in Cntnap2$^{+/+}$ (left) and Cntnap2$^{-/-}$ mice (middle). The seed region is depicted in green lettering. No change of rs-fMRI connectivity of the VPM was detected in Cntnap2$^{-/-}$ mice with respect to Cntnap2$^{+/+}$ mice (right). (D). Functional connectivity between VPM and S1 was also quantified in unilateral reference volumes of interest (green). Error bars represent SEM. S1, primary somatosensory cortex; VPM, ventral posteromedial nucleus of the thalamus; TN, trigeminal nucleus. ** $p < 0.01$ (unpaired t-test, n = 13 Cntnap2$^{+/+}$ and n = 13 Cntnap2$^{-/-}$ mice, each dot represents one animal).

The contribution of the peripheral nervous system in shaping sensory responses in Shank3b$^{-/-}$ and Cntnap2$^{-/-}$ mice.

Given the reports of aberrant somatosensory processing in the central nervous system of adult Shank3b and Cntnap2 mutant mice following whisker stimulation, we next decided to investigate a possible peripheral contribution to such defects. The first step in proper tactile perception from the whiskers starts in the trigeminal ganglion (TG) which collects the mechanosensory neurons which respond to tactile stimuli. Ideally, this structure could represent a potential site of dysfunction for sensory processing. For this reason, we decided to perform a gene expression profiling of TG in Shank3b$^{-/-}$ and Cntnap2$^{-/-}$ mice, in both adult and juvenile stages. Numerous markers for sensory neurons were significantly upregulated in the trigeminal ganglia of either Shank3b$^{-/-}$ or Cntnap2$^{-/-}$ adult mice (Fig. 27A). Cck (FC=2.164, p=0.0001), Sst (FC=1.387, p=0.0333), P2X7 (FC=1.201, p=0.0378), and Calca (FC=1.222, p=0.0019) show significant increases in expression values in Cntnap2$^{-/-}$ trigeminal ganglia, similarly as Tacr1 (FC= 1.435, p=0.0006) and Trpa1 (FC= 1.154, p=0.0185) in Shank3b$^{-/-}$ samples. As in Cntnap2 KO TG, Calca mRNA was also upregulated in Shank3b$^{-/-}$ TG (FC=1.114, p=0.0144). Shank3b$^{-/-}$ and Cntnap2$^{-/-}$ adult mice also showed significant alteration in the expression of inhibitory markers (Fig. 27B) such as a downregulation in Gabra1 (for SHK FC=1.435, p<0.0001; for CNT FC= 1.072, p=0.0038) in the trigeminal ganglia. There was a significant decrease in the genetic expression of Gad2 (FC = 0.2379, p< 0.0001) in the TG of Shank3b$^{-/-}$ adults. On the other hand, genes such as Pvalb (FC=2.313, p< 0.0001), Gabra2 (FC=1.549, p< 0.0001), Gabrb2 (FC=1.399, p=0.0021), and Gabrb3 (FC=1.450, p=0.0434) were upregulated in the TG of these same mice. Markers for excitatory neuronal subtypes were also significantly differentially expressed in the trigeminal ganglia of KO adult animals (Fig. 27B). In Shank3b KO mice, Kcna1 was downregulated (FC= 0.8985, p= 0.0447). Additionally, upregulation of mGluR2

(FC=132.0, p= 0.0103) was found in Cntnap2 KO animals. Several markers for neuroinflammation (Fig. 27C) were downregulated in the adult Shank3b$^{-/-}$ TG, namely CCL-5 (FC=0.5115, p=0.0012), Tnf (FC=0.8403, p=0.0226), Iba1 (FC=0.7728, p=0.0476), and Tmem-119 (FC=0.7799, p=0.0103). qRT-PCR showed an increased expression of S100B mRNA in Shank3b KO TG (FC=1.519, p=0.0321). In Cntnap2$^{-/-}$ mice there was also an upregulation of iNOS expression (FC=1.864, p=0.0003). Conversely, Il-1b expression showed to be significantly decreased in Cntnap2$^{-/-}$ samples (FC=0.7344, p=0.0023). Finally, a significant increase in the gene expression was found among the neurotrophic markers tested in adult samples (Fig 27D), with TrkA (FC=1.205, p= 0.0332) showing upregulation in Shank3b$^{-/-}$ samples and Gdnf (FC=1.464, p=0.0404) in Cntnap2$^{-/-}$ samples.

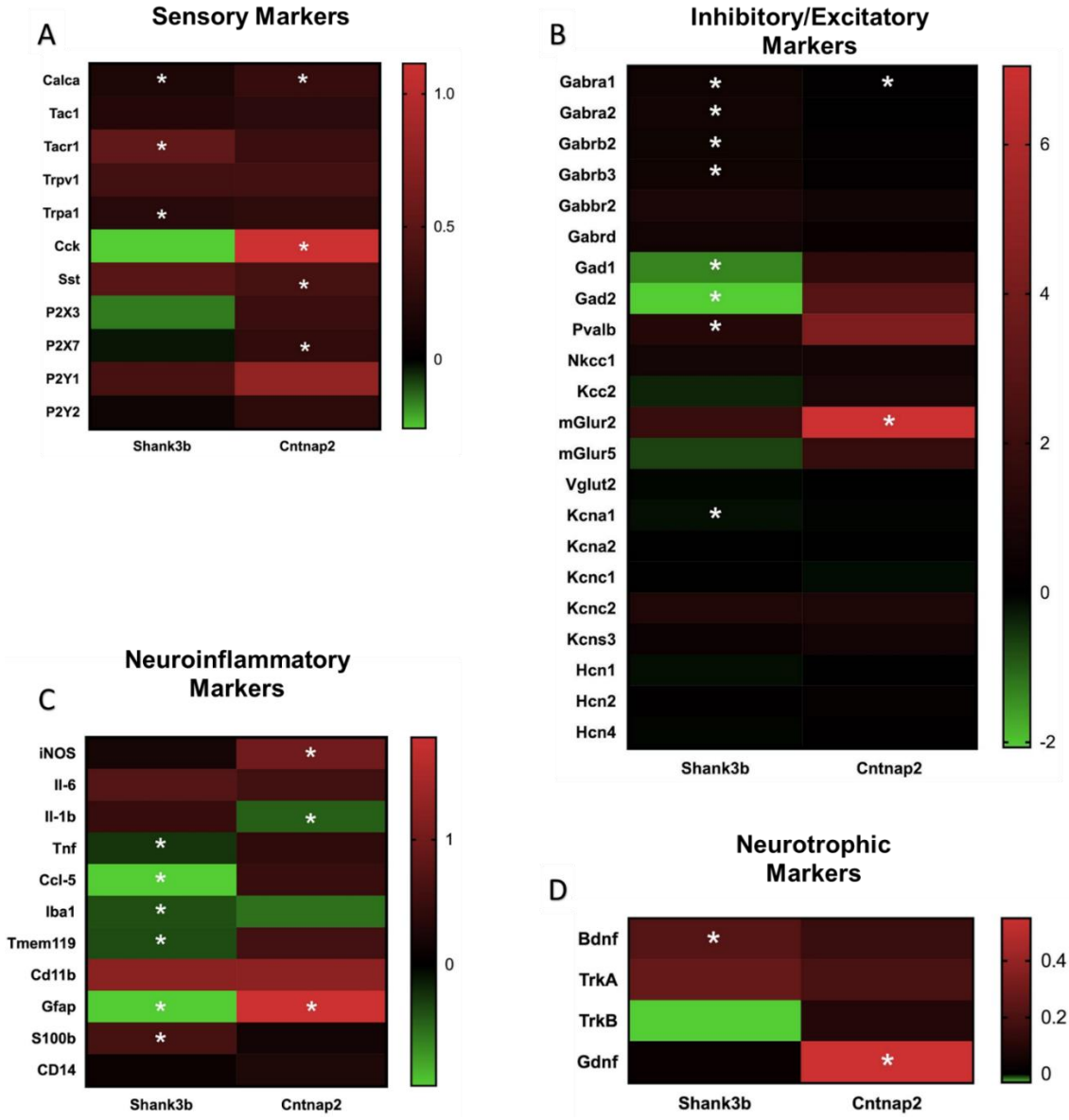

Fig. 27. Heatmap of Log2 fold change values for adult Shank3b and Cntnap2 TG. Values above 0 indicate an upregulation of the respective gene in KO mice relative to WT controls (in red). Conversely, values below 0 indicate downregulation of a gene in KO animals relative to WT controls (in green). Genes annotated with an asterisk (*) show a significant difference in expression values ($p < 0.05$).

qRT-PCR experiments on juvenile mice (Fig. 28) showed that only Shank3b$^{-/-}$ TGs display a significant difference in the expression of sensory markers, namely a decrease in P2X3 mRNA expression (FC= 0.6916, p=0.0031) and an increased expression of Cck (FC= 4.087, p=0.0220). Within the inhibitory markers tested, Gabrd was upregulated in Shank3b$^{-/-}$ trigeminal ganglia (FC=1.241, p 0.0016), while mGlur5 was upregulated in Shank3b$^{-/-}$ (FC=2.277, p= 0.0494) among the excitatory markers tested.

Of the neuroinflammatory markers tested in P30 mice, Il-1b was the only one resulting in a significant difference in fold change showing an upregulation (FC= 1.817, p= 0.0107) in Cntnap2$^{-/-}$ juvenile mice relative to controls. Lastly, in the category of neurotrophic markers, both TrkA and TrkB were downregulated (FC= 0.7446, p= 0.0472 for TrkA; FC= 0.8958, p=0.0175 for TrkB), while Gdnf was upregulated (FC= 2.086, p=0.0053) in the Shank3b$^{-/-}$ TG.

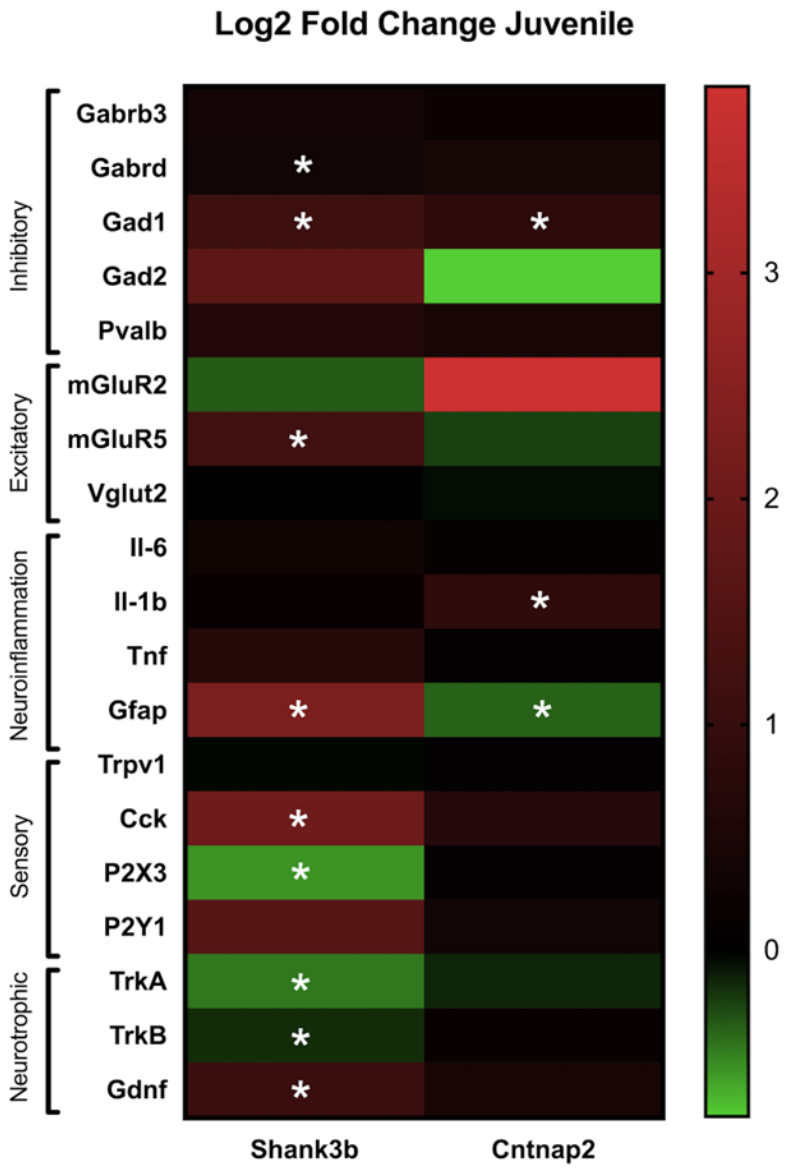

Fig. 28. Heatmap of Log2 fold change values for juvenile (P30) Shank3b and Cntnap2 TG. Values above 0 indicate an upregulation of the respective gene in KO mice relative to WT controls (in red). Conversely, values below 0 indicate downregulation of a gene in KO animals relative to WT controls (in green). Genes annotated with an asterisk (*) show a significant difference in expression values ($p < 0.05$).

Of particular interest was the expression pattern of Gad1 and GFAP transcripts as these genes showed differential expression in both adult and juvenile Shank3b$^{-/-}$ and Cntnap2$^{-/-}$ mice. At P30, Gad1 expression in both Shank3b$^{-/-}$ and Cntnap2$^{-/-}$ TG was significantly higher relative to WT controls (FC=2.193, p=0.0103 for Shank3b$^{-/-}$; FC=1.750, p=0.0397 for Cntnap2$^{-/-}$). In adulthood, a significant downregulation of this gene was found only in the case of Shank3b$^{-/-}$ TG (FC=0.3933, p<0.0001). Gfap expression showed opposed trends throughout development in the two mouse strains. Gfap mRNA was upregulated at P30 (FC=4.823, p=0.0403) and downregulated in adulthood (FC=0.5118, p=0.0030) in Shank3b$^{-/-}$ mice. In contrast, juvenile Cntnap2$^{-/-}$ mice showed Gfap downregulation (FC=0.7848, p=0.0173) followed by its upregulation in adulthood (FC=2.821, p=0.0117). These data suggest that the peripheral nervous system of Shank3b$^{-/-}$ and Cntnap2$^{-/-}$ show an aberrant regulation of genes involved in sensory and other pathways possibly contributing to behavioural abnormalities and c-*fos* deregulation in the central nervous system.

Discussion

Aberrant reactivity to sensory stimuli is a fundamental aspect of autism being reported in 90% of autistic individuals (Robertson and Baron-Cohen, 2017), yet the neuronal underpinnings of this trait are far to be understood. Both over and under-responsiveness to sensory stimulation are found in autistic individuals with a high degree of heterogeneity, a characteristic intrinsic to autism itself (DSM-V; Balasco et al., 2019). Tactile deficits, among others, appear to be the most reported by clinicians and families. Several studies point to a direct correlation between tactile deficits and ASD diagnosis, as well as to a predictive role of tactile abnormalities in the severity of autistic symptomatology developed later in life (Foss-Feig et al., 2012).

Both hyper- and hypo-sensitivity to tactile stimuli have been proposed to contribute to social deficits and other autism-related behaviours. Accordingly, sensory abnormalities are a common trait in mice harbouring ASD-relevant mutations (Balasco et al., 2019). Previous studies addressed somatosensory deficits in mouse models of ASD (He et al., 2017; Chelini et al., 2019; Chen et al., 2020; Orefice, 2020; Pizzo et al., 2020), including Shank3b$^{-/-}$ (Orefice et al., 2016; Orefice et al., 2019) and Cntnap2$^{-/-}$ mice (Peñagarikano et al., 2011; Dawes et al., 2018; Antoine et al., 2019). Mice use their whiskers for a variety of behaviours including conspecific interaction, exploration, and environmental navigation (Ahl, 1986; Brecht, 2007; Diamond et al., 2008; Diamond and Arabzadeh, 2013). Interestingly, whisker-dependent responses are affected in mouse strains bearing mutations in ASD-relevant genes (He et al. 2017; Chelini et al. 2019; Chen et al. 2020; Pizzo et al. 2020). Here we sought to investigate the neural substrates of whisker-dependent behaviours in Shank3b$^{-/-}$ and Cntnap2$^{-/-}$ mice.

We first used a version of tNORT specifically designed to favour whisker-mediated object exploration (see material and methods, Wu et al., 2013).

In this task, both Shank3b$^{-/-}$ and Cntnap2$^{-/-}$ with their relative controls showed no preference for the equally textured objects in the learning phase (Fig. 10A and C), indicating that they do not avoid object interaction with whiskers. In the testing phase, only Shank3b$^{+/+}$ and Cntnap$^{+/+}$ were able to discriminate among the textured objects (Fig. 10B and D), given their preference index score above 50% for the novel textured object. By contrast, Shank3b$^{-/-}$ mice spent significantly less time exploring the novel (differently textured) object, showing a preference for the familiar textured object instead (Fig. 10B); although a degree of variability in texture discrimination was present within mutant mice (8 out of 13 showed a preference index below 50%, while 5 out of 13 showed a preference index above 50%). In the same task, Cntnap2$^{-/-}$ mice were not able to discriminate between objects with different textures having a preference index of 50% (Fig. 10D). Together, these results indicate that Shank3b$^{-/-}$ and Cntnap2$^{-/-}$ mice do not avoid object interaction through whiskers yet show aberrant whisker-dependent texture discrimination. We cannot totally exclude the possibility that the hypo-locomotor phenotype of Shank3b$^{-/-}$ mice (Fig. 7) partially affects whisker-guided exploration, as suggested by the reduced distance travelled and velocity in both learning and testing phases of the tNORT (data not shown). However, Shank3b$^{-/-}$ mice spent the same amount of time investigating objects as controls in both the learning and testing phases of tNORT (Fig. 9A and B). In Cntnap2$^{-/-}$ mice, behavioural hyporeactivity to whisker stimulation would not be attributable to a generalized hypoactive phenotype, since Cntnap2 mutants showed hyperlocomotion in the open field arena (Fig. 8), as previously described in mice (Peñagarikano et al., 2011) and CDFE patients (Strauss et al., 2006).

We next asked whether Shank3b$^{-/-}$ and Cntnap2$^{-/-}$ mice were less prone to engage in proactive behaviours in response to novelty or threats. We

thus used the WN test to study the behavioural responses to active whisker stimulation (Fig. 5). This test has been traditionally intended to test sensory whisker-evoked reactivity in rats following traumatic brain injury (McNamara et al., 2010) and recently adapted to characterize whisker-dependent behaviours in mice harbouring ASD-relevant mutations (Chelini et al. 2019; Pizzo et al. 2020; Balasco et al., 2019). Here we used a quantitative approach to score behavioural responses to stimulus presentation (see materials and methods for details). We found a marked reduced avoidance behaviour in the Shank3b$^{-/-}$ mice following the WN test, as indicated by their lower score in the evasion and climbing and startle categories (Fig. 11C, D and E). During the sham session, both genotypes showed comparable responses in guarded, evading, climbing, and startle behaviours (Fig.11B-E), while Shank3b$^{-/-}$ mice displayed significantly more freezing (Fig. 11A). However, both Shank3b$^{+/+}$ and Shank3b$^{-/-}$ mice showed a comparable fear response (freezing and guarded behaviours) to repetitive whisker stimulation (Fig. 11A and B), suggesting that anxiety does not affect mice's performance in the WN test. Finally, we detected no major differences in behavioural scores between male and female mice of both genotypes, in line with other behavioural studies previously performed (Angelakos et al. 2019; Orefice et al. 2019). We also performed the WN test in Cntnap2 mutants and controls (Fig. 12) but did not find gross behavioural abnormalities. Both genotypes were comparable in the sham session for each behaviour analysed (Fig. 12A-E) and did not differ between genotypes across trials, suggesting an intact behavioural response to direct whisker stimulation. The hyporeactivity to whisker stimulation in Shank3b$^{-/-}$ mice and the normal behavioural response in Cntnap2$^{-/-}$ mice made us question the commonality of the two mouse models (despite common whisker-dependent texture discrimination). While both SHANK3 and CASPR2 are synaptic proteins and have in common the "location" at the synapse, their role is certainly different (SHANK3: postsynaptic scaffold protein

of glutamatergic synapses; CNTNAP2: adhesion molecule of neurexin superfamily at the synapses). Thus, a different behavioural response to whisker stimulation in the two genotypes reflects the difficulty of generalising a behavioural trait based on a mutation affecting the synapses. This led us to think that the neuronal bases of such behaviours may be divergent in the two models.

Recent studies performed in mice lacking ASD-associated genes showed that repetitive whisker stimulation modulates the expression of the immediate-early gene c-*fos* in several brain areas, including S1 (Chelini et al., 2019; Pizzo et al., 2020). For this reason, we investigated c-*fos* evoked responses following whisker stimulation in key brain areas involved in somatosensory processing. Whisker stimulation during WN resulted in c-*fos* mRNA downregulation in Shank3b$^{-/-}$ S1 but not the hippocampus (Fig. 13 and 15) and other brain areas (Fig. 16). Whisker stimulation in Shank3b$^{+/+}$ mice did not evoke an upregulation of c-*fos* expression in the hippocampus as expected, probably due to the fact the animals are freely moving in the WN test and baseline c-*fos* expression might mask the effect in this brain area. Indeed, whisker stimulation under anaesthesia, a more controlled setting, selectively downregulated c-*fos* mRNA expression in both S1 and hippocampus of Shank3b$^{-/-}$ mice (Fig. 18) but not in other brain areas analysed (Fig. 20). These results are reinforced by the fact that stimulation of whiskers in head-fixed awake Shank3b$^{-/-}$ mice showed the same pattern of c-*fos* mRNA deregulation (Fig. 17).

Recent findings showed that Shank3b$^{-/-}$ mice exhibit increased sensitivity to whisker stimulation in a vibrissae motion detection task (Chen et al. 2020). Specifically, Shank3b$^{-/-}$ mutants showed increased sensitivity to weak but not strong stimuli applied to the whiskers. The authors also showed that this hyper-reactivity to weak tactile stimulation was due to increased excitation/inhibition (E/I) balance

resulting from the increased firing of excitatory neurons and reduced firing of GABAergic interneurons in S1 (Chen et al. 2020). Accordingly, a reduced expression of the GABAergic marker parvalbumin was detected in Shank3b$^{-/-}$ brains (Filice et al. 2016; Orefice et al. 2019). Contrary to Chen et al. (2020), we show that Shank3b$^{-/-}$ mice are hypo-reactive to repetitive whisker stimulation (Fig. 11). However, the different experimental protocols used in the two studies (Chen et al. 2020: psychometric, imaging, and electrophysiological measurements following weak whisker stimulation in head-restrained mice; this study: behavioural phenotyping and c-*fos* mRNA expression analysis following repetitive whisker stimulation in freely moving animals) do not allow us to directly compare the obtained results. Further studies are needed to characterize the neuronal subtypes showing altered c-*fos* mRNA regulation in Shank3b$^{-/-}$ mice. Nevertheless, the absence of c-*fos* mRNA upregulation observed in Shank3b$^{-/-}$ S1 and hippocampus following repetitive whisker stimulation is consistent with synaptic impairment previously shown in Shank3 mutants (Bozdagi et al. 2010; Yang et al. 2012) and might reflect a diminished neuronal response to repetitive whisker stimulation.

Although Cntnap2$^{-/-}$ did not show behavioural alterations following the WN test we still decided to study c-*fos* mRNA modulation following whisker stimulation in the S1. The reasons for that were two-fold: firstly, the marked texture discrimination deficit showed by the Cntnap2$^{-/-}$ mice in the tNORT, and secondly, the fact that the absence of a hypo/hyper sensory response to whisker stimulation in the WN, per se, does not exclude the possibility of a circuit dysfunction (Liska et al., 2018). We found that, following WS, Cntnap2$^{-/-}$ mice showed c-*fos* mRNA upregulation of S1 (Fig.21) indicating an enhanced neuronal response following sensory stimulation of the whiskers. This is in line with reports of spontaneous seizure susceptibility in Cntnap2 $^{-/-}$ mice over 6 months

of age (Peñagarikano et al., 2011), a phenotype shared with CDFE patients (Strauss et al., 2006). Accordingly, we detected increased expression of excitatory but not inhibitory neuron markers in the neocortex of Cntnap2 mice (Fig. 23), confirming the increased E/I balance previously detected in these mutants (Antoine et al., 2019). Thus, the enhanced c-*fos* induction detected in the Cntnap2 S1 following WS might also depend on the hyperexcitable phenotype of Cntnap2 mutant mice. However, none of our animals tested exceeded 6 months of age, nor showed signs of epileptic seizures. Moreover, c-*fos* mRNA signal intensity in other brain regions analysed following WS tests did not show any difference between genotypes (Fig.22), thus rejecting the possibility that heightened c-*fos* mRNA expression was related to generalized hyperexcitability in this model.

GABAergic interneuron defects in Cntnap2$^{-/-}$ mice (Peñagarikano et al., 2011; Gao et al., 2018) might account for the increased neuronal activation within the S1 of Cntnap2$^{-/-}$ mice following whisker stimulation. Increased excitation/inhibition (E/I) ratio has been proposed as a common mechanism underlying the core features of ASDs (Rubenstein and Merzenich, 2003; Nelson and Valakh, 2015; Lee et al., 2017; Bozzi et al., 2018; Sohal and Rubenstein, 2019). Although recent data suggest that E/I imbalance might be a compensatory mechanism rather than the underlying cause (Antoine et al., 2019), acute changes in the E/I ratio have been reported to both induce or reduce ASD phenotypes (Yizhar et al., 2011; Selimbeyoglu et al., 2017). Increased excitability in the somatosensory cortex was indeed observed in young Cntnap2$^{-/-}$ mice, despite reduced whisker-evoked spiking (Antoine et al., 2019). Our data (Fig. 23) support the idea that E/I imbalance in the Cntnap2 neocortex is mostly due to a deregulated expression of excitatory but not inhibitory markers. Accordingly, other authors reported no change in GAD and Pvalb expression in the Cntnap2 neocortex (Lauber et al., 2018).

Moreover, previous studies showed that asynchronous firing patterns are present in S1 cortical neurons of Cntnap2$^{-/-}$ mice (Peñagarikano et al., 2011), accompanied by reduced dendritic spine density and impaired oscillations (Lazaro et al., 2019). This is in line with our data showing c-*fos* upregulation in S1 of Cntnap2 $^{-/-}$ mice following WS (Fig. 21) indicating a broad network dysfunction within S1 in these mutants.

The hippocampus receives inputs from the somatosensory cortex (Lavenex and Amaral 2000), and several studies indicate that many inputs control hippocampal neuron responses. CA1 pyramidal cells receive information from the whiskers via the somatosensory thalamus (VPM) and entorhinal cortex (Pereira et al. 2007). Somatosensory stimulation increases DG granule cell firing, while predominantly inhibitory responses occur in CA1 (Bellistri et al. 2013). Hippocampal neurons use afferent somatosensory information to dynamically update spatial maps (Pereira et al. 2007). Accordingly, a blockade of tactile transmission by applying lidocaine on the whisker pad decreased the firing rate of hippocampal place cells, resulting in expanding their place fields in the rat (Gener et al. 2013). Synchronized activity between S1 and the hippocampus is crucial for the formation of cognitive maps. In the rat, coherence between S1 firing and hippocampal activity increases when the animal collects sensory information through whiskers, and such coherence enhances the integration of somatosensory information in the hippocampus (Grion et al. 2016). In mice, tactile experience enrichment induces c-*fos* expression in the hippocampus and improves memory by modulating the activity of DG granule cells that receive sensory information from S1 via the entorhinal cortex (Wang et al. 2020). Chemogenetic activation of DG neurons receiving tactile stimuli results in memory enhancement, while inactivation of DG or S1-innervated entorhinal neurons has opposite effects (Wang et al. 2020). Thus, tactile experience modifies cognitive maps by modulating the activity of the S1

to hippocampus pathway, confirming the importance of this circuit in somatosensory information processing. Indeed, whisker stimulation in both Shank3b$^{+/+}$ and Cntnap2$^{+/+}$ mice induced upregulation of c-*fos* expression in the hippocampus (Fig. 18 for Shank3b and Fig. 22 for Cntnap2) and, while c-*fos* deregulation was found in Shank3b$^{-/-}$ mice (Fig. 17 and 18) compared to controls, Cntnap2$^{-/-}$ had intact c-*fos* expression (Fig. 22B), suggesting a common cortico-hippocampal pathway dysfunction in Shank3b mutant mice while a localised dysfunction in Cntnap2$^{-/-}$ mutants.

It is generally accepted that cognitive function relies on coordinated interactions within and across discrete neuronal networks, and several studies point to long- and short-range dysconnectivity within brain areas both in ASD patients (Müller and Fishman, 2018) and mouse models (Zerbi et al., 2021). Previous studies showed that Shank3$^{-/-}$ and Cntnap2$^{-/-}$ mice display disrupted prefronto-cortical functional connectivity (Pagani et al., 2019; Liska et al., 2018) and general patterns of hyperconnectivity across major brain structures including the neocortex were found in Cntnap2 mutants (Choe et al., 2021). Interestingly, a recent study by Choe and colleagues using two complementary whole-brain mapping approaches (rsfMRI and c-*fos*-iDISCO+ imaging) showed a high degree of correlation between activity-induced c-*fos* expression and functional connectivity maps in Cntnap2 mice, indicating that c-*fos* expression mapping represents a good proxy of functional connectivity in this ASD model (Choe et al., 2021). Within this framework, the observed rsfMRI hypo-connectivity between the dorsal hippocampus and S1 in Shank3b mutant (Fig.24) mice might represent a network substrate for the reduced activation of these areas (Fig. 14, 17 and 18) and restricted behavioural responses (Fig. 11) following repetitive whisker stimulation. This conclusion is strengthened by the observation that Shank3b$^{-/-}$ mice show a preserved

connectivity between S1 and thalamic/brainstem somatosensory areas (Fig. 25) and by the findings that sensory hyporeactivity has been reported in PMS patients (Tavassoli et al., 2021). In keeping with these findings, c-*fos* mRNA upregulation observed in Cntnap2$^{-/-}$ S1 following WS (Fig. 21) might reflect the hyperconnectivity pattern detected in this sensory area by rsfMRI (Fig. 26A and B), a phenotype shared with subjects bearing Cntnap2 polymorphisms (Scott-Van Zeeland et al., 2010). Moreover, the preserved connectivity between S1 and VPM (Fig. 26B and C) and the stronger whisker-dependent c-*fos* mRNA induction (detected in S1 but not in other brain areas; Fig. 21 and 22) suggest that abnormal whisker-dependent responses observed in Cntnap2$^{-/-}$ mice mostly depend on local circuit dysfunction within S1.

Together, the results presented so far would suggest higher-order CNS circuits as the preferred site of dysfunction in the encoding of sensory stimuli. Nonetheless, sensory neurons in the peripheral nervous system represent the very first station in the sensory system. Specifically, in the whisker somatosensory system, pseudounipolar neurons which receive sensory stimuli from the whisker pad have their cell bodies in the trigeminal ganglia. Thus, TG neurons represent the initial sites of processing of tactile stimuli then conveyed to CNS. Ideally, this structure represents a potential site of dysfunction underlying impairments in somatosensory perception in ASD individuals. While defects in the PNS have been reported in the dorsal root ganglion (DRG) of mouse models of ASD (Orefice et al., 2016; Orefice et al., 2019), there is no evidence of TG neuron dysfunctions in ASD.

To infer a possible peripheral contribution to such defects, we performed a gene expression profiling of TG in Cntnap2$^{-/-}$ and Shank3b$^{-/-}$ mice, in both adult and juvenile stages and found largely deregulated gene expression of several neuronal and non-neuronal markers (Fig. 27 and 28). Untangling the role of such markers based solely on their gene

expression throughout development carries an inherent level of difficulty as several cellular processes may interfere with and influence the resulting behavioural phenotypes. Specifically, we showed an increased mRNA expression in several sensory markers involved in nociception (Fig. 27A), such as Trap1, Calca, and Tacr1 in Shank3b$^{-/-}$ and Calca and Sst in Cntnap2$^{-/-}$ TG. Furthermore, P2X7, whose inhibition was found to ameliorate dendritic spine pathology and social deficits in Rett syndrome mice models (Garré et al., 2020) is upregulated in Cntnap2$^{-/-}$ adults. Such findings converge with previous studies reporting instances of increased pain sensitivity in ASD patients and animal models (Zhang et al., 2021; Failla et al., 2020). Other researchers however find a hyposensitivity in response to stimuli among ASD individuals and models (Dhamne et al., 2017; Allely, 2013). Altered expression of sensory markers P2X3 and Cck in juvenile Shank3b$^{-/-}$ mice (downregulated and upregulated respectively) attest to early changes in sensory marker expression which could contribute to the sensory dysfunction (Fig. 28). The purinergic P2X3 receptor (associated with nociception and hypersensitivity) is upregulated by inflammation, oxidative stress, pain, (Zhang et al., 2014; Wu et al., 2004) and epilepsy (Zhou et al., 2016), all of which have been documented in relation to ASD. A deregulated expression of these markers could directly affect the initial stages of sensory processing thereafter leading to hyper- or hyposensitivity typically seen among ASD mouse models.

Altered expression in inhibitory and excitatory markers was also found in TG from Shank3b$^{-/-}$ and Cntnap2$^{-/-}$ mice (Fig. 27B). Dysregulation in GABAergic marker expression and interneuron functioning is commonly seen among humans with ASD as well as within animal models of this disorder (Zhao et al., 2022; Cellot & Cherubini, 2014; Vogt et al., 2018). In line with this, we found that inhibitory markers, the majority of which were GABAergic, were among the most altered in Shank3b$^{-/-}$ and

Cntnap2$^{-/-}$ TG. An increase of GABAergic markers such as Gabra1, Gabra2, Gabrb2, and Gabrb3 in Shank3b$^{-/-}$ and Cntnap2$^{-/-}$ trigeminal ganglia could be interpreted as underlining increased inhibition and thus giving way to hyporeactive/hyposensitive behaviours found in adult Shank3b$^{-/-}$ and Cntnap2$^{-/-}$ mice. Our qRT-PCR results also unveiled an upregulation of excitatory markers. These results, suggesting increased excitability in both Shank3b and Cntnap2 models, seem to conflict with our findings on inhibitory markers. However, contrasting evidence exists on the role of excitatory markers in ASD (Oka & Takashima, 1999; Lohith et al., 2013; Chana et al., 2015; Cai et al., 2019). Moreover, the present results were of a smaller magnitude than that of other marker types. Our experiments showed an upregulation of inflammatory markers (Fig. 27C) such as S100b, iNOS, and Il-1b in the TG of Shank3b$^{-/-}$ and Cntnap2$^{-/-}$ mice. Other inflammatory markers (Tnf, Iba1, Ccl-5, and Tmem-119) were instead downregulated in the TG of Shank3b$^{-/-}$ and Cntnap2$^{-/-}$ mice. While no evidence of immune dysfunction in the trigeminal ganglia from ASD individuals or animal models has been reported so far, our data could signal a state of immunosuppression. Neuroinflammation has been proposed to contribute to the development of ASDs by prompting neuronal dysfunction that characterizes these conditions (Eissa et al., 2020). Our results are in line with several lines of research that document the elevated expression of inflammatory markers such as pro-inflammatory cytokines in the brain and blood of ASD subjects (Vargas et al., 2005; Zhao et al., 2021; Li et al., 2009; Rodriguez & Kern, 2011; Molloy et al., 2006). Finally, also genes encoding for neurotrophic factors and receptors were deregulated in Shank3b$^{-/-}$ and Cntnap2$^{-/-}$ TG (Fig. 27D). Growth factors have been traditionally implicated in the origins of neurodevelopmental disorders such as ASD and ADHD (Nickl-Jockschat & Michel, 2011) and both TrkB and TrkA pathways are deregulated in autism (Subramanian et al., 2015; Mostafa et al., 2021; Dinçel et al., 2013). In this context downregulation of these

neurotrophic receptors may compromise the function of crucial factors in early development.

Among the markers tested, the expression profiles of Gad1 and Gfap mRNA are particularly relevant. While Gad1 is downregulated in Shank3b$^{-/-}$ adults, its expression is upregulated in KO juveniles of both lines (Fig. 27B and Fig. 28). Gad1 encodes for the GAD67 enzyme crucial to GABA synthesis, particularly during early neurodevelopment (Feldblum et al., 1993), and its dysregulation may be involved in creating an excitatory/inhibitory imbalance (Rubenstein & Merzenich, 2003). Lower levels of both Gad1 mRNA and protein have been found in the postmortem brains of autistic adults (Fatemi et al., 2002; Chao et al., 2010; Yip et al., 2007; Zhubi et al., 2017) as well as in animal models (Peñagarikano et al., 2011) in several areas throughout the cerebral cortex. On the other hand, increased Gad1 expression has been documented in the cerebellum of postmortem autistic brains (Yip et al., 2008) and the prefrontal cortex of ASD animal models (Hou et al., 2018; El Idrissi et al., 2005). Gad1 overexpression correlates with increased GABA synthesis and therefore promotes inhibition (Dicken et al., 2015). Chemogenetic depolarization of GABAergic DRG reduces peripherally induced nociception, while decreasing inhibition by introducing GABA receptor antagonists on sensory ganglia trigger nociception (Du et al., 2017). Moreover, recent work on cortical networks (Haroush & Marom, 2019) suggests that inhibition may reduce discrimination between stimuli. Thus, upregulation of Gad1 in the TG of juvenile Shank3b$^{-/-}$ and Cntnap2$^{-/-}$ mice may lead to an increase in inhibition from sensory neurons upstream to higher-level sensory cortex leading to altered texture discrimination, as observed in these mice.

We also reported a Gfap mRNA upregulation in the juvenile Shank3b$^{-/-}$ and in the adult Cntnap2$^{-/-}$ TG (Fig. 27C and 28). Conversely, Gfap mRNA was downregulated in the TG of Shank3b$^{-/-}$ adults and Cntnap2$^{-/-}$ juveniles. The Gfap gene codes for GFAP expressed in glial cells, in the

TG specifically in satellite glial cells (Stephenson & Byers, 1995). GFAP expression has been reported to be deregulated in the brain of autistic subjects (Laurence & Fatemi, 2005; Edmonson et al., 2014; Crawford et al., 2015). Therefore, alterations in Gfap expression observed in juvenile and adult Shank3b$^{-/-}$ and Cntnap2$^{-/-}$ may reflect disturbances in astrocyte function that could compromise typical neural development and transmission as seen in ASD (Petrelli et al., 2016). A true understanding of the functional significance of these alterations in gene expression found in the TG of Shank3b$^{-/-}$ and Cntnap2$^{-/-}$ will only be achieved prior further investigations. Nonetheless, such results confirm that the trigeminal ganglion, as part of the PNS, could be involved in abnormal sensory processing in Shank3b$^{-/-}$ and Cntnap2$^{-/-}$ open avenues for the development of peripherally targeted treatments for tactile sensory deficits observed in ASD.

In this study, we report that adult Shank3b and Cntnap2 mutant mice, models of syndromic forms of autism, display aberrant whisker-dependent behaviours. This trait is associated with altered response and coupling of circuits involved in sensory processing at both central and peripheral levels. Specifically, we found that Shank3b$^{-/-}$ mice and Cntnap2$^{-/-}$ display an impaired texture discrimination ability through whiskers while showing intact exploration. While Shank3b$^{-/-}$ mice were found to be hypo-responsive to the stimulation of the whiskers compared to wild-type littermates, Cntnap2$^{-/-}$ were unaffected by the stimulation and behaved comparably to controls. Moreover, Shank3b$^{-/-}$ hypo-responsiveness was accompanied by a reduced c-*fos* mRNA expression in the primary somatosensory cortex and hippocampus. On the contrary, in Cntnap2$^{-/-}$ mice we found an increased c-*fos* mRNA induction in the primary somatosensory cortex. Using rs-fMRI, we detected decreased long-range functional connectivity between the hippocampus and the S1 in Shank3b$^{-/-}$ mice, while increased functional

connectivity within S1 in Cntnap2$^{-/-}$ mice was observed. In both mutant mice, these functional connectivity defects were specific for higher-order structures as thalamic and brainstem structures showed preserved functional connectivity. Finally, we probed the trigeminal ganglion as the first station in sensory neurotransmission in the whisker system and found deregulation of key neuronal and non-neuronal gene markers involved in cellular mechanisms (inhibition, excitation, neuroinflammation) in both adult and juvenile Shank3b$^{-/-}$ and Cntnap2$^{-/-}$ mice. Taken together, these results support the concept that impaired processing of sensory information may contribute to behavioural deficits in mouse models of ASD. However, the present study does not provide insights into the mechanisms responsible for the behavioural and circuit dysfunctions here reported. Moreover, since this study focuses on adult animals, it remains to be elucidated whether these defects appear early during development. Further studies are needed to fill these gaps and assess whether altered processing of sensory information within sensory hubs represents a common deficit in mice harbouring ASD-related mutations. Nonetheless, understanding the neuronal underpinnings of altered sensory behaviours in genetic mouse models of ASD paves the way to effective management of sensory impairments with the goal to give a better life to people with autism.

Gene Symbol	Gene name	Forward Sequence 5'->3'	Reverse Sequence 5'->3'
Beta Actin	Beta Actin	AATCGTGCGTGACATCAAAG	AAGGAAGGCTGGAAAAGAGC
Cntnap2	Contactin Associated Protein 2	GAGGGGAGAAAAAGCAAAGCAG	AACTGCTGTACCTTCCTTGGG
Shank3b	SH3 And Multiple Ankyrin Repeat Domains 3	TTACACCCACACCTGCCTTC	CACCATCCTCCTCGGGTTTC
Gad1	Glutamate Decarboxylase 1	AGATAGCCCTGAGCGACGAG	ATGGCCGATGATTCTGGTTC
Gabra2	GABA A Receptor Subunit Alpha 2	AGATTCAAAGCCACTGGAGG	CCAGCACCAACCTGACTG
Gabrb3	GABA A Receptor Subunit Beta 3	GAGGTCTTCACAAGCTCAAAATC	AGGCAGGGTAATATTTCACTCAG
Gabra1	GABA A Receptor Subunit Alpha 1	CTCTCCCACACTTTTCTCCC	CCGACAGTGTGCTCAGAATG
Gabrb2	GABA A Receptor Subunit Beta 2	TCAGAGGATGACTTTGCTA	GCACACAATAATGTTTACTAT
Gabbr2	GABA B Receptor Subunit Beta 2	TCAGAGGATGACTTTGCTA	GCACACAATAATGTTTACTAT
Gabrd	GABA A Receptor Subunit Delta	ATGCATTTGCCCACTTCAA	ATGGGTTTGAGTCTGGAACG
Gad2	Glutamate Decarboxylase 2	CATTCCTGTCCTTGCCTCTC	GTGCATCCTTTGTCCATGT
Pvalb	GABAergic Interneuron Subpopulation	TGTCGATGACAGACGTGCTC	TTCTTCAACCCCAATCTTGC
Nkcc1	SLC12A1 - Solute Carrier Family 12 Member 1	CCTCTCACGAACCCATTGG	GCTGGGATAGGTCTCTCTGT
Kcc2	SLC12A1 - Solute Carrier Family 12 Member 4	AGATCGAGAGCAACGACGAGAGG	GGTGGCGATCGAAGAAGAAT

Calca	Alpha CGRP Peptide	CCTGCAACACTGCCACCTGCG	GAAGGCTTCAGAGCCCACATTG
Tac1	Tachykinin Precursor 1 (Substance P)	ATGGCCAGATCTCTCACAAAAG	AAGATGAATAGATAGTGCGTTCAGG
Tacr1	Tachykinin Precursor 1 Receptor (Substance P-R)	GCTCTGTGCATGGGTCTCTT	AGGAAGGATGGCTCCAGGAT
Trpv1	Transient Receptor Potential Vanilloid 1	CAAACTCCACCCCACACTGA	AGGCCAAGACCCCAATCTTC
Trpa1	Transient Receptor Potential Cation Channel	AGGTGATTTTTAAAACATTGCTGAG	CTCGATAATTGATGTCTCCTAGCAT
Cck	Cholecystokinin	AGCGGCGTATGTCTGTGCGT	CACTGCGCCGGCCAAAATCC
Sst	Somatostatin	CCCCAGACTCCGTCAGTTTCT	TCTCTGTCTGGTTGGGCTCG
P2X3	Purinergic Receptor P2X 3	CAGGGCACTTCTGTCTTTGTC	AGCGGTACTTCTCCTCATTCTC
P2X7	Purinergic Receptor P2X 7	CGAGTTGGTGCCAGTGTGGA	CCTGCTGTTGGTGGCCTCTT
P2Y1	Purinergic Receptor P2Y 1	CCTGCGAAGTTATTTCATCTA	GTTGAGACTTGCTAGACCTCT
P2Y2	Purinergic Receptor P2Y 2	GCAGCATCCTCTTCCTCACCT	CATGTTGATGGCGTTGAGGGT
Cckar	Cholecystokinin Receptor A	GCTGCATAGCGTCACTTGG	GATGGAGTTAGACTGCAACC
Cckbr	Cholecystokinin Receptor B	CCAAGCTGCTGGCTAAGAAG	CTTAGCCTGGACAGAGAAGC
Cacna1c	Calcium Voltage-Gated Channel Subunit Alpha1 C	CGTTCTCATCCTGCTCAACACC	GAGCTTCAGGATCATCTCCACTG
Ramp1	Receptor (calcitonin) Activity Modifying Protein 1	GACGCTATGGTGTGACT	AGTGCAGTCATGAGCAG
Calcrl	Calcitonin Receptor-like	TGCTGGAATGACGTTGCAGC	GCCTTCACAGAGCATCCAGA
Il-6	Interleukin-6	GCCTTCTTGGGACTGATGCT	GACAGGTCTGTTGGGAGTGG
Il-1b	Interleukin-1b	ACGGACCCCAAAAGATGAAG	TTCTCCACAGCCACAATGAG
iNOS	Nitric Oxide Synthase 2, citokine - Inducible	CAGCTGGGCTGTACAAACCTT	CATTGGAAGTGAAGCGTTTCG
Tnf	Tumor Necrosis Factor	CAAAATTCGAGTGACAAGCC	TGTCTTTGAGATCCATGCCG

Ccl-5	C-C Motif Chemokine Ligand 5	AGAATACATCAACTATTTGGAGA	CCTTGCATCTGAAATTTTAATGA
Iba1	AIF1 - Allograft Inflammatory Factor 1	GTCCTTGAAGCGAATGCTGG	CATTCTCAAGATGGCAGATC
Tmem119	Transmembrane Protein 119	GTGTCTAACAGGCCCCAGAA	AGCCACGTGGTATCAAGGAG
Cd11b	IGAM - Integrin Subunit Alpha M	CCTTGTTCTCTTTGATGCAG	GTGATGACAACTAGGATCTT
Gfap	Glial Fibrillary Acidic Protein	TCCTGGAACAGCAAAACAAG	CAGCCTCAGGTTGGTTTCAT
S100b	S100 Calcium Binding Protein B	TGCCCTCATTGATGTCTTCCA	GAGAGAGCTCGTTGTTGATAAGCT
CD14	CD14 Molecule	GGCTTGTTGCTGTTGCTTC	CAGGGCTCCGAATAGAATCC
CD68	CD68 Molecule	AGGGTGGAAGAAAGGTAAAGC	AGAGCAGGTCAAGGTGAACAG
mGlurR5	Metabotropic Glutamate Receptor 5	ATCTGCCTGGGTTACTTGTG	GCAATACGGTTGGTCTTCG
mGluR2	GRM2 - Glutamate Metabotropic Receptor 2	AGGCCATGCTTTTTGCACTG	GAAGGCCTCAATGCCTGTCT
Vglut2	Vescicular Glutamatergic Transporter 2	TGCTACCTCACAGGAGAATGGA	GCGCACCTTCTTGCACAAAT
Kcna1	Voltage-Gated Potassium Channel Subunit Kv1.1	TTACCCTGGGCACGGAGATA	ACACCCTTACCAAGCGGATG
Kcna2	Voltage-Gated Potassium Channel Subunit Kv1.2	CATCTGCAAGGGCAACGTCAC	CCTTTGGAAGGAAGGAGGCA
Kcns3	Voltage-Gated Potassium Channel Subunit Kv9.3	CCCTGGACAAGATGAGGAAC	TTGATGCCCCAGTACTCGAT
Hcn2	Hyperpolarization Activated Cyclic Nucleotide Gated Potassium Channel 2	ATCGCATAGGCAAGAAGAACTC	CAATCTCCTGGATGATGGCATT

Hcn1	Hyperpolarization Activated Cyclic Nucleotide Gated Potassium Channel 1	CTCAGTCTCTTGCGGTTATTACG	TGGCGAGGTCATAGGTCAT
Kcnc1	Voltage-Gated Potassium Channel Subunit Kv3.1	GTGCCGACGAGTTCTTCTTC	GTCATCTCCAGCTCGTCCTC
Vglut1	Vescicular Glutamatergic Transporter 1	CCCCCAAATCCTTGCACTTT	AACAAATGGCCACTGAGAAACC
Knc2c	Voltage-Gated Potassium Channel Subunit Kv3.2	AGATCGAGAGCAACGAGAGG	GGTGGCGATCGAAGAAGAAT
Hcn4	Hyperpolarization Activated Cyclic Nucleotide Gated Potassium Channel 4	GCATGATGCTTCTGCTGTGT	GCTTCCCCCAGGAGTTATTC
Bdnf	Brain Derived Neurotrophic Factor	AGGCCAACTGAAGCAGTATTTC	CCGAACATACGATTGGGTAGTT
TrkA	Neurotrophic Receptor Tyrosine Kinase 1	GAAGAATGTGACGTGCTGGG	GAAGGAGACGCTGACTTGGA
TrkB	Neurotrophic Receptor Tyrosine Kinase 2	AAGGACTTTCATCGGGAAGCTG	TCGCCCTCCACACAGACAC
Gdnf	Glial Cell Derived Neurotrophic Factor	GCCACCATTAAAAGACTGAAAAGG	GCCTGCCGATTCCTCTCTCT

Table 1. Primers used for RT-qPCR.

Bibliography

Abrahams BS, Geschwind DH. Advances in autism genetics: on the threshold of a new neurobiology. Nat Rev Genet (2008) 9:341–55. doi: 10.1038/nrg2346

Ahl AS. 1986. The role of vibrissae in behavior: a status review. Vet Res Commun. 10:245–268.

Alarcon M, Abrahams BS, Stone JL, Duvall JA, Perederiy JV, Bomar JM, et al. Linkage, association, and gene-expression analyses identify CNTNAP2 as an autism-susceptibility gene. Am J Hum Genet (2008) 82:150–9. doi: 10.1016/j.ajhg.2007.09.005

Allely C. S. 2013. Pain sensitivity and observer perception of pain in individuals with autistic spectrum disorder. The Scientific World Journal, 2013, 916178

American Psychiatric A. Diagnostic and statistical manual of mental disorders: DSM-5. Arlington, VA: American Psychiatric Association (2013). doi: 10.1176/appi.books.9780890425596

American Psychiatric A. Diagnostic and statistical manual of mental disorders: DSM-3. Arlington, VA: American Psychiatric Association (1980).

Anderson GR, Galfin T, Xu W, Aoto J, Malenka RC, Südhof TC. 2012. Candidate autism gene screen identifies critical role for cell-adhesion molecule CASPR2 in dendritic arborization and spine development. Proc. Natl. Acad. Sci. U. S. A., 109 (2012), pp. 18120-18125

Angelakos CC, Tudor JC, Ferri SL, Jongens TA, Abel T. 2019. Home-cage hypoactivity in mouse genetic models of autism spectrum disorder. Neurobiol Learn Mem. 165:107000.

Antoine MW, Langberg T, Schnepel P, Feldman DE. 2019. Increased excitation-inhibition ratio stabilizes synapse and circuit excitability in four autism mouse models. Neuron, 101 (2019), pp. 648-661.e644

Arking DE, Cutler DJ, Brune CW, Teslovich TM, West K, Ikeda M, et al. A common genetic variant in the neurexin superfamily member CNTNAP2 increases familial risk of autism. Am J Hum Genet (2008) 82:160–4. doi: 10.1016/j.ajhg.2007.09.015

Ayres AJ, Robbins J. Sensory integration and the child. Torrance, CA: Western Psychological Services (1979).

Bailey A, Le Couteur A, Gottesman I, Bolton P, Simonoff E, Yuzda E, et al. Autism as a strongly genetic disorder: evidence from a British twin study. Psychol Med (1995) 25:63–77. doi: 10.1017/S0033291700028099

Balasco L, Chelini G, Bozzi Y, Provenzano G. 2019. Whisker nuisance test: a valuable tool to assess tactile hypersensitivity in mice. Bio Protocol. 9:e3331.

Balasco L, Provenzano G, Bozzi Y. 2020. Sensory abnormalities in autism spectrum disorders: a focus on the tactile domain, from genetic mouse models to the clinic. Front Psych. 10:1016.

Baranek GT, Berkson G. Tactile defensiveness in children with developmental disabilities: responsiveness and habituation. J Autism Dev Disord (1994) 24:457–71. doi: 10.1007/BF02172128

Baranek GT, Foster LG, Berkson G. Tactile defensiveness and stereotyped behaviors. Am J Occup Ther (1997) 51:91–5. doi: 10.5014/ajot.51.2.91

Baranek GT, Watson LR, Boyd BA, Poe MD, David FJ, Mcguire L. Hyporesponsiveness to social and nonsocial sensory stimuli in children with autism, children with developmental delays, and typically developing children. Dev Psychopathol (2013) 25:307–20. doi: 10.1017/S0954579412001071

Barnett K. A theoretical construct of the concepts of touch as they relate to nursing. Nurs Res (1972) 21:102–10. doi: 10.1097/00006199-197203000-00002

Bellistri E, Aguilar J, Brotons-Mas JR, Foffani G, de la Prida LM. 2013. Basic properties of somatosensory-evoked responses in the dorsal hippocampus of the rat. J Physiol. 591:2667–2686.

Ben-Sasson A, Cermak SA, Orsmond GI, Tager-Flusberg H, Carter AS, Kadlec MB, et al. Extreme sensory modulation behaviors in toddlers with autism spectrum disorders. Am J Occup Ther (2007) 61:584–92. doi: 10.5014/ajot.61.5.584

Bergman P, Escalona SK. Unusual sensitivities in very young children. Psychoanal Study Child (2001) 3(1):333–352. doi: 10.1080/00797308.1947.11823091

Bjornsdotter M, Gordon I, Pelphrey K, Olausson H, Kaiser M. Development of brain mechanisms for processing affective touch. Front In Behav Neurosci (2014) 8–24. doi: 10.3389/fnbeh.2014.00024

Blakemore S-J, Tavassoli T, Calò S, Thomas RM, Catmur C, Frith U, et al. Tactile sensitivity in Asperger syndrome. Brain Cogn (2006) 61:5–13. doi: 10.1016/j.bandc.2005.12.013

Bonnel A, Mottron L, Peretz I, Trudel M, Gallun E, Bonnel AM. Enhanced pitch sensitivity in individuals with autism: a signal detection analysis. J Cognit Neurosci (2003) 15:226–35. doi: 10.1162/089892903321208169

Bozdagi O, Sakurai T, Papapetrou D, Wang X, Dickstein DL, Takahashi N, Kajiwara Y, Yang M, Katz AM, Scattoni ML, et al. 2010. Haploinsufficiency of the autism-associated Shank3 gene leads to deficits in synaptic function, social interaction, and social communication. Mol Autism. 1:15.

Bozzi Y, Provenzano G, Casarosa S. Neurobiological bases of autism-epilepsy comorbidity: a focus on excitation/inhibition imbalance. Eur J Neurosci (2018) 47:534–48. doi: 10.1111/ejn.13595

Brauer J, Xiao Y, Poulain T, Friederici AD, Schirmer A. Frequency of maternal touch predicts resting activity and connectivity of the developing social brain. Cereb Cortex (2016) 26:3544–52. doi: 10.1093/cercor/bhw137

Brecht M. 2007. Barrel cortex and whisker-mediated behaviors. Curr Op Neurobiol. 17:408–416.

Cai, G., Wang, M., Wang, S., Liu, Y., Zhao, Y., Zhu, Y., Zhao, S., Zhang, M., Guo, B., Yao, H., Wang, W., Wang, J., & Wu, S. 2019. Brain mGluR5 in Shank3B-/- mice studied

with in vivo [18F]FPEB PET imaging and ex vivo immunoblotting. Frontiers in psychiatry, 10, 38

Cascio C, Mcglone F, Folger S, Tannan V, Baranek G, Pelphrey KA, et al. Tactile perception in adults with autism: a multidimensional psychophysical study. J Autism Dev Disord (2008) 38:127–37. doi: 10.1007/s10803-007-0370-8

Cascio CJ, Lorenzi J, Baranek GT. Self-reported pleasantness ratings and examiner-coded defensiveness in response to touch in children with ASD: effects of stimulus material and bodily location. J Autism Dev Disord (2016) 46:1528–37. doi: 10.1007/s10803-013-1961-1

Cellot, G., & Cherubini, E. 2014. GABAergic signaling as therapeutic target for autism spectrum disorders. Frontiers in pediatrics, 2, 70.

Chana, G., Laskaris, L., Pantelis, C., Gillett, P., Testa, R., Zantomio, D., Burrows, E. L., Hannan, A. J., Everall, I. P., & Skafidas, E. 2015. Decreased expression of mGluR5 within the dorsolateral prefrontal cortex in autism and increased microglial number in mGluR5 knockout mice: Pathophysiological and neurobehavioral implications. Brain, behavior, and immunity, 49, 197–205.

Chao, H. T., Chen, H., Samaco, R. C., Xue, M., Chahrour, M., Yoo, J., Neul, J. L., Gong, S., Lu, H. C., Heintz, N., Ekker, M., Rubenstein, J. L., Noebels, J. L., Rosenmund, C., & Zoghbi, H. Y. 2010. Dysfunction in GABA signalling mediates autism-like stereotypies and Rett syndrome phenotypes. Nature, 468(7321), 263–269.

Chelini G, Zerbi V, Cimino L, Grigoli A, Markicevic M, Libera F, Robbiati S, Gadler M, Bronzoni S, Miorelli S, et al. 2019. Aberrant somatosensory processing and connectivity in mice lacking Engrailed-2. The J Neurosci. 39:1525–1538.

Chen P, Hong W. Neural circuit mechanisms of social behavior. Neuron (2018) 98:16–30. doi: 10.1016/j.neuron.2018.02.026

Chen Q, Deister CA, Gao X, Guo B, Lynn-Jones T, Chen N, Wells MF, Liu R, Goard MJ, Dimidschstein J, et al. 2020. Dysfunction of cortical GABAergic neurons leads to sensory hyper-reactivity in a Shank3 mouse model of ASD. Nat Neurosci. 23:520–532.

Choe KY, Bethlehem RAI, Safrin M, Dong H, Salman E, Li Y, Grinevich V, Golshani P, Denardo LA, Peñagarikano O, Harris NG, Geschwind DH. 2021. Oxytocin normalizes altered circuit connectivity for social rescue of the Cntnap2 knockout mouse. Neuron., 110 (2021), pp. 795-808

Christian SL, Brune CW, Sudi J, Kumar RA, Liu S, Karamohamed S, et al. Novel submicroscopic chromosomal abnormalities detected in autism spectrum disorder. Biol Psychiatry (2008) 63:1111–7. doi: 10.1016/j.biopsych.2008.01.009

Coletta L, Pagani M, Whitesell JD, Harris JA, Bernhardt B, Gozzi A. 2020. Network structure of the mouse brain connectome with voxel resolution. Sci. Adv., 6 (eabb7187) (2020)

Connor C, Johnson K. Neural coding of tactile texture: comparison of spatial and temporal mechanisms for roughness perception. J Neurosci (1992) 12:3414–26. doi: 10.1523/JNEUROSCI.12-09-03414.1992

Crane L, Goddard L, Pring L. Sensory processing in adults with autism spectrum disorders. Autism (2009) 13:215–28. doi: 10.1177/1362361309103794

Crawford, J. D., Chandley, M. J., Szebeni, K., Szebeni, A., Waters, B., & Ordway, G. A. 2015. Elevated GFAP Protein in Anterior Cingulate Cortical White Matter in Males With Autism Spectrum Disorder. Autism research: official journal of the International Society for Autism Research, 8(6), 649–657.

Crawley JN. Designing mouse behavioral tasks relevant to autistic-like behaviors. Ment Retard Dev Disabil Res Rev (2004) 10:248–58. doi: 10.1002/mrdd.20039

D. Sinclair, B. Oranje, K.A. Razak, S.J. Siegel, S. Schmid. Sensory processing in autism spectrum disorders and fragile X syndrome - from the clinic to animal models Neurosci. Biobehav. Rev., 76 (2017), pp. 235-253

Dawes JM, Weir GA, Middleton SJ, Patel R, Chisholm KI, Pettingill P, Peck LJ, Sheridan J, Shakir A, Jacobson L, Gutierrez-Mecinas M, Galino J, Walcher J, Kühnemund J, Kuehn H, Sanna MD, Lang B, Clark AJ, Themistocleous AC, Iwagaki N, West SJ, Werynska K, Carroll L, Trendafilova T, Menassa DA, Giannoccaro MP, Coutinho E, Cervellini I, Tewari D, Buckley C, Leite MI, Wildner H, Zeilhofer HU, Peles E, Todd AJ, Mcmahon SB, Dickenson AH, Lewin GR, Vincent A, Bennett DL. 2018. Immune or genetic-mediated disruption of CASPR2 causes pain hypersensitivity due to enhanced primary afferent excitability. Neuron, 97 (2018), pp. 806-822

De La Torre-Ubieta L, Won H, Stein JL, Geschwind DH. Advancing the understanding of autism disease mechanisms through genetics. Nat Med (2016) 22:345. doi: 10.1038/nm.4071

Delorey TM. GABRB3 gene deficient mice: a potential model of autism spectrum disorder. In: International Review of Neurobiology. Cambridge, MA: Academic Press (2005). p. 359–82. doi: 10.1016/S0074-7742(05)71015-1

Dhamne, S. C., Silverman, J. L., Super, C. E., Lammers, S., Hameed, M. Q., Modi, M. E., Copping, N. A., Pride, M. C., Smith, D. G., Rotenberg, A., Crawley, J. N., & Sahin, M. 2017. Replicable in vivo physiological and behavioral phenotypes of the Shank3B null mutant mouse model of autism. Molecular autism, 8, 26.

Di Martino, A., Yan, CG., Li, Q. et al. The autism brain imaging data exchange: towards a large-scale evaluation of the intrinsic brain architecture in autism. Mol Psychiatry 19, 659–667 (2014). https://doi.org/10.1038/mp.2013.78

Diamond ME, Arabzadeh E. 2013. Whisker sensory system - from receptor to decision. Prog. Neurobiol., 103 (2013), pp. 28-40.

Diamond ME, Armstrong-James M, Budway MJ, Ebner FF. Somatic sensory responses in the rostral sector of the posterior group (POm) and in the ventral posterior medial nucleus (VPM) of the rat thalamus: dependence on the barrel field cortex. J Comp Neurol (1992) 319:66–84. doi: 10.1002/cne.903190108

Diamond ME, von Heimendahl M, Knutsen PM, Kleinfeld D, Ahissar E. 2008. 'Where' and 'what' in the whisker sensorimotor system. Nat Rev Neurosci. 9:601–612.

Dicken, M. S., Hughes, A. R., & Hentges, S. T. 2015. Gad1 mRNA as a reliable indicator of altered GABA release from orexigenic neurons in the hypothalamus. The European journal of neuroscience, 42(9), 2644–2653.

Dinçel N., Ünalp A., Kutlu A., Öztürk A., Uran N., Ulusoy S. Serum nerve growth factor levels in autistic children in Turkish population: a preliminary study. Indian J Med Res. 2013 Dec;138(6):900–3.

Dinstein I, Heeger D, Lorenzi L, Minshew N, Malach R, Behrmann M. Unreliable evoked responses in autism. Neuron (2012) 75:981–91. doi: 10.1016/j.neuron.2012.07.026

Domínguez-Iturza N, Lo AC, Shah D, Armendáriz M, Vannelli A, Mercaldo V, Trusel M, Li KW, Gastaldo D, Santos AR, et al. 2019. The autism- and schizophrenia-associated protein CYFIP1 regulates bilateral brain connectivity and behaviour. Nat Commun. 10:3454

Du, X., Hao, H., Yang, Y., Huang, S., Wang, C., Gigout, S., Ramli, R., Li, X., Jaworska, E., Edwards, I., Deuchars, J., Yanagawa, Y., Qi, J., Guan, B., Jaffe, D. B., Zhang, H., & Gamper, N. 2017. Local GABAergic signaling within sensory ganglia controls peripheral nociceptive transmission. The Journal of clinical investigation, 127(5), 1741–1756

Dunbar RIM. The social role of touch in humans and primates: behavioural function and neurobiological mechanisms. Neurosci Biobehavioral Rev (2010) 34:260–8. doi: 10.1016/j.neubiorev.2008.07.001

Durand CM, Betancur C, Boeckers TM, Bockmann J, Chaste P, Fauchereau F, et al. Mutations in the gene encoding the synaptic scaffolding protein SHANK3 are associated with autism spectrum disorders. Nat Genet (2007) 39:25–7. doi: 10.1038/ng1933

Dykes RW, Landry P, Metherate R, Hicks TP. Functional role of GABA in cat primary somatosensory cortex: shaping receptive fields of cortical neurons. J Neurophysiol (1984) 52:1066–93. doi: 10.1152/jn.1984.52.6.1066

Edmonson, C., Ziats, M. N., & Rennert, O. M. 2014. Altered glial marker expression in autistic post-mortem prefrontal cortex and cerebellum. Molecular autism, 5(1), 3.

Eissa, N., Sadeq, A., Sasse, A., & Sadek, B. 2020. Role of Neuroinflammation in Autism Spectrum Disorder and the Emergence of Brain Histaminergic System. Lessons Also for BPSD?. Frontiers in pharmacology, 11, 886.

El Idrissi, A., Ding, X. H., Scalia, J., Trenkner, E., Brown, W. T., & Dobkin, C. 2005. Decreased GABA(A) receptor expression in the seizure-prone fragile X mouse. Neuroscience letters, 377(3), 141–146.

Estes A, Zwaigenbaum L, Gu H, St John T, Paterson S, Elison JT, et al. Behavioral, cognitive, and adaptive development in infants with autism spectrum disorder in the first 2 years of life. J Neurodev Disord (2015) 7:24. doi: 10.1186/s11689-015-9117-6

Eveloff HH. The autistic child. Arch Gen Psychiatry (1960) 3:66–81. doi: 10.1001/archpsyc.1960.01710010068010

Failla, M. D., Gerdes, M. B., Williams, Z. J., Moore, D. J., & Cascio, C. J. 2020. Increased pain sensitivity and pain-related anxiety in individuals with autism. Pain reports, 5(6), e861.

Fatemi, S. H., Halt, A. R., Stary, J. M., Kanodia, R., Schulz, S. C., & Realmuto, G. R. 2002. Glutamic acid decarboxylase 65 and 67 kDa proteins are reduced in autistic parietal and cerebellar cortices. Biological psychiatry, 52(8), 805–810.

Feldblum, S., Erlander, M. G., & Tobin, A. J. 1993. Different distributions of GAD65 and GAD67 mRNAs suggest that the two glutamate decarboxylases play distinctive functional roles. Journal of neuroscience research, 34(6), 689–706.

Fernandez BA, Roberts W, Chung B, Weksberg R, Meyn S, Szatmari P, et al. Phenotypic spectrum associated with de novo and inherited deletions and duplications at 16p11.2 in individuals ascertained for diagnosis of autism spectrum disorder. J Med Genet (2010) 47:195–203. doi: 10.1136/jmg.2009.069369

Fernandez T, Morgan T, Davis N, Klin A, Morris A, Farhi A, et al. Disruption of contactin 4 (CNTN4) results in developmental delay and other features of 3p deletion syndrome. Am J Hum Genet (2004) 74:1286–93. doi: 10.1086/421474

Filice F, Vörckel KJ, Sungur AÖ, Wöhr M, Schwaller B. 2016. Reduction in parvalbumin expression not loss of the parvalbumin-expressing GABA interneuron subpopulation in genetic parvalbumin and shank mouse models of autism. Mol Brain. 9:10.

Filipkowski RK, Rydz M, Berdel B, Morys J, Kaczmarek L. 2000. Tactile experience induces c-fos expression in rat barrel cortex. Learn Mem. 7:116–122.

Foss-Feig JH, Heacock JL, Cascio CJ. 2012. Tactile responsiveness patterns and their association with core features in autism spectrum disorders. Res Autism Spectr Disord. 6:337–344.

Galle SA, Courchesne V, Mottron L, Frasnelli J. Olfaction in the autism spectrum. Perception (2013) 42:341–55. doi: 10.1068/p7337

Gao R, Piguel NH, Melendez-Zaidi AE, Martin-De-Saavedra MD, Yoon S, Forrest MP, Myczek K, Zhang G, Russell TA, Csernansky JC, Surmeier DJ, Penzes P. 2018. CNTNAP2 stabilizes interneuron dendritic arbors through CASK. Mol. Psychiatry, 23 (2018), pp. 1832-1850

Garré J.M., Silva H.M., Lafaille J.J., Yang G. 2020. P2X7 receptor inhibition ameliorates dendritic spine pathology and social behavioral deficits in Rett syndrome mice.Nat Commun. 11(1):1784.

Gener T, Perez-Mendez L, Sanchez-Vives MV. 2013. Tactile modulation of hippocampal place fields. Hippocampus. 23:1453–1462.

Ghaziuddin M, Ghaziuddin N, Greden J. Depression in persons with autism: implications for research and clinical care. J Autism Dev Disord (2002) 32:299–306. doi: 10.1023/A:1016330802348

Glessner JT, Wang K, Cai G, Korvatska O, Kim CE, Wood S, et al. Autism genome-wide copy number variation reveals ubiquitin and neuronal genes. Nature (2009) 459:569–73. doi: 10.1038/nature07953

Gliga T, Jones EJ, Bedford R, Charman T, Johnson MH. From early markers to neuro-developmental mechanisms of autism. Dev Rev (2014) 34:189–207. doi: 10.1016/j.dr.2014.05.003

Gordon A, Salomon D, Barak N, Pen Y, Tsoory M, Kimchi T, Peles E. 2016. Expression of Cntnap2 (Caspr2) in multiple levels of sensory systems. Mol. Cell. Neurosci., 70 (2016), pp. 42-53

Grandin T. An inside View of Autism. In: Schopler E, Mesibov GB, editors. High-Functioning Individuals with Autism. Springers: Boston, MA (1992). doi: 10.1007/978-1-4899-2456-8_6

Green SA, Rudie JD, Colich NL, et al. Over-reactive brain responses to sensory stimuli in youth with autism spectrum disorders. J Am Acad Child Adolesc Psychiatry. 2013;52:1158–1172

Grion N, Akrami A, Zuo Y, Stella F, Diamond ME. 2016. Coherence between rat sensorimotor system and hippocampus is enhanced during tactile discrimination. PLoS Biol. 14:e1002384.

Guclu B, Tanidir C, Mukaddes NM, Unal F. Tactile sensitivity of normal and autistic children. Somatosens Mot Res (2007) 24:21–33. doi: 10.1080/08990220601179418

Haigh SM, Gupta A, Barb SM, Glass SAF, Minshew NJ, Dinstein I, et al. Differential sensory fMRI signatures in autism and schizophrenia: analysis of amplitude and trial-to-trial variability. Schizophr Res (2016) 175:12–9. doi: 10.1016/j.schres.2016.03.036

Haroush, N., & Marom, S. 2019. Inhibition increases response variability and reduces stimulus discrimination in random networks of cortical neurons. Scientific reports, 9(1), 4969.

He CX, Cantu DA, Mantri SS, Zeiger WA, Goel A, Portera-Cailliau C. 2017. Tactile defensiveness and impaired adaptation of neuronal activity in the Fmr1 knock-out mouse model of autism. J Neurosci. 37:6475–6487.

Hertenstein MJ, Verkamp JM, Kerestes AM, Holmes RM. The communicative functions of touch in humans, nonhuman primates, and rats: a review and synthesis of the empirical research. Genet Soc Gen Psychol Monogr (2006b) 132:5–94. doi: 10.3200/MONO.132.1.5-94

Hertenstein MJ. Touch: its communicative functions in infancy. Hum Dev (2002) 45:70–94. doi: 10.1159/000048154

Hill RS, Walsh CA. Molecular insights into human brain evolution. Nature (2005) 437:64–7. doi: 10.1038/nature04103

Hilton CL, Harper JD, Kueker RH, Lang AR, Abbacchi AM, Todorov A, et al. Sensory responsiveness as a predictor of social severity in children with high functioning autism spectrum disorders. J Autism Dev Disord (2010) 40:937–45. doi: 10.1007/s10803-010-0944-8

Hollins M, Bensmaia SJ. The coding of roughness. Can J Exp Psychol (2007) 61:184–95. doi: 10.1037/cjep2007020

Hou, Q., Wang, Y., Li, Y., Chen, D., Yang, F., & Wang, S. 2018. A Developmental Study of Abnormal behaviors and altered GABAergic signaling in the VPA-treated rat model of autism. Frontiers in behavioral neuroscience, 12, 182.

Huguet G, Ey E, Bourgeron T. The Genetic Landscapes of Autism Spectrum Disorders. Annu Rev Genomics Hum Genet (2013) 14:191–213. doi: 10.1146/annurev-genom-091212-153431

Hussman JP. Suppressed GABAergic inhibition as a common factor in suspected etiologies of autism. J Autism Dev Disord (2001) 31:247–8. doi: 10.1023/a:1010715619091

Iurilli G, Datta SR. Population Coding in an Innately Relevant Olfactory Area. Neuron. 2017 Mar 8;93(5):1180-1197.e7. doi: 10.1016/j.neuron.2017.02.010.

Jabaudon D. Fate and freedom in developing neocortical circuits. Nat Commun (2017) 8:16042. doi: 10.1038/ncomms16042

Jamain S, Quach H, Betancur C, Rastam M, Colineaux C, Gillberg IC, et al. Mutations of the X-linked genes encoding neuroligins NLGN3 and NLGN4 are associated with autism. Nat Genet (2003) 34:27–9. doi: 10.1038/ng1136

Jiang YH, Ehlers MD. 2013. Modeling autism by SHANK gene mutations in mice. Neuron. 78:8–27

Juliano SL, Whitsel BL, Tommerdahl M, Cheema SS. Determinants of patchy metabolic labeling in the somatosensory cortex of cats: a possible role for intrinsic inhibitory circuitry. J Neurosci (1989) 9:1–12. doi: 10.1523/JNEUROSCI.09-01-00001.1989

Kaas JH. Somatosensory Cortex. In: Squire LR, editor. Encyclopedia of Neuroscience. Oxford Academic Press: (2004). p. 73–7. doi: 10.1016/B978-008045046-9.02028-3

Kanner L. Autistic disturbances of affective contact. Acta Paedopsychiatr (1968) 35:100–36.

Kerns CM, Kendall PC. The presentation and classification of anxiety in autism spectrum disorder. Clin Psychol: Sci Pract (2012) 19:323–47. doi: 10.1111/cpsp.12009

Kim HG, Kishikawa S, Higgins AW, Seong IS, Donovan DJ, Shen Y, et al. Disruption of neurexin 1 associated with autism spectrum disorder. Am J Hum Genet (2008) 82:199–207. doi: 10.1016/j.ajhg.2007.09.011

Lainhart JE. Brain imaging research in autism spectrum disorders: in search of neuropathology and health across the lifespan. Curr Opin Psychiatry. 2015 Mar;28(2):76-82. doi: 10.1097/YCO.0000000000000130. PMID: 25602243; PMCID: PMC4465432.

Lauber E, Filice F, Schwaller B. 2018. Dysregulation of parvalbumin expression in the Cntnap2-/- mouse model of autism spectrum disorder. Front. Mol. Neurosci., 11 (2018), p. 262.

Laurence, J. A., & Fatemi, S. H. 2005. Glial fibrillary acidic protein is elevated in superior frontal, parietal and cerebellar cortices of autistic subjects. Cerebellum, 4(3), 206–210.

Lavallee P, Deschenes M. Dendroarchitecture and lateral inhibition in thalamic barreloids. J Neurosci (2004) 24:6098–105. doi: 10.1523/JNEUROSCI.0973-04.2004

Lavenex P, Amaral DG. 2000. Hippocampal-neocortical interaction: a hierarchy of associativity. Hippocampus. 10:420–430.

Lawson-Yuen A, Saldivar JS, Sommer S, Picker J. Familial deletion within NLGN4 associated with autism and Tourette syndrome. Eur J Hum Genet (2008) 16:614–8. doi: 10.1038/sj.ejhg.5202006

Lazaro MT, Taxidis J, Shuman T, Bachmutsky I, Ikrar T, Santos R, Marcello GM, Mylavarapu A, Chandra S, Foreman A, Goli R, Tran D, Sharma N, Azhdam M, Dong H, Choe KY, Peñagarikano O, Masmanidis SC, Rácz B, Xu X, Geschwind DH, Golshani P. Reduced Prefrontal Synaptic Connectivity and Disturbed Oscillatory Population Dynamics in the CNTNAP2 Model of Autism. Cell Rep. 2019 May 28;27(9):2567-2578.e6. doi: 10.1016/j.celrep.2019.05.006. PMID: 31141683; PMCID: PMC6553483.

Le Couteur A, Bailey A, Goode S, Pickles A, Robertson S, Gottesman I, et al. A broader phenotype of autism: the clinical spectrum in twins. J Child Psychol Psychiatry (1996) 37:785–801. doi: 10.1111/j.1469-7610.1996.tb01475.x

Leblanc JJ, Fagiolini M. Autism: a "critical period" disorder? Neural Plast (2011) 2011:921680. doi: 10.1155/2011/921680

Lee E, Lee J, Kim E. 2017. Excitation/inhibition imbalance in animal models of autism spectrum disorders. Biol. Psychiatry, 81 (2017), pp. 838-847

Li, X., Chauhan, A., Sheikh, A. M., Patil, S., Chauhan, V., Li, X. M., Ji, L., Brown, T., & Malik, M. 2009. Elevated immune response in the brain of autistic patients. Journal of neuroimmunology, 207(1-2), 111–116.

Liska A, Bertero A, Gomolka R, Sabbioni M, Galbusera A, Barsotti N, Panzeri S, Scattoni ML, Pasqualetti M, Gozzi A. 2018. Homozygous loss of autism-risk gene CNTNAP2 results in reduced local and long-range prefrontal functional connectivity. Cereb. Cortex, 28 (2018), pp. 1141-1153.

Lohith, T.G., Osterweil, E.K., Fujita, M. et al. 2013. Is metabotropic glutamate receptor 5 upregulated in prefrontal cortex in fragile X syndrome?. Molecular Autism 4, 15

Lottem E, Azouz R. Mechanisms of tactile information transmission through whisker vibrations. J Neurosci (2009) 29:11686–97. doi: 10.1523/JNEUROSCI.0705-09.2009

Ma PM. The barrelettes–architectonic vibrissal representations in the brainstem trigeminal complex of the mouse. I. Normal structural organization. J Comp Neurol (1991) 309:161–99. doi: 10.1002/cne.903090202

Marco EJ, Hinkley LB, Hill SS, Nagarajan SS. Sensory processing in autism: a review of neurophysiologic findings. Pediatr Res (2011) 69:48R–54R. doi: 10.1203/PDR.0b013e3182130c54

Marco EJ, Khatibi K, Hill SS, Siegel B, Arroyo MS, Dowling AF, et al. Children with autism show reduced somatosensory response: an MEG study. Autism Res (2012) 5:340–51. doi: 10.1002/aur.1247

Markram H, Toledo-Rodriguez M, Wang Y, Gupta A, Silberberg G, Wu C. Interneurons of the neocortical inhibitory system. Nat Rev Neurosci (2004) 5:793. doi: 10.1038/nrn1519

Mccormick DA. GABA as an inhibitory neurotransmitter in human cerebral cortex. J Neurophysiol (1989) 62:1018–27. doi: 10.1152/jn.1989.62.5.1018

McNamara KC, Lisembee AM, Lifshitz J. The whisker nuisance task identifies a late-onset, persistent sensory sensitivity in diffuse brain-injured rats. J Neurotrauma. 2010 Apr;27(4):695-706. doi: 10.1089/neu.2009.1237. PMID: 20067394; PMCID: PMC2867628.

Mikkelsen M, Wodka EL, Mostofsky SH, Puts NAJ. Autism spectrum disorder in the scope of tactile processing. Dev Cogn Neurosci (2018) 29:140–50. doi: 10.1016/j.dcn.2016.12.005

Molloy, C. A., Morrow, A. L., Meinzen-Derr, J., Schleifer, K., Dienger, K., Manning-Courtney, P., Altaye, M., & Wills-Karp, M. 2006. Elevated cytokine levels in children with autism spectrum disorder. Journal of neuroimmunology, 172(1-2), 198–205.

Monteiro P, Feng G. 2017. SHANK proteins: roles at the synapse and in autism spectrum disorder. Nat Rev Neurosci. 18:147–157

Morrison I, Loken LS, Olausson H. The skin as a social organ. Exp Brain Res (2010) 204:305–14. doi: 10.1007/s00221-009-2007-y

Mostafa, G. A., Meguid, N. A., Shehab, A., Elsaeid, A., & Maher, M. 2021. Plasma levels of nerve growth factor in Egyptian autistic children: relation to hyperserotonemia and autoimmunity. Journal of neuroimmunology, 358, 577638.

Müller RA, Fishman I. 2018. Brain connectivity and neuroimaging of social networks in autism. Trends Cogn. Sci., 22 (2018), pp. 1103-1116.

Nelson RJ, Sur M, Felleman DJ, Kaas JH. Representations of the body surface in postcentral parietal cortex of Macaca fascicularis. J Comp Neurol (1980) 192:611–43. doi: 10.1002/cne.901920402

Nelson SB, Valakh V. 2015. Excitatory/inhibitory balance and circuit homeostasis in autism spectrum disorders. Neuron, 87 (2015), pp. 684-698

Nickl-Jockschat, T., & Michel, T. M. 2011. The role of neurotrophic factors in autism. Molecular psychiatry, 16(5), 478–490.

O'riordan M, Passetti F. Discrimination in autism within different sensory modalities. J Autism Dev Disord (2006) 36:665–75. doi: 10.1007/s10803-006-0106-1

Oka, A., & Takashima, S. 1999. The up-regulation of metabotropic glutamate receptor 5 (mGluR5) in Down's syndrome brains. Acta neuropathologica, 97(3), 275–278.

Orefice LL, Mosko JR, Morency DT, Wells MF, Tasnim A, Mozeika SM, Ye M, Chirila AM, Emanuel AJ, Rankin G, et al. 2019. Targeting peripheral somatosensory neurons to improve tactile-related phenotypes in ASD models. Cell. 178:867–886.

Orefice LL, Zimmerman AL, Chirila AM, Sleboda SJ, Head JP, Ginty DD. Peripheral mechanosensory neuron dysfunction underlies tactile and behavioral deficits in mouse models of ASDs. Cell (2016) 166:299–313. doi: 10.1016/j.cell.2016.05.033

Orefice LL. 2020. Peripheral somatosensory neuron dysfunction: emerging roles in autism spectrum disorders. Neuroscience. 445:120–129.

Pagani M, Barsotti N, Bertero A, Trakoshis S, Ulysse L, Locarno A, Miseviciute I, De Felice A, Canella C, Supekar K, Galbusera A, Menon V, Tonini R, Deco G, Lombardo MV, Pasqualetti M, Gozzi A. 2021. mTOR-related synaptic pathology causes autism spectrum disorder-associated functional hyperconnectivity. Nat. Commun., 12 (2021), p. 6084

Pagani M, Bertero A, Liska A, Galbusera A, Sabbioni M, Barsotti N, Colenbier N, Marinazzo D, Scattoni ML, Pasqualetti M, et al. 2019. Deletion of autism risk gene Shank3 disrupts prefrontal connectivity. J Neurosci. 39:5299.

Pagani M, Damiano M, Galbusera A, Tsaftaris SA, Gozzi A. 2016. Semi-automated registration-based anatomical labelling, voxel based morphometry and cortical thickness mapping of the mouse brain. J. Neurosci. Methods, 267 (2016), pp. 62-73.

Paxinos G. Paxinos and Franklin's the mouse brain in stereotaxic coordinates. 4th ed. Franklin KBJ, editor. Boston: Amsterdam (2013).

Peça J, Feliciano C, Ting JT, Wang W, Wells MF, Venkatraman TN, Lascola CD, Fu Z, Feng G. 2011. Shank3 mutant mice display autistic-like behaviours and striatal dysfunction. Nature. 472:437–442.

Peñagarikano O, Abrahams BS, Herman EI, Winden KD, Gdalyahu A, Dong H, Sonnenblick LI, Gruver R, Almajano J, Bragin A, Golshani P, Trachtenberg JT, Peles E, Geschwind DH. 2011. Absence of CNTNAP2 leads to epilepsy, neuronal migration abnormalities, and core autism-related deficits. Cell, 147 (2011), pp. 235-246

Penfield W, Boldrey E. Somatic motor and sensory representation in the cerebral cortex of man as studied by electrical stimulation. Brain (1937) 60:389–443. doi: 10.1093/brain/60.4.389

Pereira A, Ribeiro S, Wiest M, Moore LC, Pantoja J, Lin S-C, Nicolelis MAL. 2007. Processing of tactile information by the hippocampus. Proc Natl Acad Sci U S A. 104:18286–18291.

Petersen CC. 2007. The functional organization of the barrel cortex. Neuron. 56:339–355.

Petrelli, F., Pucci, L., & Bezzi, P. 2016. Astrocytes and Microglia and Their Potential Link with Autism Spectrum Disorders. Frontiers in cellular neuroscience, 10, 21.

Phelan K, McDermid HE. 2012. The 22q13.3 deletion syndrome (Phelan-McDermid syndrome). Mol Syndromol. 2:186–201.

Pizzo R, Lamarca A, Sassoè-Pognetto M, Giustetto M. 2020. Structural bases of atypical whisker responses in a mouse model of CDKL5 deficiency disorder. Neuroscience. 445:130–143.

Poliak S, Gollan L, Martinez R, Custer A, Einheber S, Salzer JL, Trimmer JS, Shrager P, Peles E. 1999. Caspr2, a new member of the neurexin superfamily, is localized at the juxtaparanodes of myelinated axons and associates with K+ channels. Neuron, 24 (1999), pp. 1037-1047

Poliak S, Salomon D, Elhanany H, Sabanay H, Kiernan B, Pevny L, Stewart CL, Xu X, Chiu SY, Shrager P, Furley AJ, Peles E. 2003. Juxtaparanodal clustering of shaker-like K+ channels in myelinated axons depends on Caspr2 and TAG-1. J. Cell Biol., 162 (2003), pp. 1149-1160

Provenzano G, Pangrazzi L, Poli A, Pernigo M, Sgadò P, Genovesi S, Zunino G, Berardi N, Casarosa S, Bozzi Y. 2014. Hippocampal dysregulation of neurofibromin-dependent pathways is associated with impaired spatial learning in engrailed 2 knock-out mice. J Neurosci. 34:13281–13288

Puts N.A.J., Wodka EL, Harris AD, Crocetti D, Tommerdahl M, Mostofsky SH. Reduced GABA and altered somatosensory function in children with autism spectrum disorder. Autism Res (2017) 10:608–19. doi: 10.1002/aur.1691

Puts NA, Wodka EL, Tommerdahl M, Mostofsky SH, Edden RA. Impaired tactile processing in children with autism spectrum disorder. J Neurophysiol (2014) 111:1803–11. doi: 10.1152/jn.00890.2013

Robertson CE, Baron-Cohen S. Sensory perception in autism. Nat Rev Neurosci (2017) 18:671–84. doi: 10.1038/nrn.2017.112

Rodriguez, J. I., & Kern, J. K. 2011. Evidence of microglial activation in autism and its possible role in brain underconnectivity. Neuron glia biology, 7(2-4), 205–213

Rogers SJ, Hepburn S, Wehner E. Parent reports of sensory symptoms in toddlers with autism and those with other developmental disorders. J Autism Dev Disord (2003b) 33:631–42. doi: 10.1023/B:JADD.0000006000.38991.a7

Rozenkrantz L, Zachor D, Heller I, Plotkin A, Weissbrod A, Snitz K, et al. A mechanistic link between olfaction and autism spectrum disorder. Curr Biol (2015) 25:1904–10. doi: 10.1016/j.cub.2015.05.048

Rubenstein JL, Merzenich MM. Model of autism: increased ratio of excitation/inhibition in key neural systems. Genes Brain Behav (2003) 2:255–67. doi: 10.1034/j.1601-183X.2003.00037.x

Rubenstein JL, Merzenich MM. Model of autism: increased ratio of excitation/inhibition in key neural systems. Genes Brain Behav (2003) 2:255–67. doi: 10.1034/j.1601-183X.2003.00037.x

Rutter M. Cognitive deficits in the pathogenesis of autism. J Child Psychol Psychiatry (1983) 24:513–31. doi: 10.1111/j.1469-7610.1983.tb00129.x

Schmucker C, Seeliger M, Humphries P, Biel M, Schaeffel F. 2005. Grating acuity at different luminances in wild-type mice and in mice lacking rod or cone function. Invest Ophthalmol Vis Sci. 46:398–407

Scott KE, Kazazian K, Mann RS, Möhrle D, Schormans AL, Schmid S, Allman BL. 2020. Loss of Cntnap2 in the Rat Causes Autism-Related Alterations in Social Interactions, Stereotypic Behavior, and Sensory Processing. Autism Res. 2020 Oct;13(10):1698-1717. doi: 10.1002/aur.2364. Epub 2020 Sep 11. PMID: 32918359.

Scott-Van Zeeland AA, Abrahams BS, Alvarez-Retuerto AI, Sonnenblick LI, Rudie JD, Ghahremani D, Mumford JA, Poldrack RA, Dapretto M, Geschwind DH, Bookheimer SY. 2010. Altered functional connectivity in frontal lobe circuits is associated with variation in the autism risk gene CNTNAP2. Sci. Transl. Med., 2 (2010), p. 56ra80

Selimbeyoglu A, Kim CK, Inoue M, Lee SY, Hong ASO, Kauvar I, Ramakrishnan C, Fenno LE, Davidson TJ, Wright M, Deisseroth K. 2017. Modulation of prefrontal cortex excitation/inhibition balance rescues social behavior in CNTNAP2-deficient mice. Sci. Transl. Med., 9 (2017)

Sgadò P, Provenzano G, Dessi E, Adami V, Zunino G, Genovesi S, Casarosa S, Bozzi Y. 2013. Transcriptome profiling in engrailed-2 mutant mice reveals common molecular pathways associated with autism spectrum disorders. Molecular Autism, 4 (2013), p. 51

Silverman JL, Yang M, Lord C, Crawley JN. Behavioural phenotyping assays for mouse models of autism. Nat Rev Neurosci (2010) 11:490–502. doi: 10.1038/nrn2851

Simmons DR, Robertson AE, Mckay LS, Toal E, Mcaleer P, Pollick FE. Vision in autism spectrum disorders. Vision Res (2009) 49:2705–39. doi: 10.1016/j.visres.2009.08.005

Sohal VS, Rubenstein JLR. 2019. Excitation-inhibition balance as a framework for investigating mechanisms in neuropsychiatric disorders. Mol. Psychiatry, 24 (2019), pp. 1248-1257

Stephenson, J. L., & Byers, M. R. 1995. GFAP immunoreactivity in trigeminal ganglion satellite cells after tooth injury in rats. Experimental neurology, 131(1), 11–22.

Strauss KA, Puffenberger EG, Huentelman MJ, Gottlieb S, Dobrin SE, Parod JM, Stephan DA, Morton DH. 2006. Recessive symptomatic focal epilepsy and mutant contactin-associated protein-like 2. N. Engl. J. Med., 354 (2006), pp. 1370-1377

Subramanian, M., Timmerman, C. K., Schwartz, J. L., Pham, D. L., & Meffert, M. K. 2015. Characterizing autism spectrum disorders by key biochemical pathways. Frontiers in neuroscience, 9, 313.

Tavassoli T, Auyeung B, Murphy LC, Baron-Cohen S, Chakrabarti B. Variation in the autism candidate gene GABRB3 modulates tactile sensitivity in typically developing children. Mol Autism (2012) 3:6. doi: 10.1186/2040-2392-3-6

Tavassoli T, Baron-Cohen S. Taste identification in adults with autism spectrum conditions. J Autism Dev Disord (2012) 42:1419–24. doi: 10.1007/s10803-011-1377-8

Tavassoli T, Hoekstra RA, Baron-Cohen S. The sensory perception quotient (SPQ): development and validation of a new sensory questionnaire for adults with and without autism. Mol Autism (2014) 5:29. doi: 10.1186/2040-2392-5-29

Tavassoli T, Layton C, Levy T, Rowe M, George-Jones J, Zweifach J, Lurie S, Buxbaum JD, Kolevzon A, Siper PM. 2021. Sensory reactivity phenotype in Phelan-McDermid syndrome is distinct from idiopathic ASD. Genes (Basel). 12:977. https://doi.org/10.3390/genes12070977.

Tripathi PP, Sgadò P, Scali M, Viaggi C, Casarosa S, Simon HH, Vaglini F, Corsini GU, Bozzi Y. 2009. Increased susceptibility to kainic acid-induced seizures in Engrailed-2 knockout mice. Neuroscience. 159:842–849.

Turner-Brown LM, Baranek GT, Reznick JS, Watson LR, Crais ER. The first year inventory: a longitudinal follow-up of 12-month-old to 3-year-old children. Autism (2013) 17:527–40. doi: 10.1177/1362361312439633

Unichenko P, Yang JW, Kirischuk S, Kolbaev S, Kilb W, Hammer M, Krueger-Burg D, Brose N, Luhmann HJ. 2018. Autism related neuroligin-4 knockout impairs intracortical processing but not sensory inputs in mouse barrel cortex. Cereb Cortex. 28:2873–2886.

Van Der Loos H. Barreloids in mouse somatosensory thalamus. Neurosci Lett (1976) 2:1–6. doi: 10.1016/0304-3940(76)90036-7

Vargas, D. L., Nascimbene, C., Krishnan, C., Zimmerman, A. W., & Pardo, C. A. 2005. Neuroglial activation and neuroinflammation in the brain of patients with autism. Annals of neurology, 57(1), 67–81.

Vogt, D., Cho, K., Shelton, S. M., Paul, A., Huang, Z. J., Sohal, V. S., & Rubenstein, J. 2018. Mouse Cntnap2 and human CNTNAP2 ASD alleles cell autonomously regulate PV+ cortical interneurons. Cerebral cortex, 28(11), 3868–3879.

Wang C, Liu H, Li K, Wu ZZ, Wu C, Yu JY, Gong Q, Fang P, Wang XX, Duan SM, et al. 2020. Tactile modulation of memory and anxiety requires dentate granule cells along the dorsoventral axis. Nat Commun. 11:6045

Wing L. The handicaps of autistic children–a comparative study. J Child Psychol Psychiatry (1969) 10:1–40. doi: 10.1111/j.1469-7610.1969.tb02066.x

Woolsey TA, Van Der Loos H. The structural organization of layer IV in the somatosensory region (SI) of mouse cerebral cortex. The description of a cortical field composed of discrete cytoarchitectonic units. Brain Res (1970) 17:205–42. doi: 10.1016/0006-8993(70)90079-X

Wu G., Whiteside G.T., Lee G., Nolan S., Niosi M., Pearson M.S., Ilyin V.I. 2004. A-317491, a selectiveP2X3/P2X2/3 receptor antagonist, reverses inflammatory mechanical hyperalgesia through action at peripheral receptors in rats. Eur J Pharmacol., 504(1-2), 45–53

Wu HP, Ioffe JC, Iverson MM, Boon JM, Dyck RH. 2013. Novel, whisker-dependent texture discrimination task for mice. Behav Brain Res. 237:238–242.

Yang M, Bozdagi O, Scattoni ML, Wöhr M, Roullet FI, Katz AM, Abrams DN, Kalikhman D, Simon H, Woldeyohannes L, et al. 2012. Reduced excitatory neurotransmission and mild autism-relevant phenotypes in adolescent Shank3 null mutant mice. J Neurosci. 32:6525–6541.

Yip J., Soghomonian J.J., Blatt G.J. 2007. Decreased GAD67 mRNA levels in cerebellar Purkinje cells in autism: pathophysiological implications. Acta neuropathologica, 113(5), 559–568.

Yip, J., Soghomonian, J. J., & Blatt, G. J. 2008. Increased GAD67 mRNA expression in cerebellar interneurons in autism: implications for Purkinje cell dysfunction. Journal of neuroscience research, 86(3), 525–530.

Yizhar, O., Fenno, L., Prigge, M. et al. Neocortical excitation/inhibition balance in information processing and social dysfunction. Nature 477, 171–178 (2011). https://doi.org/10.1038/nature10360

Zerbi V, Pagani M, Markicevic M, Matteoli M, Pozzi D, Fagiolini M, Bozzi Y, Galbusera A, Scattoni ML, Provenzano G, Banerjee A, Helmchen F, Basson MA, Ellegood J, Lerch JP, Rudin M, Gozzi A, Wenderoth N. 2021. Brain mapping across 16 autism mouse models reveals a spectrum of functional connectivity subtypes. Mol. Psychiatry, 26 (2021), pp. 7610-7620.

Zhang, Q., Siroky, M., Yang, J. H., Zhao, Z., & Azadzoi, K. 2014. Effects of ischemia and oxidative stress on bladder purinoceptors expression. Urology, 84 (5).

Zhang, Z., Yao, Z., Wu, K., Zhang, T., Xing, C., & Xing, X. L. 2021. Resveratrol rescued the pain related hypersensitivity for Cntnap2-deficient mice. European journal of pharmacology, 891, 173704.

Zhao, H., Mao, X., Zhu, C., Zou, X., Peng, F., Yang, W., Li, B., Li, G., Ge, T., & Cui, R. 2022. GABAergic system dysfunction in Autism Spectrum Disorders. Frontiers in cell and developmental biology, 9, 781327.

Zhao, H., Zhang, H., Liu, S., Luo, W., Jiang, Y., & Gao, J. 2021. Association of peripheral blood levels of cytokines with Autism Spectrum Disorder: A meta-analysis. Frontiers in psychiatry, 12, 670200.

Zhou, X., Ma, L. M., Xiong, Y., Huang, H., Yuan, J. X., Li, R. H., Li, J. N., & Chen, Y. M. 2016. Upregulated P2X3 receptor expression in patients with intractable temporal lobe epilepsy and in a rat model of epilepsy. Neurochemical research, 41(6), 1263–1273.

Zhubi, A., Chen, Y., Guidotti, A., & Grayson, D. R. 2017. Epigenetic regulation of RELN and GAD1 in the frontal cortex (FC) of autism spectrum disorder (ASD) subjects. International journal of developmental neuroscience: the official journal of the International Society for Developmental Neuroscience, 62, 63–72.